Thesis for Doctor of Philosophy

Application of Lower Bainite Microstructure for Bearing Steels and Acceleration of Transformation Kinetics

Chae, Jae-Yong   (채 재 용)

Computational Metallurgy

Graduate Institute of Ferrous Technology

Pohang University of Science and Technology

2012

Application of Lower Bainite Microstructure for Bearing Steels and Acceleration of Transformation Kinetics

2012

Chae, Jae-Yong

베어링강 최종 미세조직으로서의
저온 베이나이트 적용 가능성
및 변태 가속화

Application of Lower Bainite
Microstructure for Bearing Steels
and
Acceleration of Transformation Kinetics

Application of Lower Bainite Microstructure for Bearing Steels and Acceleration of Transformation Kinetics

By

Chae, Jae-Yong

Computational Metallurgy

Graduate Institute of Ferrous Technology

Pohang University of Science and Technology

A thesis submitted to the faculty of Pohang University of Science and Technology in partial fulfillments of the requirements for the degree of Doctor of Philosophy in the Graduate Institute of Ferrous Technology (Computational Metallurgy)

Pohang, Korea

7 December 2012

Approved by

Prof. Suh, Dong-Woo   Prof. Bhadeshia, H. K. D. H.

_____   _____

Major Advisor   Co-advisor

Application of Lower Bainite Microstructure for Bearing Steels and Acceleration of Transformation Kinetics

Chae, Jae-Yong

This dissertation is submitted for the degree of Doctor of Philosophy at the Graduate Institute of Ferrous Technology of Pohang University of Science and Technology. The research reported herein was approved by the committee of Thesis Appraisal

7 December 2012

Thesis Review Committee

Chairman: Suh, Dong-Woo   (signature)

Member: Lee, Jae-Sang   (signature)

Member: Huh, Yoon-Uk   (signature)

Member: Lee, Chang-Hoon   (signature)

Member: Kim, Dae-Woo   (signature)

Preface

This dissertation is submitted for the degree of Doctor of Philosophy at Pohang University of Science and Technology. The research described herein was conducted under the supervision of Professor H. K. D. H. Bhadeshia, Professor of Computational Metallurgy in the Graduate Institute of Ferrous Technology, Pohang University of Science and Technology and Professor of Physical Metallurgy, University of Cambridge, between September 2008 and December 2012

This work is to the best of my knowledge original, except where acknowledgements and references are made to previous work. Neither this, nor any substantially similar dissertation has been or is being submitted for any other degree, diploma or other qualification at any other university. This dissertation does not exceed 60,000 words in length.

Part of this work has been submitted to appear in the following publications:

J. Y. Chae, J. H. Jang, G. Zhang, K. H. Kim, J. S. Lee, H. K. D. H. Bhadeshia, and D. W. Suh, "Dilatometric analysis of cementite dissolution in hypereutectoid steels containing Cr." *Scripta Materialia*, 65:245-248, 2011.

Jae Yong Chae

December, 2012

Abstract

Conventional martensitic SAE52100 steel has been the most commonly used material for bearing applications. Lower bainitic microstructure was suggested as an alternative microstructure to replace the martensitic structure, since it showed an equivalent fatigue life to martensite under normal environments, and offers a superior fatigue life in water-containing environments. There have been many studies about lower bainitic SAE52100 steel, but most of them were attempted without consideration about spheroidization.

The purpose in the present research was therefore to examine the bainite transformation kinetics of SAE52100 steel, with a microstructure containing spheroidized cementite in a ferrite matrix as an initial state. The effect of various solutes such as Si, Cr, Al, and Co on the acceleration of bainite was also demonstrated. Then the mechanical properties of resultant bainitic SAE52100 steels were evaluated and compared with the literatures.

The reaction kinetics was evaluated using dilatometry and microstructural observations. As a result, bainite transformation for SAE52100 could be completed in 30 min at 250℃, which is much faster than previous studies based on a non-spheroidized starting structures. Moreover, the transformation of Al-, Co-added, and Cr-decreased alloys has been completed in shorter isothermal transformation compared with SAE52100, while the transformation kinetics of Si-added alloy was

delayed. Thermodynamic calculations and experimental observations were performed to measure the quantity of cementite during austenitization, and hence the optimum heat treatment process could be designed for each alloy.

The mechanical properties were measured by ultrasonic fatigue testing and Rockwell hardness testing. The fatigue property of lower bainitic SAE52100 could be enhanced by changing the concentration of Cr, Al, and Co, without a particular change in hardness. However, the presence of spheroidized cementite particle was adversely affected on the fatigue property of bainitic SAE52100 steel, since the measured results were inferior to the reported results with non-spheroidized microstructures.

Contents

Nomenclature

A_A	Area fraction
A_{CM}	Temperature limit on the equilibrium phase boundaries of austenite / (cementite + austenite)
A_{e1}	Lower temperature limit of the equilibrium phase boundary ferrite + austenite phase field
ASTM	American Society for Testing and Materials
B	Bainite
C_i	Mass fraction of carbon in i phase
DET	Divorced Eutectoid Transformation
D_α	Diffusivity of carbon in ferrite
D_γ	Diffusivity of carbon in austenite
EDS	Energy Dispersive X-Ray spectroscopy
FESEM	Field-Emission Scanning Electron Microscopy
f_i	Volume fraction of i phase
H	Hardness of steel
H_i	The specific hardness of the i phase
HIC	Hydrogen-Induced Cracking
k	Scale factor
L	Specimen length
L_0	Specimen length at reference temperature
L_{10}	The number of cycles until 10 % of samples were failed by fatigue
M/A	Mixture of martensite and retained austenite

M_i	Atomic mass of i phase
M_S	Martensite-start temperature
P_p	Point fraction
P_T	Total number of grid points
P_x	The number of grid points lying inside x phase
r_{cem}	Radius of cementite region
r_{total}	Radius of whole system
SEM	Scanning Transmission Electron Microscopy
$S\text{-}N$	Stress amplitude versus the logarithm of the number of cycles
T	Temperature in Kelvin
TTT	Time-temperature-transformation
V	Velocity of moving austenite/ferrite boundary
V	Atomic volume of specimen
V_0	Average volume at reference temperature
V_{cem}	Volume of cementite
V_{cem}^f	Volume fraction of cementite
V_i	The volume fraction of the i phase
V_{total}	Volume of whole system
V_V	Volume fraction
X_c	Carbon concentration in austenite
α	ferrite
γ	austenite

Δk The intensity of the stress field in the crack tip region

ΔT Undercooling below A_1

θ cementite

λ_α Diffusion distance of carbon in ferrite

λ_γ Diffusion distance of carbon in austenite

ρ_i Mass density of i phase

a_α Lattice parameter of ferrite

a_γ Lattice parameter of austenite

a_θ Lattice parameter of cementite

Chapter 1: Introduction and aim

SAE52100 is one of the most common materials for bearing applications. It has been used as a standard material especially in ball bearing industry since 1920s. The conventional heat treatment for this steel is designed to produce a martensitic microstructure by appropriate quenching and following low-temperature tempering, in order to obtain adequate mechanical properties required for bearing (Burrier 1987). The martensitic microstructure exhibits a reasonable bearing lifetime due to high strength and high resistance to fatigue (Hengerer 1987, Tsubota *et al.* 1998, Cappel *et al.* 2004).

Studies (Hollox *et al.* 1981, Akbasoglue *et al.* 1990, Luzgivova 2007) have demonstrated that SAE52100 steel with bainitic microstructure, under some environments, provides improved mechanical properties as compared to that of martensitic. Lower bainitic SAE52100 steel showed an equivalent fatigue life to martensite under normal environments, and offers a superior fatigue life in water-containing environments. In spite of those advantages, however, lower bainitic microstructure has not been regarded as an attractive proposition for conventional 52100 steel, due to kinetic constraints and complexity of the heat treatment. Thus, there have been many attempts (Beswick 1989, Olund *et al.* 1998, Chakraborty *et al.* 2008, Luzginova *et al.* 2008, Chakraborty *et al.* 2009) to accelerate the bainite transformation of SAE52100 steel, but most of them did not consider spheroidization, which is an essential process for manufacturing bearing steel.

The purpose in the present research was therefore to examine the bainite transformation kinetics of SAE52100 steel, with a microstructure containing spheroidized cementite in a ferrite matrix as an initial state. The effect of various solutes such as Si, Cr, Al, and Co on the acceleration of bainite was also demonstrated. Then the mechanical properties of resultant bainitic SAE52100 steels were evaluated and compared with the literatures. In the course of doing those works, it was necessary to understand the dissolution behavior of spheroidized cementite during austenitization.

Chapter 2: Literature review of SAE52100 bearing steel

2.1 SAE52100 steel

2.1.1 Introduction

A Bearing is a mechanical component which fixes the axle into a regular position, supports its weight and helps its rotation. In a broad sense, the device which helps relative movement between two or more parts is also referred as bearing. The bearings can be made using wood, ceramic, plastic and metals including steel. Bearing steel is used for the rolling components in machinery ranging from bicycles to wind turbines. It should maintain high precision and rotation accuracy under the condition of repeated high strength. The prime requirements are mechanical properties such as high hardness, tensile strength, fatigue property, toughness, wear resistant, and shape stability. One of the most common bearing steel is SAE52100 type which contains high carbon (about 1.0 wt%) for the strength and high chromium (1.3 ~ 1.6 wt%) for the hardenability. It has been used as a standard material especially in ball bearing industry since 1920s, and also referred as SUJ2, AISI 52100, 100Cr6, EN31, etc. The chemical composition of SAE52100 steel is represented in Table 1.

Table 1 : Chemical composition of SAE52100 steel.

Component	Composition (wt%)
Carbon	0.95 – 1.10
Manganese	0.2 – 0.45
Silicon	0.25 – 0.35
Phosphorus	0.025 Max.
Sulfur	0.025 Max
Chromium	1.30 – 1.60
Ferrous	Balanced

2.1.2 Manufacturing process

 The general manufacturing process of ball bearing steel is illustrated in Figure 1. The microstructure of SAE52100 type steel when supplied from steel manufacturer is generally pearlite including proeutectoid cementite at the prior austenite grain boundaries. Then, the microstructure is transformed to the mixture of coarse cementite and ferrite by spheroidization process. The main purpose of spheroidization is to facilitate the forging process in the next stage by reducing the hardness of the steel. Recent work has shown that the fatigue life of SAE52100 could be also improved by spheroidization, when it was transformed into tempered martensite microstructure (Kim *et al.* 2012). In addition, the cementite in the final microstructure helps improve the resistance of steel to wear (Monma *et al.* 1968). The details of spheroidization will be discussed in the following section.

```
┌─────────────────────────────┐
│    Steel manufacturer       │
│                             │
│  General steel making process│
└─────────────────────────────┘
              ↓
┌─────────────────────────────┐
│    Wire drawing factory     │
│                             │
│     Softening annealing     │
│          Drawing            │
│       Spheroidization       │
└─────────────────────────────┘
              ↓
┌─────────────────────────────┐
│      Ball manufacturer      │
│                             │
│        Ball forging         │
│     Heat treatment (Q/T)    │
└─────────────────────────────┘
              ↓
┌─────────────────────────────┐
│    Bearing manufacturer     │
│                             │
│        Ball assembly        │
└─────────────────────────────┘
```
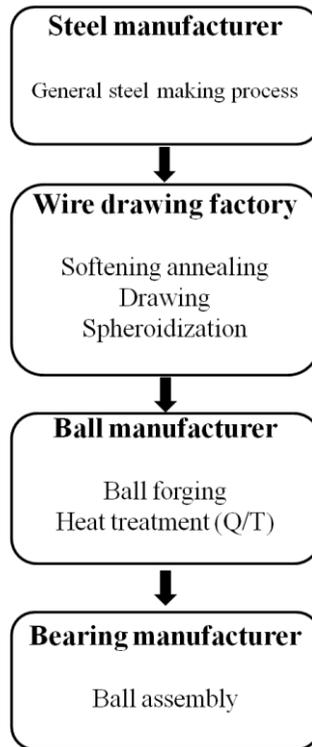
Figure 1: A typical manufacturing process of the steel for ball bearing.

2.1.3 Microstructure

Conventional SAE52100 steel is often heat treated to obtain martensitic microstructure, so quenching and tempering treatment is necessary. The purpose of quenching process is to transform the austenite into martensite, which is harder phase. Then the tempering process is followed. During tempering, martensite is reheated into temperature below the eutectoid, kept for specified time period, and air cooled. Ductility and toughness can be enhanced, residual stress be removed, and the microstructure be stabilized by the tempering process. This process allows carbon saturated martensite to transform to the tempered martensite which consists of ferrite and cementite phases.
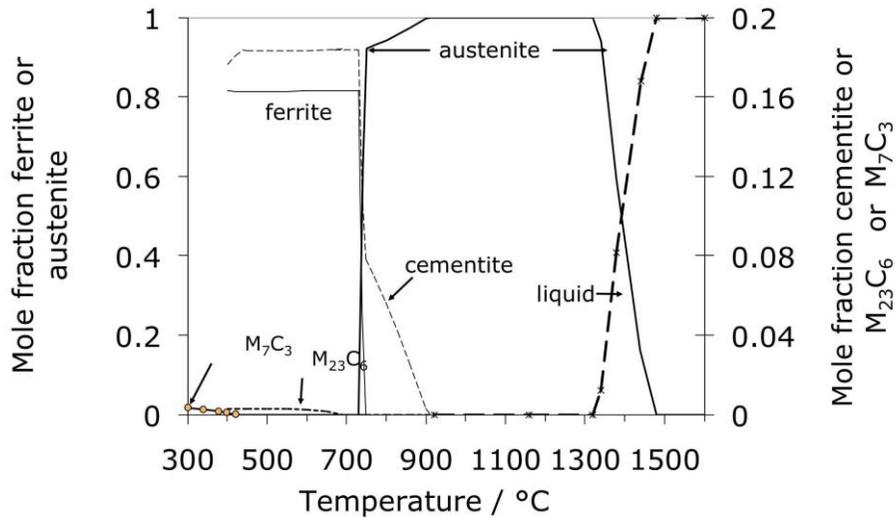
Figure 2: Phase fractions calculated using MTDATA, for SAE52100 steel, as a function of temperature (Bhadeshia 2012).

The calculated equilibrium phase fractions for SAE52100 as a function of temperature are illustrated in Figure 2 (Bhadeshia 2012). Typical austenitization process for quenching and tempering process for SAE52100 is implemented at 850℃ for 20 min, where equilibrium cementite fraction is about 3%. The equilibrium cannot be reached within 20 min of austenitization; Figure 3 illustrates the reported kinetics of cementite dissolution in 52100 type steel (Guillot *et al.* 1982). Therefore, the subsequent quenching process after austenitization occurs from the microstructure which consists of more than 3% of undissolved cementite and rest of austenite. Then, the resultant microstructure contains martensite, about 6% of retained austenite, and 3~4% of undissolved cementite particle (Tsubota *et al.* 1998, Beswick 1989). The steel is then tempered at about 250℃. The decomposition of

retained austenite and precipitation of some transition carbide from supersaturated martensite may be occurred during tempering process (Hirotsu *et al.* 1972, Hägg 1934), which can lead to the softening of the steel.
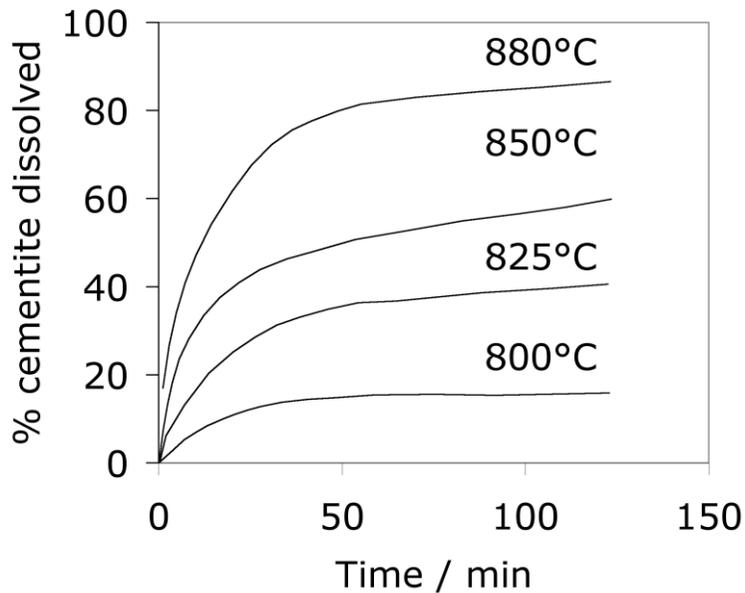
Figure 3: Kinetics of cementite dissolution in 52100 steels, beginning with spheroidized structure, as a function of austenitization temperature (Guillot *et al.* 1982).

2.2 Spheroidization process

2.2.1 Microstructural change

The aim of spheroidization is to facilitate machining and forming operations by softening the material (Knorr *et al.* 1992). The microstructure which consists of

pearlite and proeutectoid cementite in prior austenite grain boundary is transformed into the microstructure consists of coarse cementite particle in ferrite matrix during spheroidization. In spheroidized condition, 52100 steel shows about 230HV of hardness (Li *et al.* 2005), 466 and 635 MPa of yield and ultimate tensile strength respectively, with 36% of elongation (McNelley *et al.* 1983). Figure 4 illustrates the microstructural change of 52100 steel by spheroidization (Luzginova *et al.* 2008).
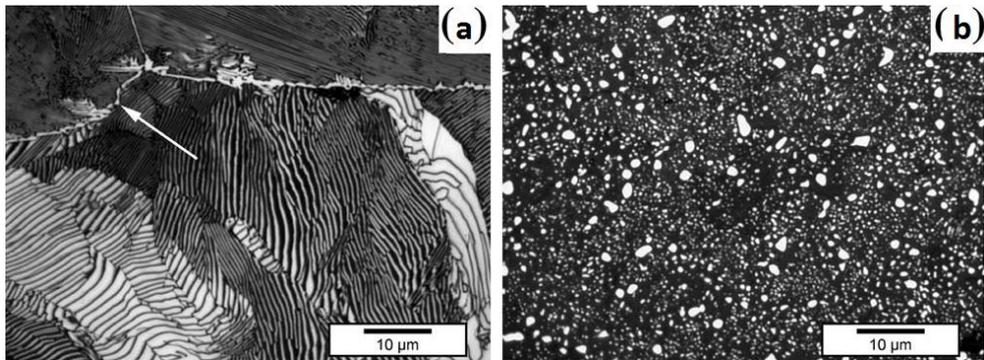
Figure 4: Change in microstructure (a) before and (b) after spheroidization (Luzginova *et al.* 2008).

2.2.2 Divorced eutectoid transformation

Two types of spheroidization methods are generally used. The first method includes subcritical annealing at the temperature below A_1, and mainly applied for hypoeutectoid steels. The other method, which will mainly be focused in this review, involves intercritical annealing at the temperature above A_1 but below A_{cm}, and mainly applied for hypereutectoid steels such as 52100 type steel. During intercritical annealing in the latter method, an incomplete dissolution of cementite occurs. The cementite lamella is broken into spheroids, and the part of grain boundary cementite is dissolved. The resultant microstructure of fine cementite particle with austenite transforms into a mixture of ferrite and cementite by either

the pearlitic reaction or by the 'divorced eutectoid transformation' reaction (DET) during slow cooling to the temperature below A_1 (Mehl *et al.* 1956, Oyama *et al.* 1984, Verhoeven 1998, Verhoeven *et al.* 2000). The ferrite and cementite grow as coupled pairs at the growth fronts and produce pearlite structure by the pearlitic reaction, whereas the ferrite and cementite grow uncooperatively and produce a spherical array of cementite particles in a ferrite matrix by DET reaction. The mechanisms of two reactions are schematically illustrated in Figure 5 (Verhoeven *et al.* 1998).
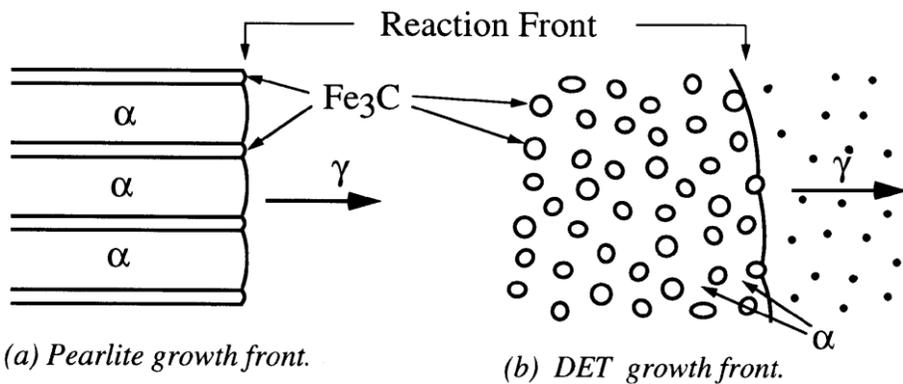
Figure 5: The growth front geometry for (a) lamellar pearlite transformation (b) divorced eutectoid transformation (Verhoeven *et al.* 1998).

A kinetic model for DET reaction has been proposed by Verhoeven (Verhoeven *et al.* 1998). During the transformation when the austenite and cementite is cooled to the temperature below A_1, a schematic illustration of the transformation front is shown in top of Figure 6. The carbon compositions at the cementite particles in both ferrite and austenite, and at the γ/α boundary can be determined in Fe-C phase diagram. If ΔT is the undercooling below the A_1, then the carbon composition labeled C_1 though C_4 in bottom of Figure 6 can be given from phase diagram in Figure 7. Therefore, as the γ/α boundary moves into the austenite during austenite to ferrite

transformation, carbon diffused away from the interface into cementite particles in both the austenite and ferrite. The carbon diffusion fluxes make the cementite particles grow without nucleation of new cementite particles. When the γ/α boundary moves at a velocity V, carbon flux balance at the boundary gives the following equation:

$$(C_4 - C_2)V = D_\gamma \frac{(C_4 - C_3)}{\lambda_\gamma} + D_\alpha \frac{(C_2 - C_1)}{\lambda_\alpha} \qquad (2\text{-}1)$$

If the transformation temperature is 700℃, the terms in equation (2-1) are determined as $(C_4 - C_2) \approx 0.75 + \Delta T(0.225/27)$, $(C_4 - C_3) \approx \Delta T(0.28/27)$, and $(C_2 - C_1) \approx \Delta T(0.009/27)$. Then an approximate equation for the velocity of the γ/α boundary is given by:

$$V \approx \frac{2D_\alpha}{\lambda_\gamma + \lambda_\alpha} \times \frac{\frac{\Delta T}{27}[\frac{0.28}{D_\alpha/D_\gamma} + 0.009]}{0.75 + \frac{\Delta T}{27}(0.225)} \qquad (2\text{-}2)$$

Verhoeven also compared this DET growth velocity with Mehl's experimental data for the velocity of the lamellar pearlite transformation (Mehl *et al.* 1956), and found a transition line for undercooling and cementite spacing below which the DET reaction is completed before pearlite has had time to nucleate (Figure 8).
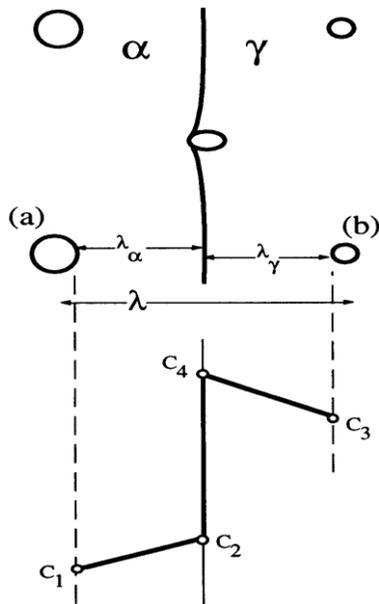
Figure 6: Schematic illustration of DET front (top) and carbon concentration profile (bottom) (Verhoeven *et al.* 1998).
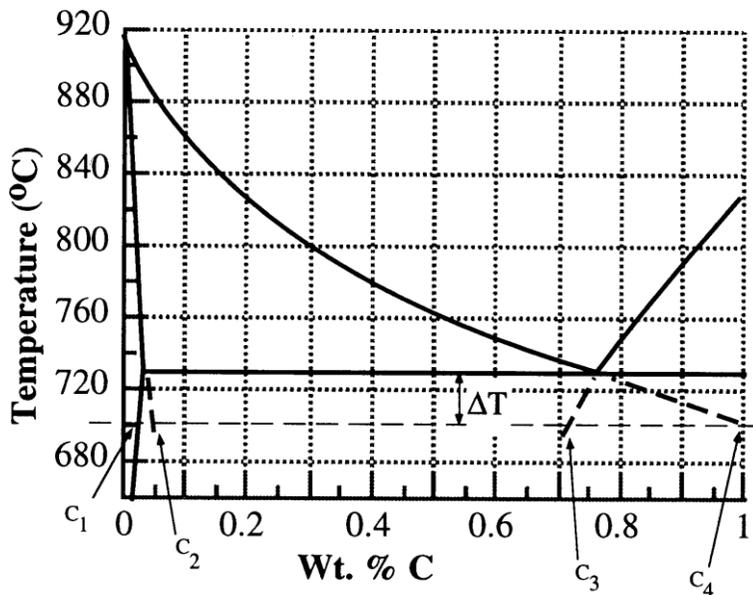
Figure 7: The Fe-C phase diagram (Verhoeven *et al.* 1998).
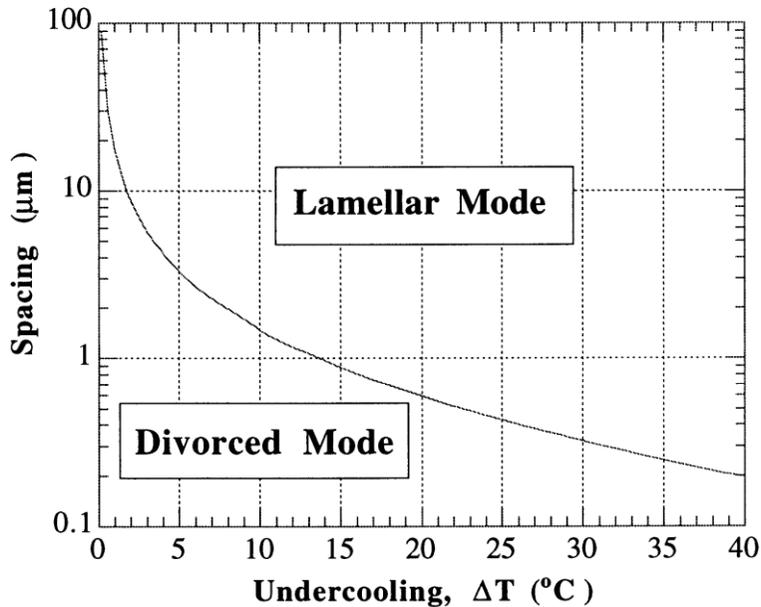
Figure 8: Predicted transition line for undercooling and cementite spacing (Verhoeven *et al.* 1998).

2.3 Lower bainite for SAE52100 steel

2.3.1 Bainite transformation for SAE52100

Lower bainite microstructure has been suggested as an alternative for martensitic 52100 type steel, for further improvement in mechanical properties. The bainitic microstructure can be made by isothermal transformation in the temperature range 200-450℃, especially lower bainite dominates when the transformation temperature is less than 350℃ (Hollox *et al.* 1981). Figure 9 illustrates the measured time-temperature transformation diagram for SAE52100, austenitized at 850℃ (Silva 2001). It took about 4 h to complete bainite transformation at a temperature just above martensite start temperature. The observed lower bainitic microstructure is illustrated in Figure 10 (Vetters *et al.* 2006), isothermal transformation of 52100 steel at 230℃ for 10 h.
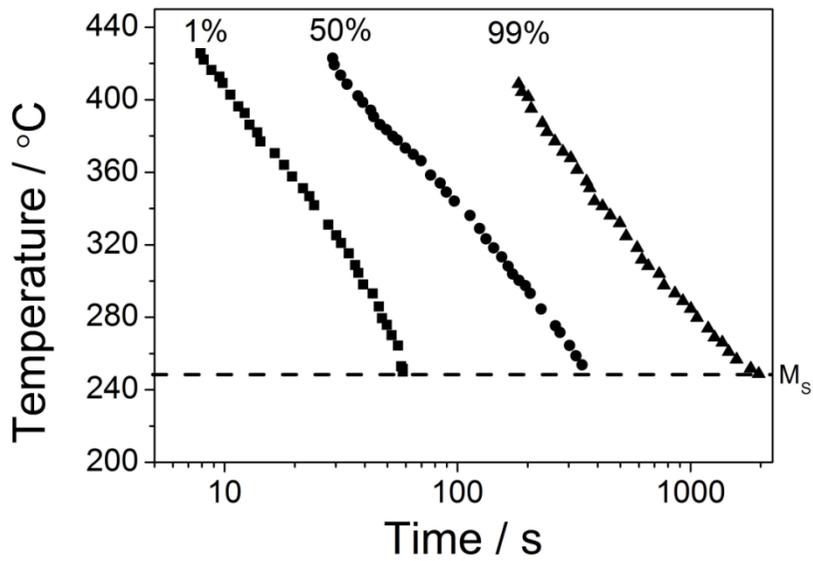
Figure 9: Measured time-temperature transformation diagram for SAE52100, austenitized at 850℃ (Silva 2001).

Figure 10: Lower bainitic microstructure of 52100 steel, isothermal holding at 230℃ for 10 h (Vetters *et al.* 2006).

2.3.2 Mechanical property

Bainitic microstructures in the 52100 type in some respects outperform those which contain tempered martensite. Hollox compared the bearing life of martensite and lower bainite under several conditions (Hollox *et al.* 1981). Lower bainite structure, in the study, was produced by the austenitization at 840℃ and following isothermal treatment at temperature between 250℃ and 300℃. Bearing life was measured by assessing the L_{10} life, the number of cycles until 10 % of samples were failed. The Lower bainite showed a superior life to that of the martensite under the conditions where water and other detrimental constituents were an inherent part of lubricant, as illustrated in Figure 11 and Figure 12, respectively.
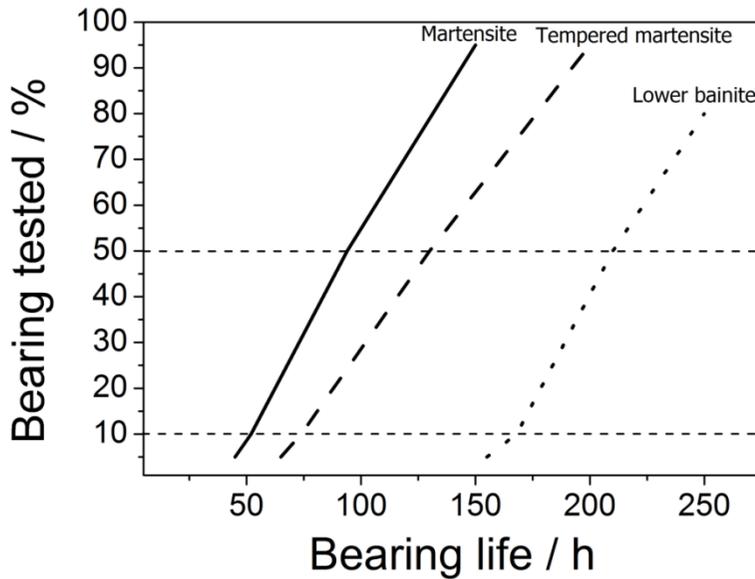
Figure 11: Bearing life of martensite, tempered martensite, and lower bainite in 52100 type steel with water lubricant (Hollox *et al.* 1981).
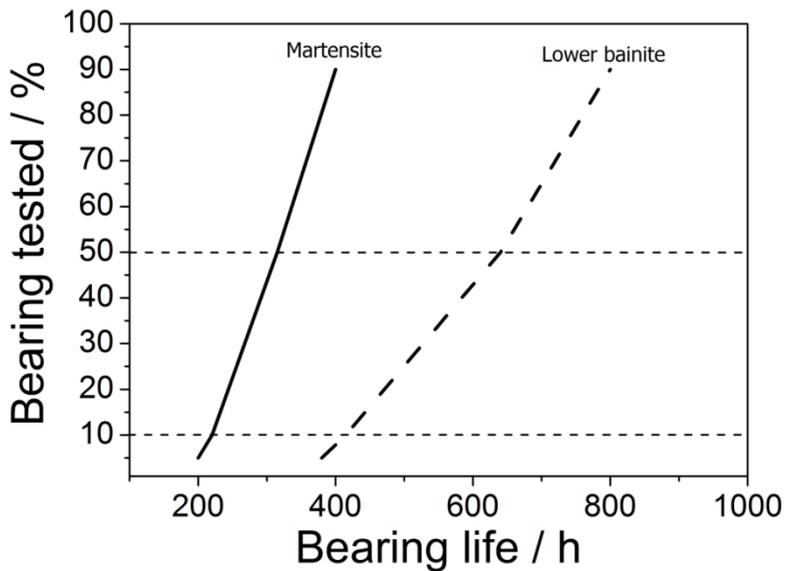
Figure 12: Bearing life of martensite and lower bainite in 52100 type steel with coal dust slurry (Hollox *et al.* 1981).

Akbasoglue has demonstrated that 52100 steel with bainitic microstructure provides improved resistance to wear and hydrogen embrittlement as compared to that of martensitic (Akbasoglue *et al.* 1990). The microstructure of martensite in the research was obtained by austenitization at 840℃ for 20 min and quenching in oil, while additional tempering at 250℃ for 60 min was performed for tempered martensite microstructure. The lower bainite microstructure was obtained by same austenitization condition, and following isothermal treatment at 250℃ for 40 min. In water-based lubricant condition, the higher fracture toughness and superior fatigue crack growth resistance of the lower bainite, compared with both the martensite and tempered martensite, was observed. Figure 13 illustrates the fatigue crack growth curves for three microstructures tested in the water-based lubricant. Stress intensity factor of horizontal axis gives a measure of the intensity of the stress field in the crack tip region.
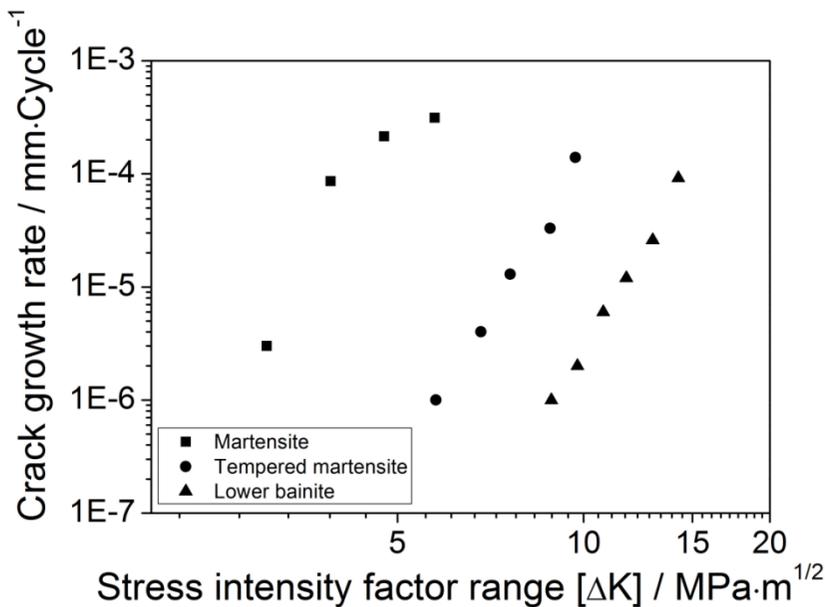
Figure 13: Fatigue crack growth rate of 52100 steel with martensite, tempered martensite, and bainite structure, tested in the water-based lubricant (Akbasoglue *et al.* 1990)

2.3.3 Bainite transformation kinetics of 52100 steel

In spite of the advantages in several mechanical properties, lower bainitic microstructure has not been regarded as an attractive proposition for 52100 steel, due to kinetic constraints and complexity of the heat treatment. It took about 240 min at 250℃ for isothermal heat treatment to obtain full bainitic microstructure of 52100 steel, whereas the maximum tempering time for martensite is about 120 min (Sakanaka 2009). Furthermore, as the isothermal temperature is closer to martensite start temperature, isothermal holding time generally needs to be increased much more (Luzginova *et al.* 2008). Figure 14 illustrates bainite transformation kinetics curves of 52100 steel for different isothermal temperatures after austenitizing at 850℃ for 30 min.
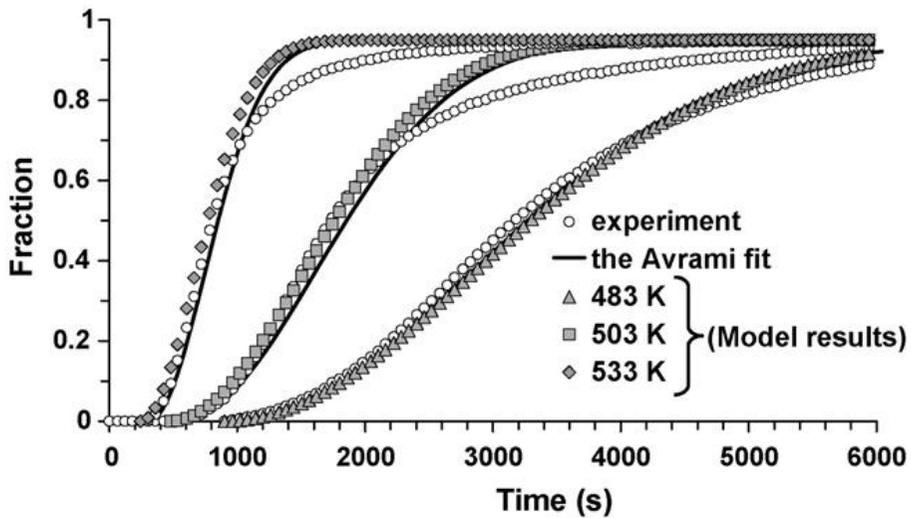
Figure 14: Calculated and measured bainite fraction as a function of isothermal holding time at different isothermal holding temperatures (Luzginova *et al.* 2008).

A combination of bainite and martensite, instead of full bainitic microstructure, has proven superior in terms of mechanical properties as compared to tempered martensite (Young 1994). When bainite forms it enriches the residual austenite with carbon, so that the strength of the subsequent martensite increases. In addition, during its deformation, the strength of the bainite is enhanced via plastic constraint by the surrounding stronger martensite. Thus the optimum isothermal heat treatment condition for 52100 steel has been investigated to develop a duplex bainitic and martensitic microstructure for improved mechanical properties (Chakraborty *et al.* 2008). Figure 15 shows the variation of hardness with isothermal holding temperature and time. The hardness of 52100 steel, austenitized at 950℃ for 30 min, reached a peak between 30 and 60 min for isothermal holding at 270℃. Figure 16 illustrates the tensile and impact test results of 52100 steel as a function of isothermal holding time. The maximum strength was obtained at about 30 min of isothermal holding at 270℃. The relative amount of phases as a function of isothermal holding time is illustrated in Table 2 (Chakraborty *et al.* 2009).
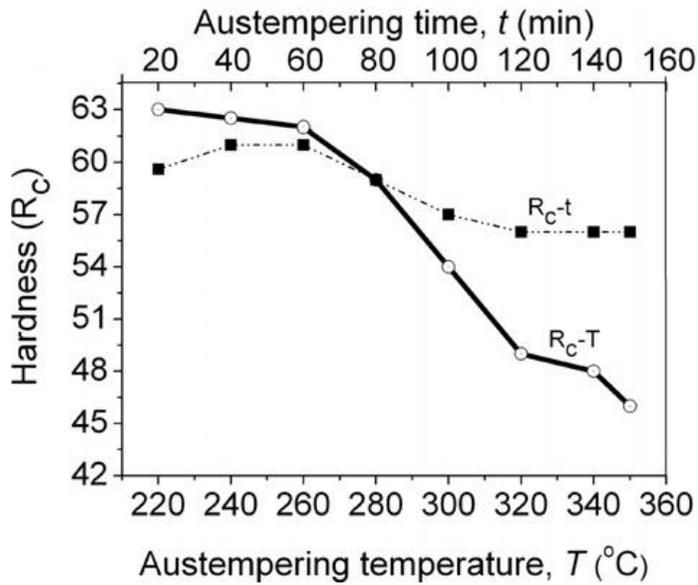
Figure 15 Variation of hardness as a function of isothermal holding time and temperature of SAE52100 steel after austenitized at 950℃ for 30 min (Chakraborty *et al.* 2008).
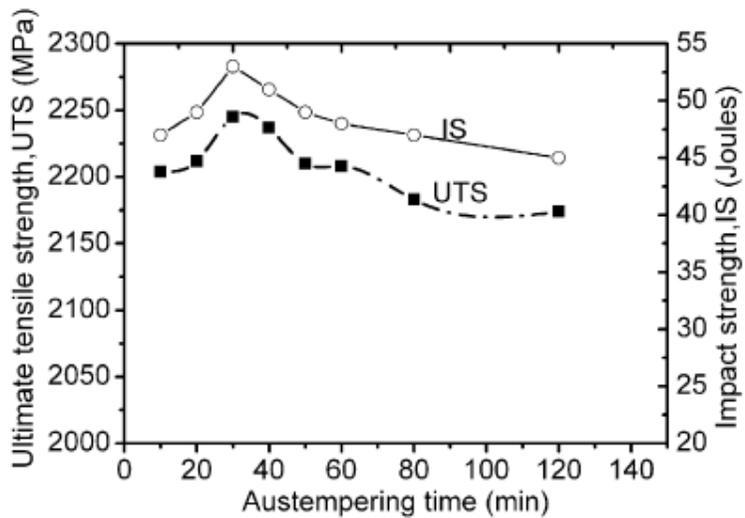
Figure 16 Variation of impact and yield strength as a function of isothermal holding time of SAE52100 steel, after austenitized at 950℃ for 30 min and isothermal holding at 270℃ (Chakraborty *et al.* 2008).

Table 2: Relative amounts of bainite, martensite, carbide, and retained austenite for 52100 steel, as a function of isothermal holding time at 270℃ (Chakraborty *et al.* 2009).

Isothermal holding time at 270℃ (min)	% Bainite	% Martensite	% Carbide	% Retained austenite
15	10	77	1	12
30	35	52	3	10
60	40	47	5	8
120	42	48	5	5

2.4 Mechanical property of SAE52100

2.4.1 Hardness

The hardness of the steel can be typically expressed as a linear combination of the contributions from individual phases:

$$H = \sum V_i H_i \qquad (2\text{-}3)$$

Here, V_i is the volume fraction of the i phase, and H_i is the specific hardness of the i phase. It has been assumed for 52100 steel that the hardness of martensite, bainite, pearlite and austenite are given by 64, 35, 29, and 17 HRC (Umbrello *et al.* 2010). However, the hardness of bainite in that assumption may not be reasonable, since much higher values have been reported in many studies (Akbasoglu *et al.* 1990, Beswick 1989, Chakraborty *et al.* 2008, Wang *et al.* 1990).

The hardness of martensitic 52100 steels reported to be decreased as an increase of tempering temperature, as shown in Figure 17 (Huh *et al.* 1982) and Figure 18 (Hokkirigawa *et al.* 1988). Meanwhile, increasing the austenitization temperature beyond 840℃ did not increase the hardness of the martensitic SAE52100 steels, since the increase in the amount of soft retained austenite coincided with the

increase in carbon concentration of austenite (to be transformed into martensite during quenching).
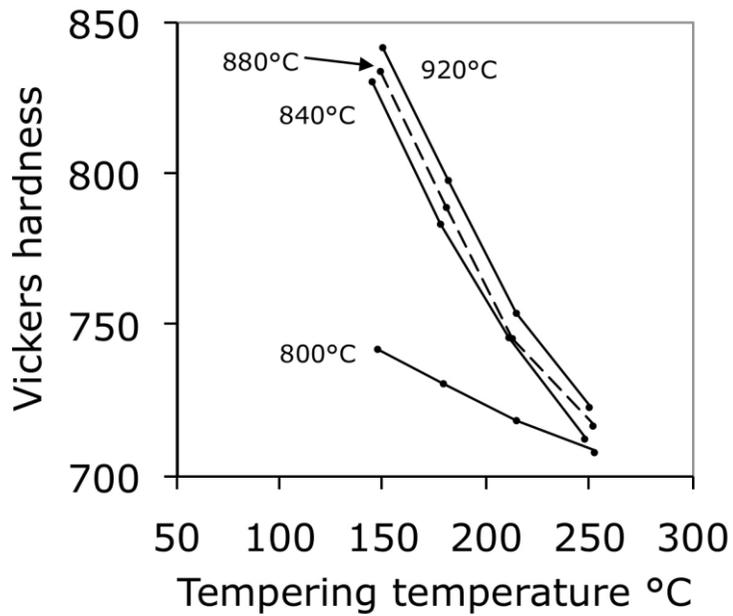
Figure 17: Hardness of 52100 steel as a function of tempering temperature, and of austenitization temperature (Huh *et al.* 1982).
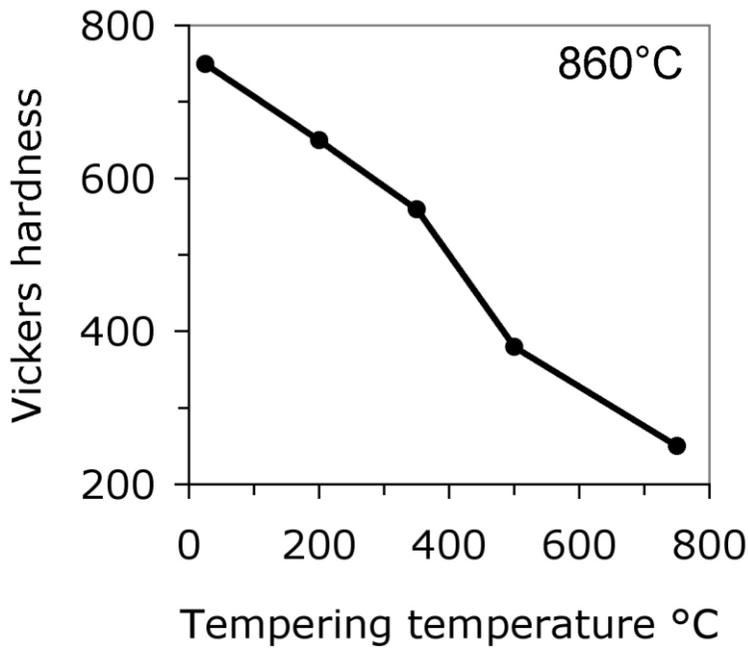
Figure 18: Hardness of 52100 steel as a function of tempering temperature (Hokkirigawa *et al.* 1988).

2.4.2 Fatigue property

Fatigue is the form of failure subjected to dynamic and fluctuating stresses. The fatigue test measures number of cycles to failure by the stress cycling. Parameters which characterize the stress cycle are schematically illustrated in Figure 19. The result of fatigue test is generally expressed as "*S-N*" curves, by plotting the alternating stress amplitude versus the logarithm of the number of cycles that cause failure, Figure 20. Fatigue limit is defined as the largest value of stress below which failure will not occur. For materials which do not exhibit a fatigue limit (red curve in Figure 20), it is conventional to define an endurance limit; the stress amplitude corresponding to a greater fatigue life (recently 10^8 cycles).
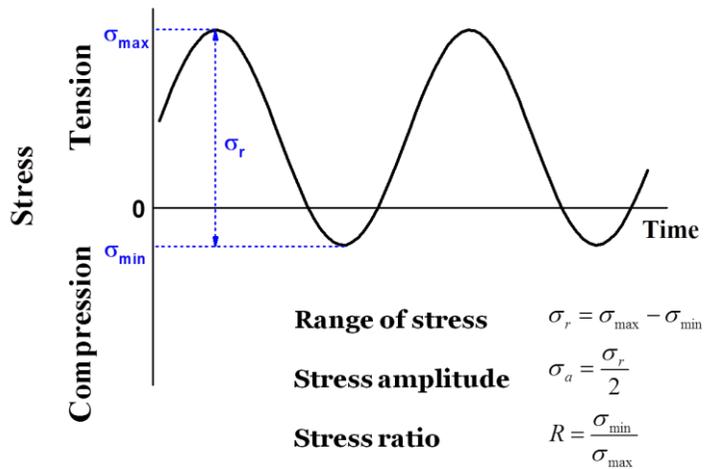
Figure 19: Repeated stress cycle, in which maximum and minimum stresses are asymmetrical relative to the zero-stress level. Parameters characterizing stress cycles are defined.
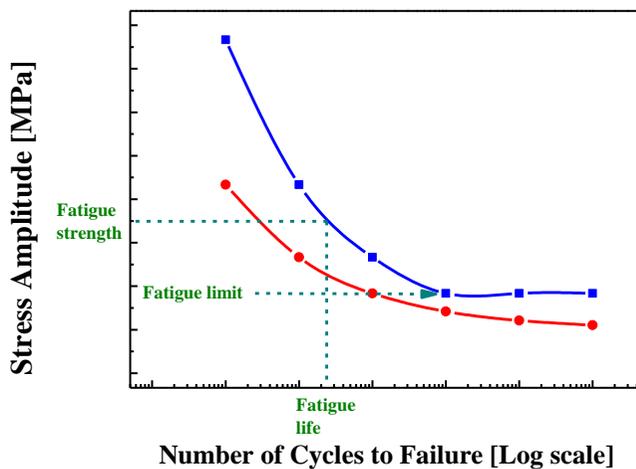
Figure 20: Schematic *S-N* curves for fatigue.

The process of fatigue failure is characterized by three steps: (1) crack initiation from a point of high stress concentration; (2) crack propagation, during which the crack advances incrementally with each stress cycle; and (3) final failure, which occurs very rapidly once the advancing crack has reached a critical size. Thus the fatigue fracture surface is generally divided into three regions according to their features; origin, fatigue zone, and instantaneous zone, Figure 21 (Sachs 2005). A single origin usually indicates a failure with low stress, while the multiple origins may be the result of high stress concentrations. During slow crack propagation, there are variations in the load that resulted progression marks in fatigue zone. Eventually the crack reaches the point where the remaining material is overstressed, and the ductile or brittle fracture may be developed in the instantaneous zone. Figure 22 illustrates typical fatigue fractograph, in which crack initiated from lower left of image. Meanwhile, the fatigue fracture surface can exhibit a shape of 'fish-eye' when the crack initiates from an internal inclusion, Figure 23. It was reported that surface crack initiation was common at high stress amplitudes in martensitic 52100 steel as illustrated in Figure 24 (Sakai 2002).
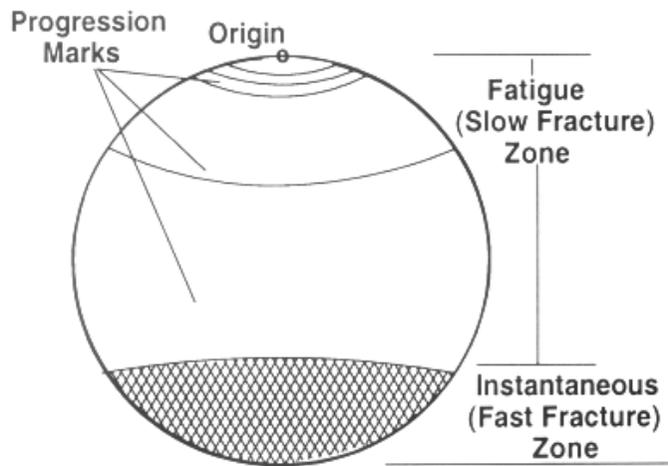
Figure 21: Schematic illustration of macroscopic fatigue fracture surface (Sachs 2005).
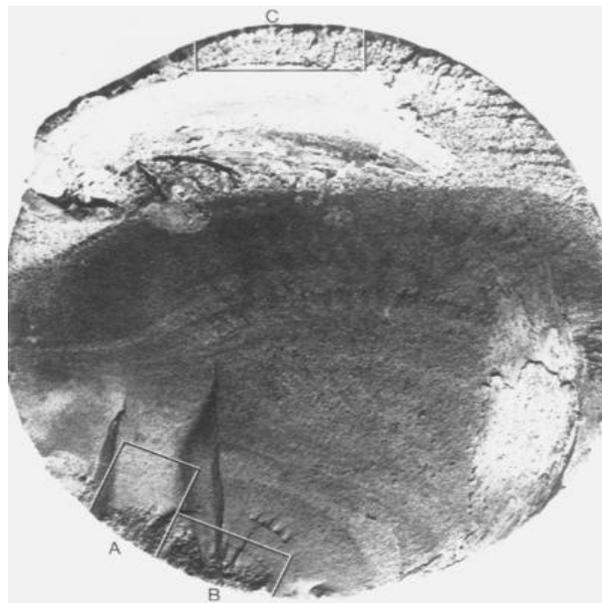
Figure 22: Fatigue fracture surface in surface induced fracture (Joyce 1992).
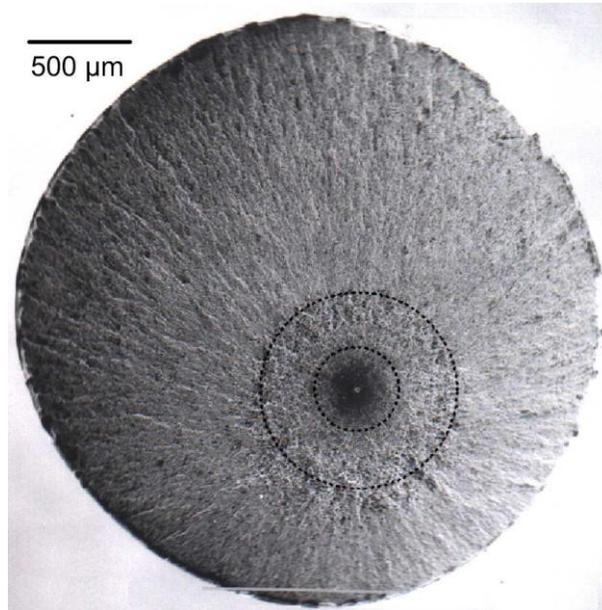
Figure 23: Fracture surface in interior inclusion induced fracture. Referred as 'Fish eye' (Sakai 2005).
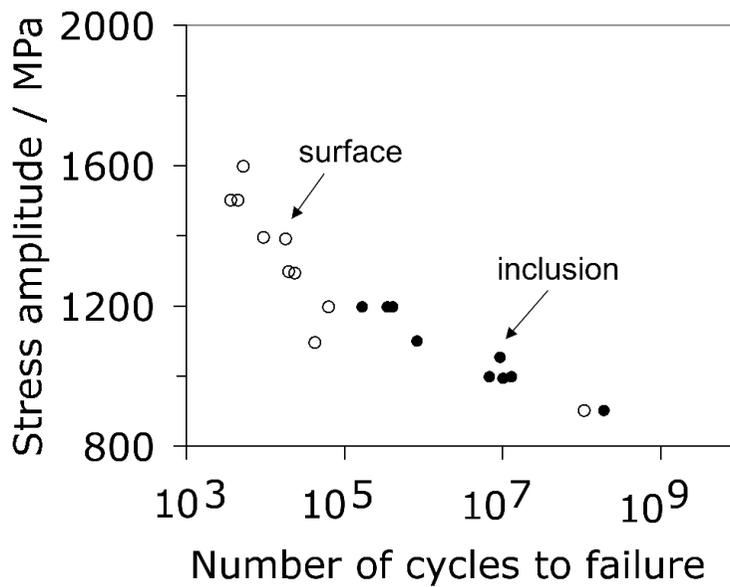
Figure 24: S-N curve for martensitic 52100 steel. The open circles represent crack initiated at the free surface, and the filled circles crack originating from internal inclusion (Sakai 2002).

2.4.3 Ultrasonic fatigue testing

Ultrasonic fatigue testing involves cyclic stressing of material at frequencies typically in the range of 15 to 25 kHz, while typical rotating-bending fatigue testing at about 50 Hz (ASM 2000, Berger et al 2008) . The major advantage of using ultrasonic fatigue is rapid evaluation of the high-cycle fatigue limit. Conventional tests for some 10^9 cycles would take about a year, whereas ultrasonic fatigue test would be completed in 14 hours. The ultrasonic fatigue testing is generally performed by a resonant test method using elastic vibration wave generated by piezoelectric ceramic.

Marines (Marines *et al.* 2003) has compared fatigue life of martensitic 52100 steels obtained in a conventional test at 35 Hz (Sakai 1999) and those measured using 20 kHz ultra sonic loading, Figure 25. The result shows a discrepancy between the two kinds of tests, with the ultrasonic tests consistently indicating lower fatigue stress. The reason for this discrepancy is not clear.
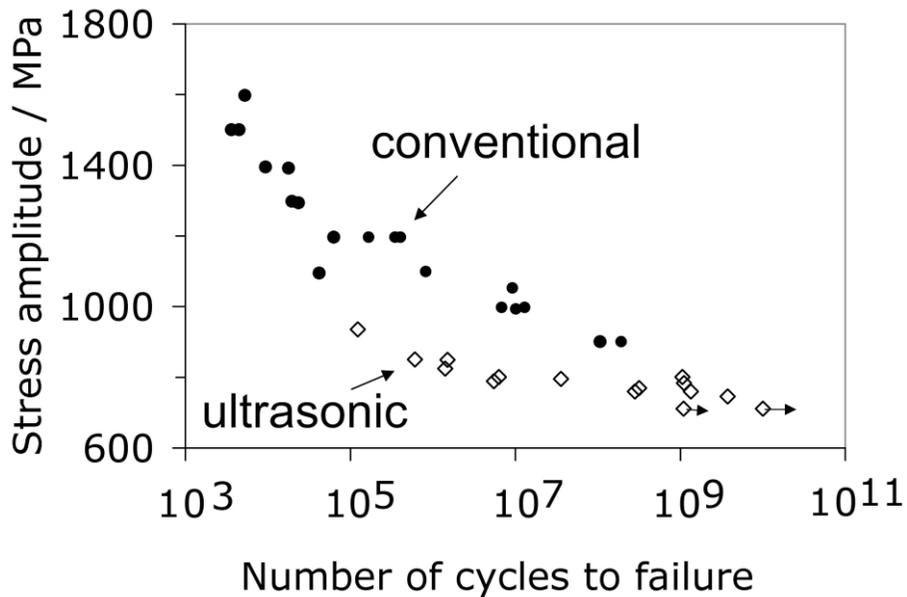
Figure 25 Comparison of conventional rotating bending and ultrasonic testing data for martensitic 52100 steel (Marines *et al.* 2003).

Fatigue property of bainitic 52100 steel has been investigated using ultrasonic testing method (Mayer *et al.* 2009). The bainitic microstructure was obtained by austenitizing at 850℃, then following isothermal holding at 220℃ for 20min first and 260℃ for 280min afterward. The resultant *S-N* curve is illustrated in Figure 26. Cracks initiated either at internal inclusions or at the surface at entire stress amplitude; internal crack initiation in about 1/3 and surface crack initiation in about 2/3.
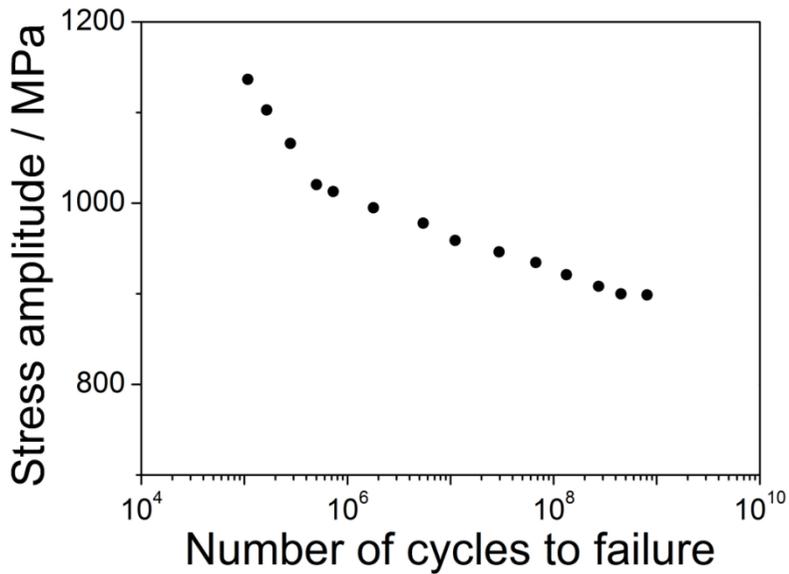
Figure 26: S-N curve of lower bainitic 52100 steel, austenitizing at 850℃ following isothermal holding at 220℃ for 20min (Mayer *et al.* 2009).

Figure 27 illustrates the reported fatigue properties of 52100 type steels in bainitic or martensitic conditions, which were commonly evaluated by ultrasonic testing at a frequency of 20 kHz (Bathias 2010, Marines *et al.* 2003, Mayer *et al.* 2009). The fatigue property of bainitic microstructure consistently indicates higher fatigue stress then that of martensitic.
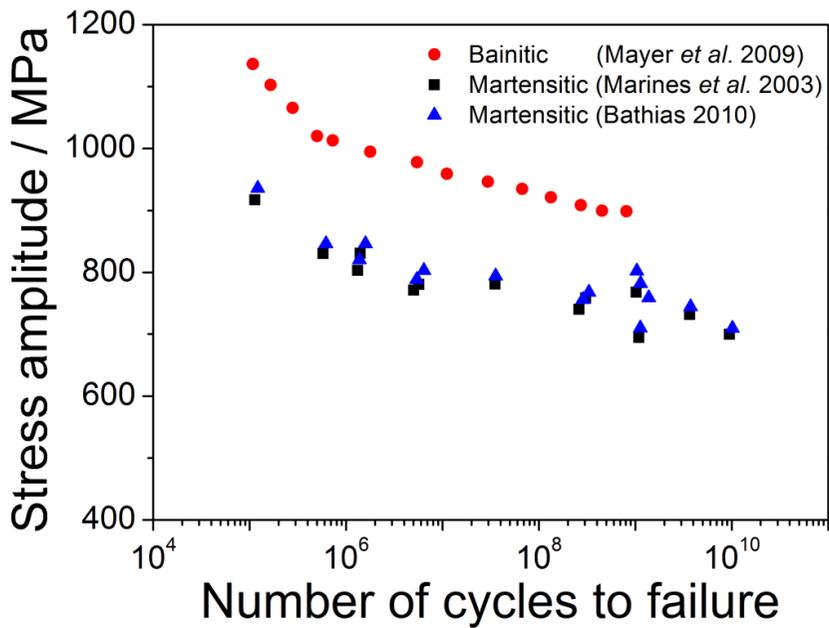
Figure 27: Reported fatigue properties of 52100 type steels in bainitic or martensitic conditions, which were commonly evaluated by ultrasonic testing. The data for the bainitic microstructure is the same as illustrated in Figure 26 (Bathias 2010, Marines *et al.* 2003, Mayer *et al.* 2009).

Chapter 3: Comparison of tempered martensite and lower bainite for SAE52100 bearing steel

3.1 Introduction

Conventional martensitic SAE52100 steel has been the most commonly used material for bearing applications. The hardened martensitic microstructure, by an appropriate quenching and tempering process, exhibits adequate mechanical properties, which satisfies the requirements for bearings (Burrier 1987). Lower bainitic microstructure was suggested as an alternative microstructure to replace martensite, since it showed an equivalent fatigue life to martensite under normal environments, and offers a superior fatigue life in water-containing environments (Hollox *et al.* 1981, Akbasoglue *et al.* 1990, Luzgivova 2007). However, bainitic bearing steels are not as popular in practice due to the higher cost for the extra duration of isothermal heat treatment. It takes about 240 min to complete bainite transformation for SAE52100 at 250℃ after austenitization at 850℃, whereas the maximum tempering time for tempered martensite is 120 min (Silva 2001, Sakanaka 2009). Furthermore, as the isothermal temperature is closer to martensite-start temperature (M_S), the isothermal holding time generally needs to be increased much more (Luzginova 2008).

However, most of studies for bainitic 52100 steel have been attempted without consideration about spheroidization. In high-carbon, chromium steel such as SAE52100, spheroidized cementite performs an important role in the acquisition of the required mechanical properties. It contributes to the enhancement of wear resistance and fatigue properties, and maintenance of alloy composition (Krauss 1980, Monma *et al.* 1998). Furthermore, the microstructure which consists of uniformly dispersed spheroidized cementite in ferrite matrix makes subsequent

forging process easy, by lowering the hardness level compared with the lamellar pearlite structure. Thus, spheroidization is an essential process for the manufacturing bearing steel.

In the present work, the bainite transformation of SAE52100 steel was attempted with a microstructure containing spheroidized cementite in a ferrite matrix. Then the resultant microstructure and hardness were compared with those of tempered martensite.

3.2 Experimental

Table 1: Alloy composition of SAE52100 (wt %).

Alloy	C	Mn	Si	Cr
SAE52100	1.0	0.35	0.25	1.4

Alloy composition of SAE52100 steel used in the present work is illustrated in Table 1. The spheroidization of the steel was performed using a tube furnace containing helium atmosphere before attempting any other heat treatment. The heat treatment for spheroidization was referred from the POSCO manufacturing process as illustrated in Figure 1. Thermodynamic calculations of the equilibrium phase fraction using ThermoCalc TCFE6 database confirm that 790℃ is just above A_1 temperature and 735℃ is just below as intended, Figure 2.
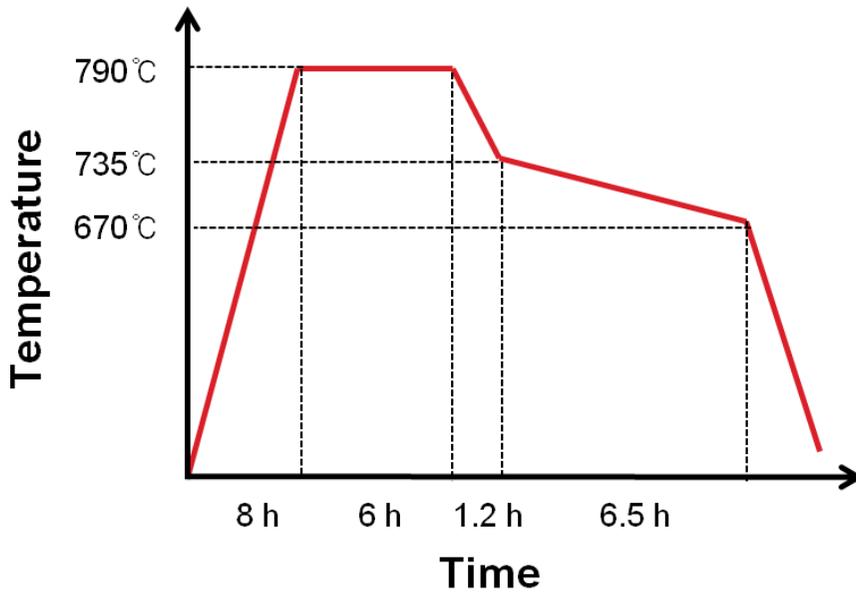
Figure 28: Spheroidization process for SAE52100 steel, referred from the POSCO manufacturing process.
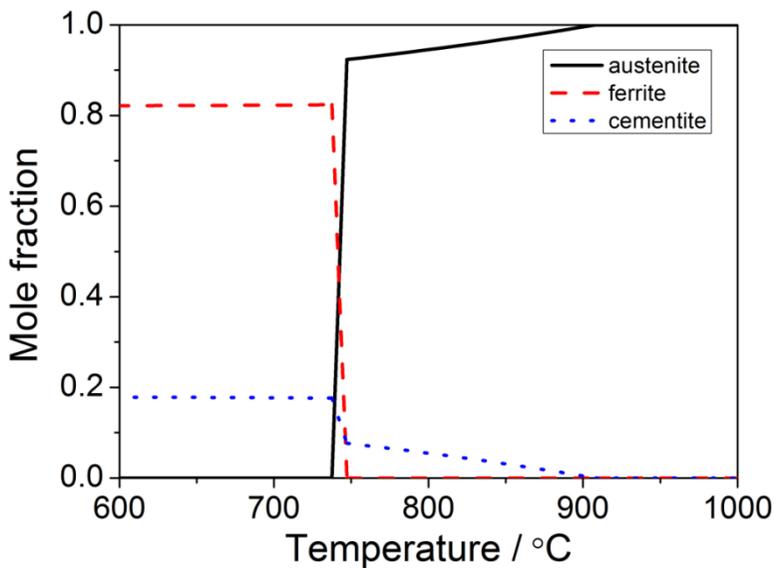
Figure 29: Equilibrium phase fraction of SAE52100 steel as a function of temperature, calculated by ThermoCalc TCFE6 database.

The spheroidized samples were machined and then heat treated in two ways; lower bainite evolves through isothermal transformation, while tempered martensite is generated by quenching from austenite, followed by isothermal tempering. These processes are illustrated in Figs 3 and 4 respectively, based on Sakanaka's research about axial-loading fatigue properties of bainitic SAE52100 steels (Sakanaka 2009). It is noted that the research did not include the spheroidization. In both processes, samples were commonly heated into the austenite-cementite two-phase region (850℃) rather than the full austenitic state in order to retain a certain amount of spheroidized cementite in the final microstructure.

Isothermal transformation for bainite was attempted at the fixed temperature (250℃) just above the martensite-start temperature to form lower bainite, and the progress of the transformation could be followed by attempting various heat-treatment times.

In the case of martensite, after rapid quenching to room temperature, the samples were tempered at three different temperatures (180℃, 230℃, and 250℃) for 120 min to see the effect of the tempering temperature on mechanical properties.
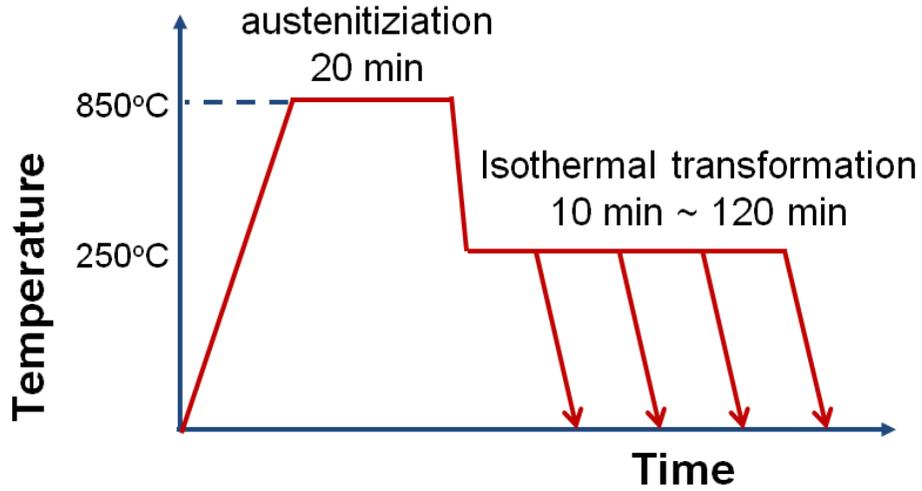
Figure 30: Heat treatment to obtain bainite in SAE52100 steel.
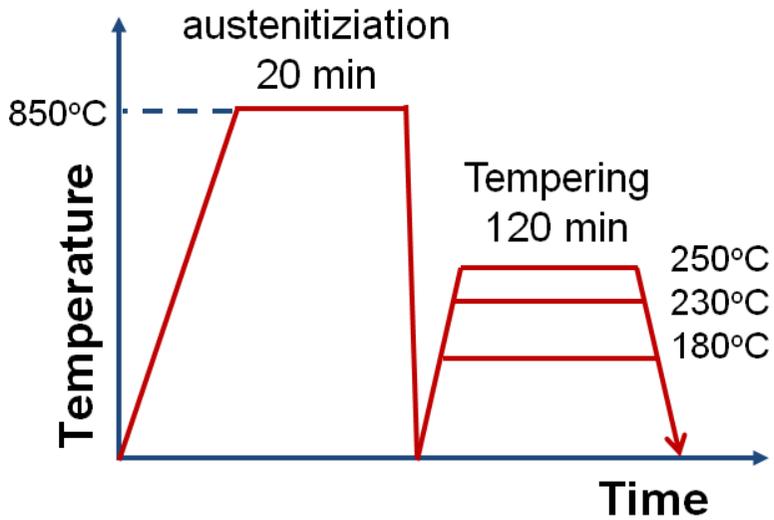
Figure 31: Heat treatment to obtain tempered martensite in SAE52100 steel.

To evaluate the suitability of the heat treatment processes, equilibrium phase fraction calculations using ThermoCalc TCFE6 database and transformation temperature measurements using dilatometry (BAHR DIL805) were exploited.

Calculated equilibrium phase fractions (Figure 2) indicate that at the temperature of 850℃, the steel is in the austenite-cementite two-phase region, where the equilibrium cementite fraction is about 0.03. However, the actual observed cementite fraction just after austenitization for 20 min is about 0.10, since it probably takes more than 20 min to arrive at the equilibrium state. This will be discussed in detail in a later chapter.

Dilatometry reveals that the martensite-start temperature following the 850℃ heat-treatment is about 210℃, as shown in Figure 5. Thus 250℃ seems to be a suitable temperature to obtain lower bainite by isothermal transformation. Furthermore, the reduction of the martensite-start temperature due to heat-treatment in the fully austenitic region (1100℃) confirms that cementite is retained after 20 min at 850℃. The dissolution of cementite between 850℃ to 1100℃ would increase the carbon concentration of austenite, thus reducing the martensite-start temperature.
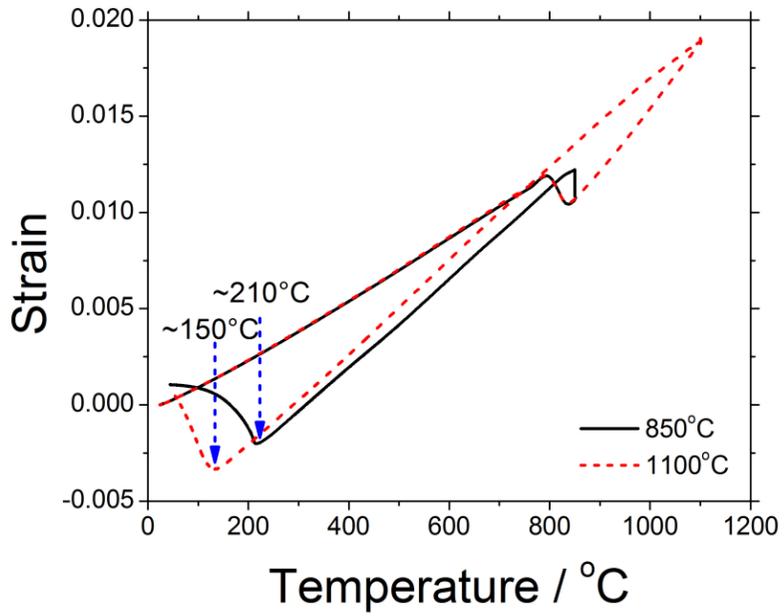
Figure 32: Martensite-start temperatures determined using dilatometry, after soaking at 850℃ and 1100℃ for 20 min.

3.3 Spheroidization

Figure 6 illustrates the observed microstructures using scanning electron microscopy (FE-SEM, Carl-Zeiss Ultra 55) before and after spheroidization. The pearlitic structure is changed into one containing spherical cementite particles in a ferrite matrix. Vickers hardness test using Wilson Wolpert 430/450-SVD system with a load of 1kg verifies decrease of hardness from 350 ± 6.0 HV to 175 ± 1.7 HV, Figure 7. The hardness values plotted represent the average of at least 5 test values.
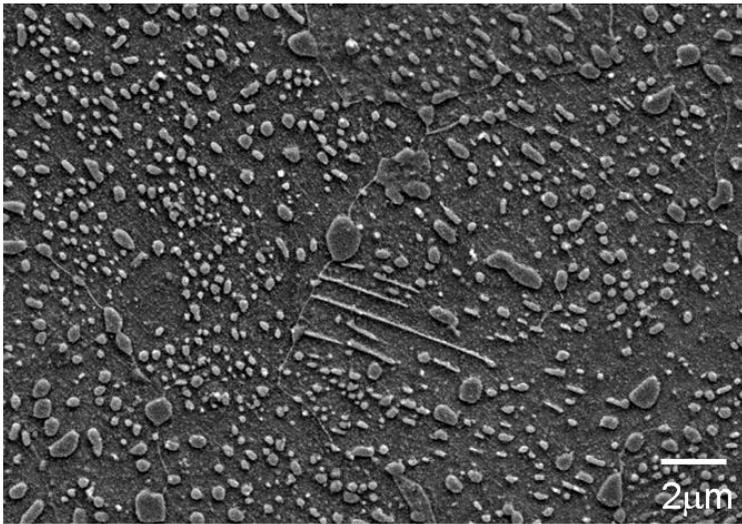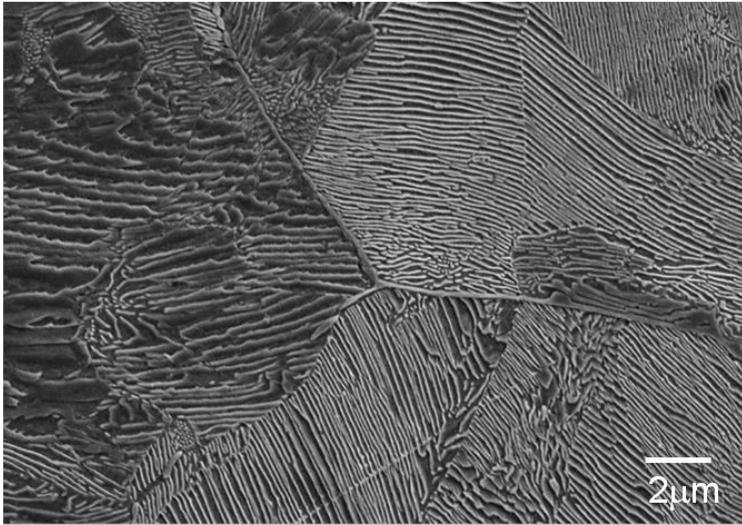
Figure 33: Microstructural change before (top) and after (bottom) spheroidization, observed by scanning electron microscopy (SEM).
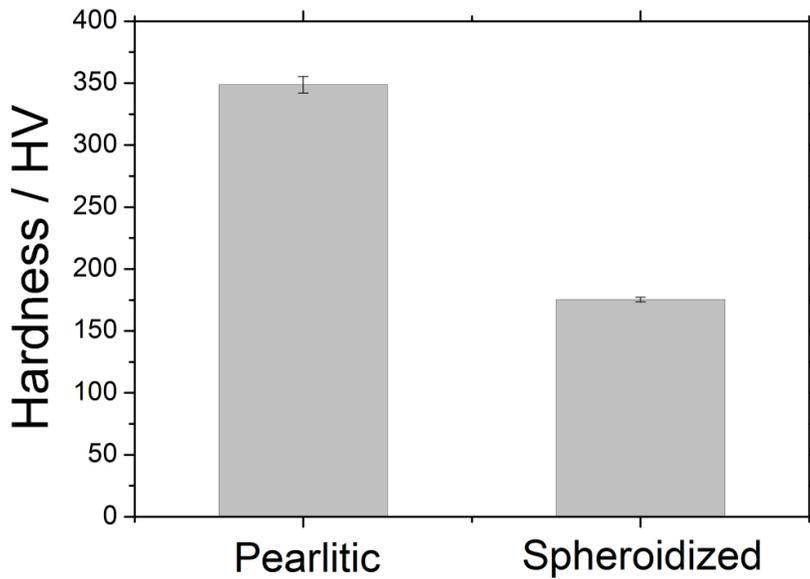
Figure 34: Hardness change through spheroidization.

3.4 Bainite transformation kinetics

To investigate the bainite transformation kinetics of SAE52100 steel, a variety of isothermal transformation periods were implemented using dilatometry, from 10 to 120 min. Then the strain measured was analyzed for investigating the transformation process. Microstructural observations were conducted on each sample using scanning electron microscopy (SEM).
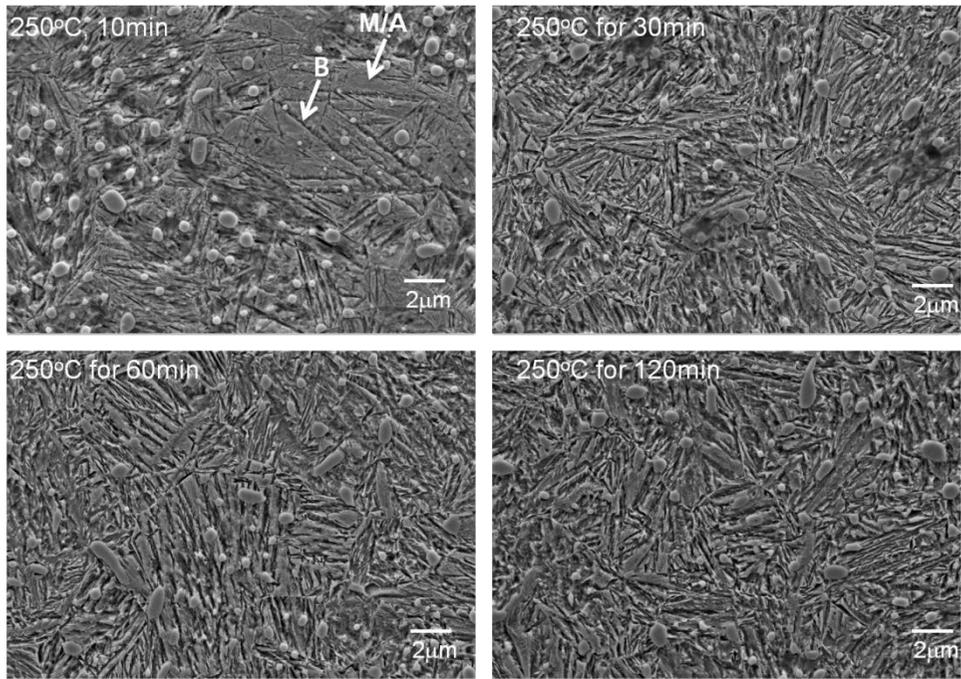
Figure 35: SEM images illustrating the microstructure as a function of isothermal transformation time. The specimens were austenitized at 850℃ for 20 min, and then transformed at 250℃.

The resultant microstructure after 10, 30, 60, and 120 min of change throughout isothermal transformation times are illustrated in Figure 8. The plate-shaped structure marked 'B' is considered to be bainite, and the neighboring plane structure marked 'M/A' is a mixture of martensite and retained austenite. The spherical cementite particles are consistently observed in all microstructure. Any changes in microstructure after 30 min of isothermal transformation became minimized. Thus bainite transformation is supposed to be almost completed in about 30 min.
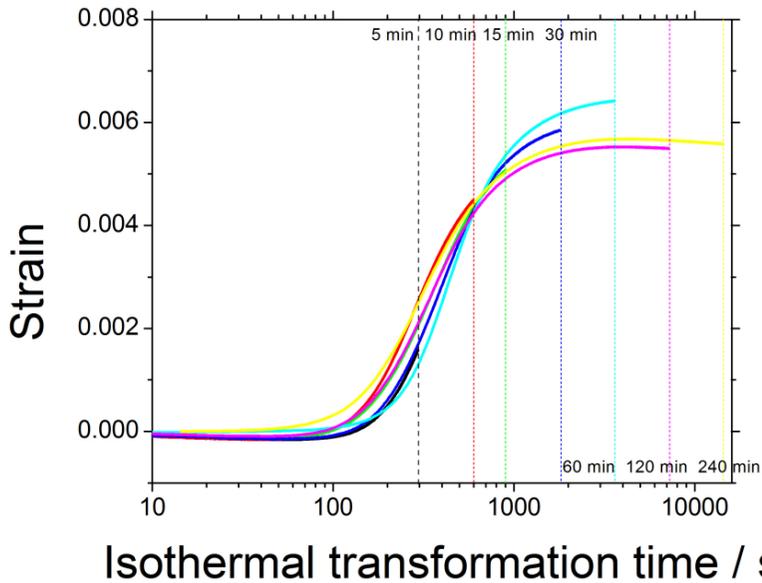
Figure 36: Strain during isothermal transformation at 250℃, measured using dilatometry.

Dilatometry also supports the interpretation of the SEM images. Strains of SAE52100 steels during transformation are presented as a function of time in Figure 9. Original dilatometry data of strain versus log scale time is arranged by fitting into the point where the isothermal transformation just started. The expansion of dilatometry specimen during transformation is mainly caused by the austenite to bainite transformation, so the bainite transformation kinetics can be understood by the degree of strain.

Bainite transformation initiates after about 100 s at 250℃. There seems to be a negligible length change after about 30 min at the transformation temperature, which is in agreement with the SEM observations.
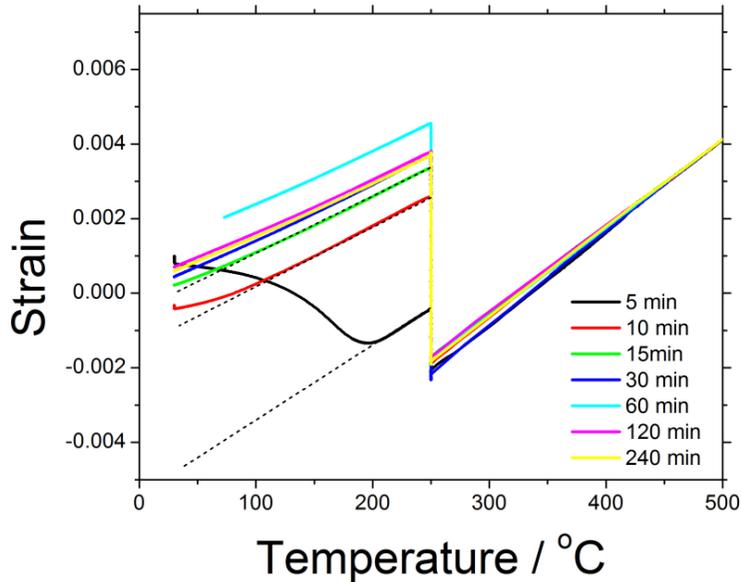
Figure 37: Strain during quenching to room temperature after isothermal transformation at 250℃ for a variety of time periods.

Another dilatometry result during cooling to room temperature after isothermal transformation also supports the interpretation about the bainite transformation kinetics, Figure 10. An expansion of the specimen, caused by the austenite to martensite transformation, is observed during quenching after 15 min at 250℃, whereas negligible expansion is observed following 30 min at 250℃. The stability of the austenite is less after the 15 min, since the amount of bainite formed is smaller than after the 30 min transformation. In the latter case, the bainite transformation is almost completed, so that the stability of austenite can be achieved by carbon partitioning. For that reason, the strain due to martensitic transformation

does not appear any more.

From the SEM observations and dilatometry results, it can be concluded that the bainite transformation of SAE52100 at 250℃ is initiated at about 100 s of isothermal transformation and almost completed in 30 min at temperature. It is much faster than reported in the literatures (Vetter *et al.* 2006, Sakanaka 2009). This is presumed to be an effect of the spheroidized cementite, and the phenomenon will be discussed in detail in Chapter 4.

3.5 Mechanical properties of bainitic SAE52100 versus martensitic

A tempered martensite microstructure was generated for comparison of mechanical properties using the heat treatment process illustrated in Figure 4. The resultant microstructure observed using SEM is shown as a function of the tempering temperature in Figure 11. The changes to the quenched microstructure increase naturally as the tempering temperature is raised. Proeutectoid spheroidized cementite is observed in every tempering condition, and the maximum size is about 2 μm as in the bainitic microstructure.
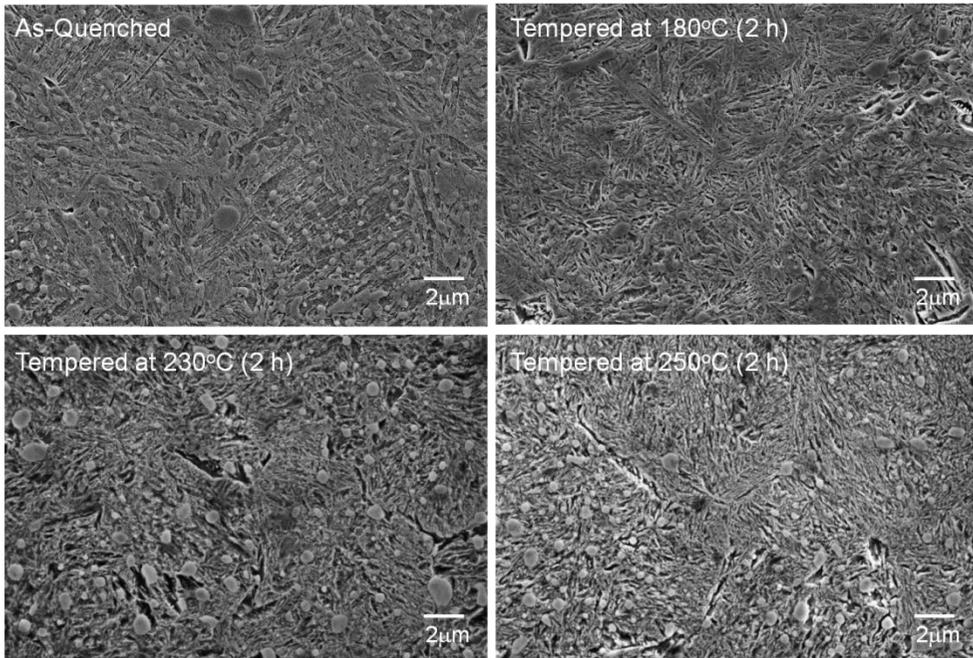
Figure 38: SEM images illustrating the microstructure following quenching and tempering. The specimen were austenitized at 850℃ for 20 min, quenched to room temperature, and then tempered at 180℃, 230℃, and 250℃ for 2 h.
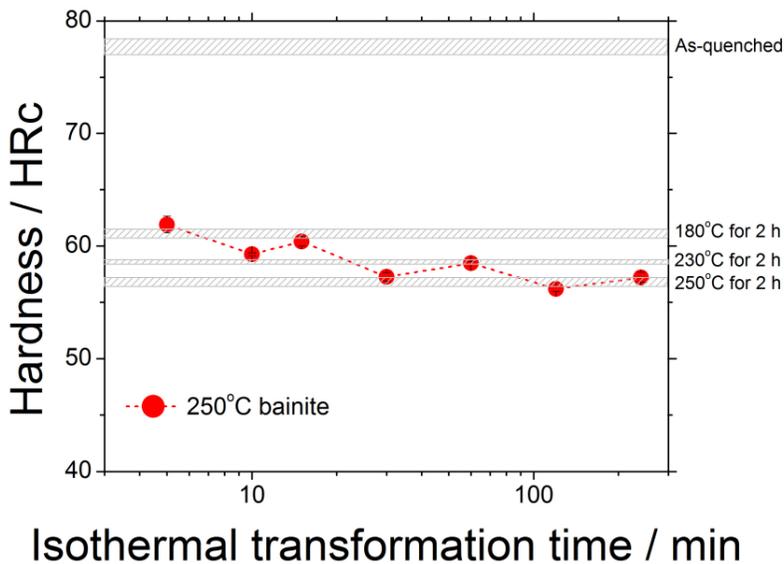
Figure 39: Rockwell hardness data for bainitic SAE52100 steel as a function of isothermal transformation time, and martensitic SAE52100 steel as a function of tempering temperature. The hardness of martensite for as-quenched, tempered at 180℃, 230℃, and 250℃ conditions are 78±0.67 HRc, 61±0.41 HRc, 59±0.24 HRc, and 57±0.41HRc, respectively.

Rockwell hardness data following tempering are represented in Figure 12, measured using a Mitutoyo HR-522 hardness testing system with a load of 1 kg. Corresponding values for the bainitic microstructure are listed as a function of the isothermal transformation time, while values for martensitic are separately marked with horizontal lines through the tempering temperature. As expected, the hardness of the martensitic structure decreased as tempering temperature increased, and that of the bainitic decreased with transformation time. At early stages of isothermal transformation, a certain amount of martensite forms as cooling to room temperature is also included in the microstructure with bainite and spheroidized

cementite. Thus, the hardness of the early stage of bainite evolution is relatively high. The hardness value of the fully bainitic microstructure, supposed to be the values after 30 min of transformation, shows a similar level to that of martensite tempered at 250℃. However, the value is lower than the hardness of martensite tempered at 230℃ and 180℃.

To examine the development of hardness of the bainitic structure, a lower transformation temperature was attempted. Bainite is known to be harder when transformation at a lower temperature due to the refinement of the bainite plates, although the time required to the initiate bainite reaction becomes longer (Caballero *et al.* 2002, Garcia-Mateo *et al.* 2003, Caballero *et al.* 2004). In that context, SAE52100 steel was therefore transformed at 230℃ to check the extent of hardness increase and any delay in transformation time. Figs 13 and 14 show the dilatometry results. Bainite is delayed a little compared with transformation at 250℃, resulting completion between 30 to 60 min. Hardness test result for the 230℃ experiments are represented with previous data in Figure 15. The result shows a similar tendency to the 250℃ data, but enhanced hardness for all transformation times. Indeed, the hardness exceeds that of martensitic tempered at 180℃. Thus, it can be concluded that a judicious decrease of isothermal transformation temperature can contribute to the enhancement of bainite hardness in SAE52100 steel without an intolerable particular delay in isothermal transformation kinetics.
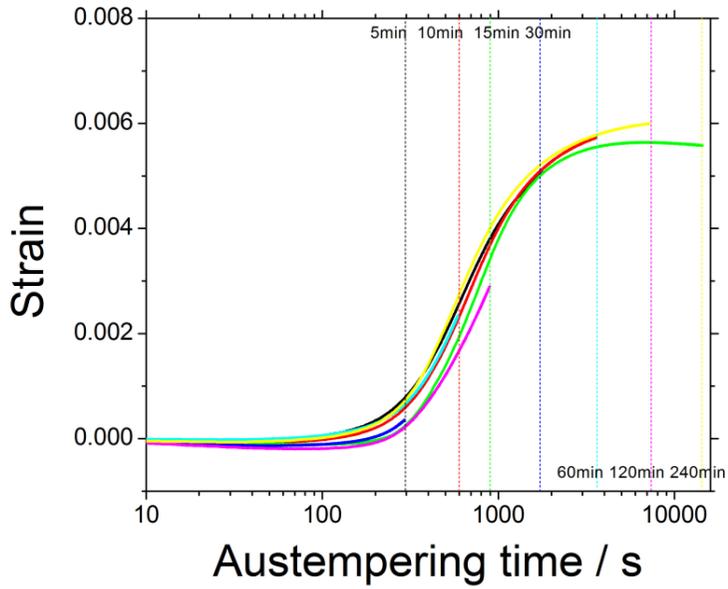
Figure 40: Strain during isothermal transformation at 230℃, measured using dilatometry.
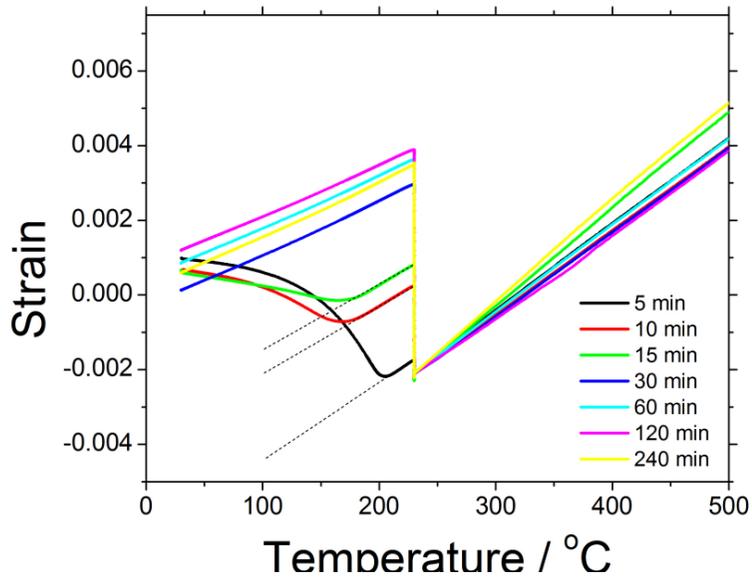
Figure 41: Strain during quenching to room temperature after isothermal transformation at 230℃ for a variety of time periods.
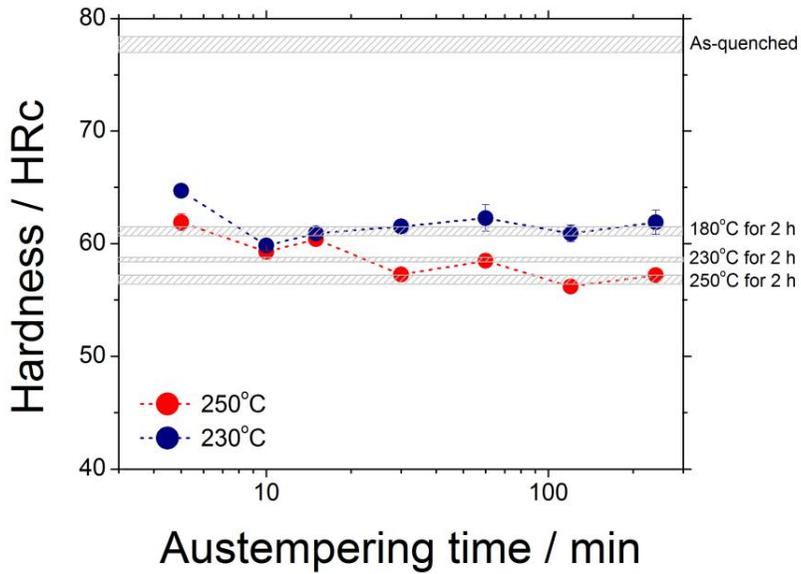
Figure 42: Rockwell hardness data for bainitic SAE52100 steel as a function of isothermal transformation time, and martensitic SAE52100 steel as a function of tempering temperature. The data for martensite and bainite at 250℃ transformation is the same as illustrated in Figure 12.

3.6 Summary

SAE52100 bearing steel was heat-treated to generate lower bainite instead of the traditional tempered martensite, with a microstructure containing spheroidized cementite in a ferrite matrix as an initial state. Bainite transformation could be completed in 30 min at 250℃, which is much faster than previous studies based on a non-spheroidized starting structures. Fully bainitic SAE52100 steel showed a similar hardness level compared with martensite at the same transformation temperature. Moreover, an enhancement of hardness could be achieved by lowering the isothermal temperature to 230℃, without retardation of transformation kinetics.

Chapter 4: Effect of alloying elements on bainite transformation kinetics of SAE52100

4.1 Introduction

It has been discussed in the previous chapter that a fully bainitic microstructure can be obtained by austempering at 250℃ for 30 min using the SAE52100 alloy. The hardness of that microstructure was comparable to that of martensite tempered at same temperature for 2 h.

A lower bainitic microstructure can also have sufficient hardness for bearing manufacture but only by transformation at low temperature, where the time required to complete transformation is prolonged (Caballero *et al.* 2002, Garicia-Mateo *et al.* 2003, Caballero *et al.* 2004). The long-time heat treatment means a decrease in productivity and increase in cost. So the acceleration of bainite transformation kinetics is an important issue for the exploitation of bainitic steels. It is known that bainite kinetics can be accelerated by changing the alloy composition. The addition of Al and Co can accelerate the transformation kinetics by increasing the free energy change accompanying transformation of austenite to ferrite (Garicia-Mateo *et al.* 2003). Cr is the alloying element which can increase the hardenability and hence retards the formation of bainite (Bhadeshia 2001). Thus, a reduction of Cr can also accelerate the bainite transformation.

To understand the effect of various solutes on the acceleration of bainite, several alloys were designed beginning with the SAE52100 base alloy. The kinetics data were then measured and compared against SAE52100. The main purpose of the work presented in this chapter was, therefore, to verify the role of solutes on reaction kinetics in the context of lower bainite.

4.2 Alloy design and experimental

Table 2 : Alloy compositions (wt%)

Alloy	C	Mn	Si	Cr	Al	Co
B1	1.0	0.35	0.25	1.4		
B2	1.0	0.35	1.25	1.4		
B3	1.0	0.35	0.25	1.0		
B4	1.0	0.35	0.25	1.4	1.0	
B5	1.0	0.35	0.25	1.4		1.5

Several alloys were designed as shown in Table 1. B1 is the SAE52100 base alloy. B2 has Si added for the purpose of another study aimed at improving the spheroidization process (Kim *et al.*, 2010). The effect of Si on the acceleration of bainite transformation has not been reported clearly. Nevertheless, a Si added alloy is included in this study, since it is known to have a similar role with Al on the bainite transformation (Etienne *et al.* 2001, Kiani-Rashid 2004). B3 is the Cr reduced alloy, with consequently reduced hardenability. B4 and B5 are Al and Co added alloys, respectively. They are designed to accelerate bainite transformation by increasing free energy difference between austenite and ferrite.
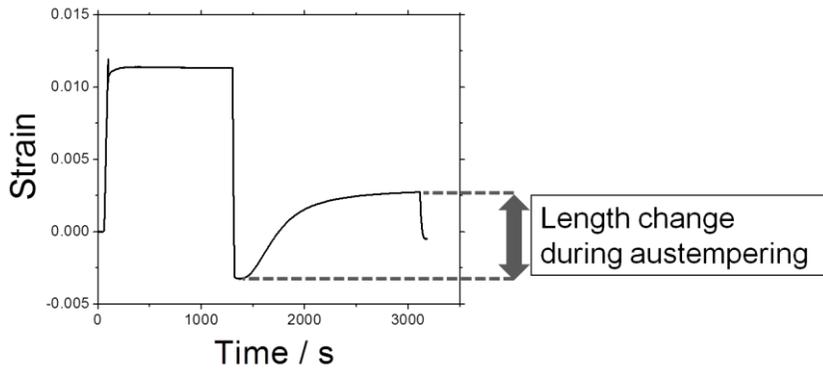
Figure 43: General dilatometer curve for bainite transformation of SAE52100 based alloys. SAE52100 alloy austenitized at 850℃ for 20 min, austempered at 250℃ for 30 min.

The reaction rates were evaluated using dilatometry. During the bainite transformation, the volume of specimen is increased as austenite transformed into bainite. The resulting volume change of the specimen can be observed as a length change of specimen by dilatometer. Thus, the length change during austempering is approximately proportional to the amount of transformed bainite. Figure 1 shows general form of the dilatometer curve for SAE52100 based alloys, in which the strain is illustrated as a function of time. The length change attributed to the bainite transformation is marked on the figure. The data are fitted into the point where the austempering heat treatment just started, and then the bainite transformation kinetics of the different alloy are compared.

4.3 Spheroidization process

Spheroidization process of SAE52100 (B1) was introduced in previous chapter. Based on that heat treatment process, the highest soaking temperature for the segmentation of the cementite lamellar structure was related to the change in the A_1 temperature for each alloy. For example, A_1 temperature of B2 alloy is increased by the addition of Si, which is a ferrite stabilizing element. So, B2 must be heat treated at a higher temperature for the segmentation of cementite lamellae compared with B1. Thus, 810℃ was applied for spheroidization of B2 instead of 790℃ of B1. The A_1 temperature of each alloy was calculated using ThermoCalc TCFE6 database (Figure 2). As a result, B3 and B5 was heat treated at 790℃ (same as B1), while B2 and B4 were heat treated at 810℃.

The change in microstructure before and after spheroidization were observed using scanning electron microscopy, and illustrated in Figure 3. The lamellar structure of pearlite is transformed into spheroidized cementite in a ferrite matrix as intended. Hardness is reduced about 50% to 67% that of a pearlite structure (Figure 4). The cementite fraction after spheroidization was measured by a point counting method using SEM images. B5 was containing about 0.20 of cementite, while other alloys were containing about 0.15±0.002 to 0.17±0.017. The detailed results are shown in Table 2.
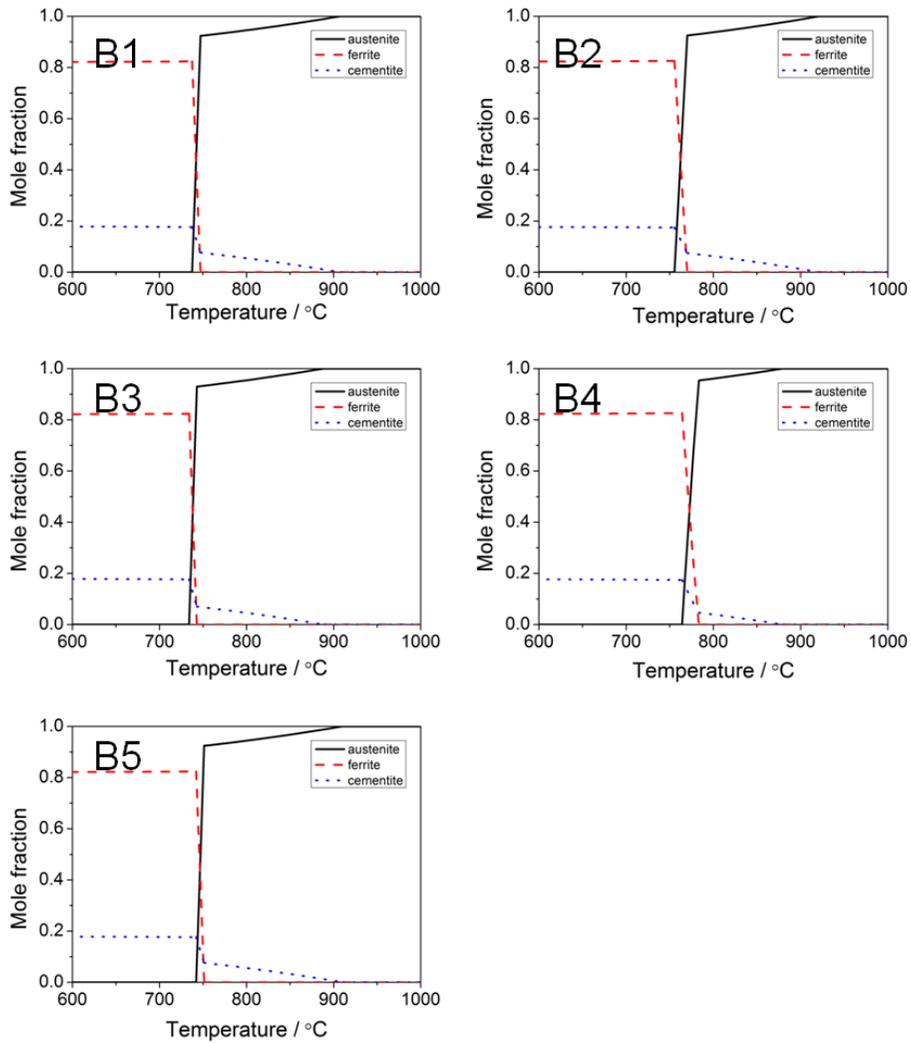
Figure 44 : Calculated equilibrium phase fractions using ThermoCalc TCFE6 database.
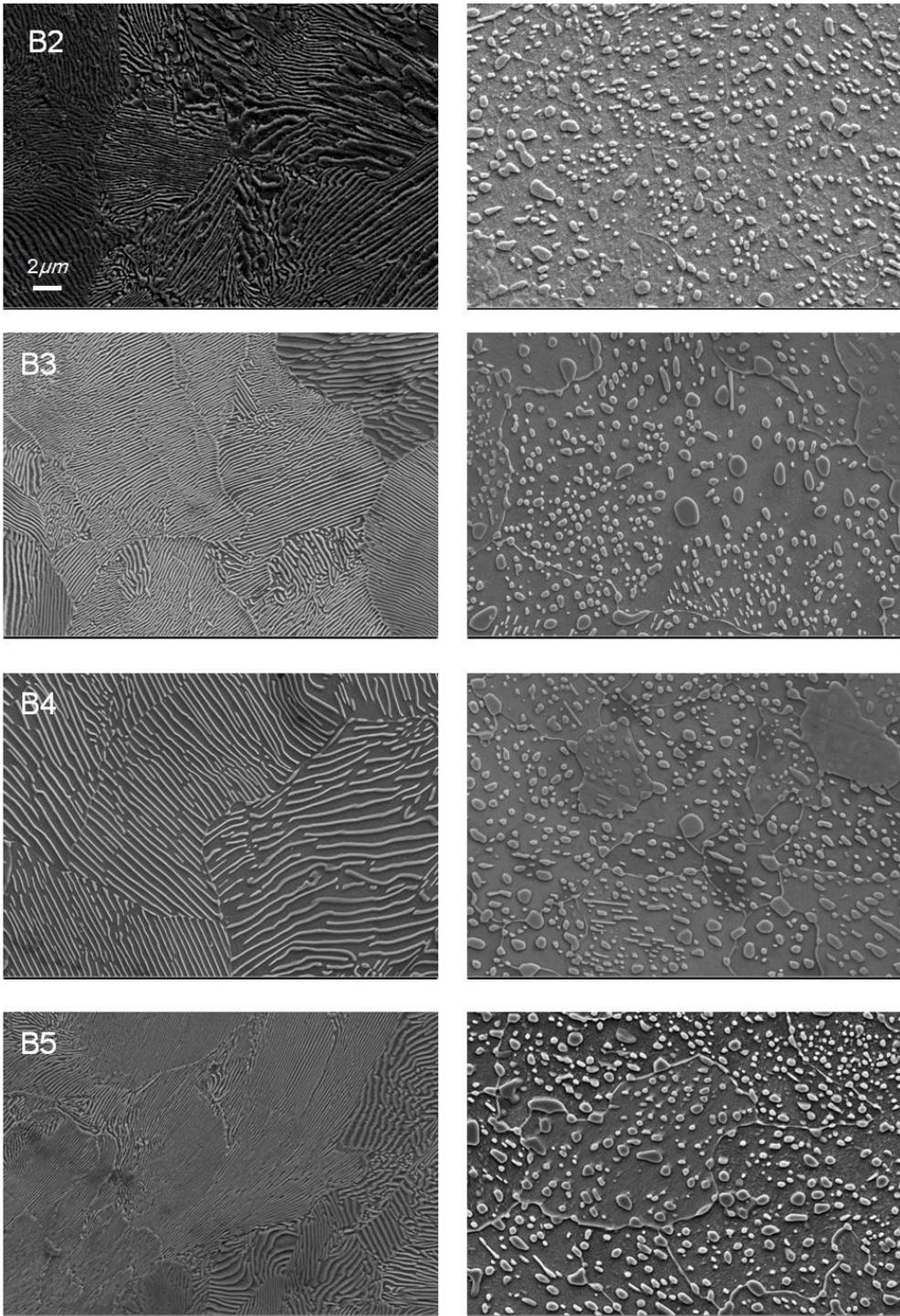
Figure 45: SEM images of microstructures before and after spheroidization.
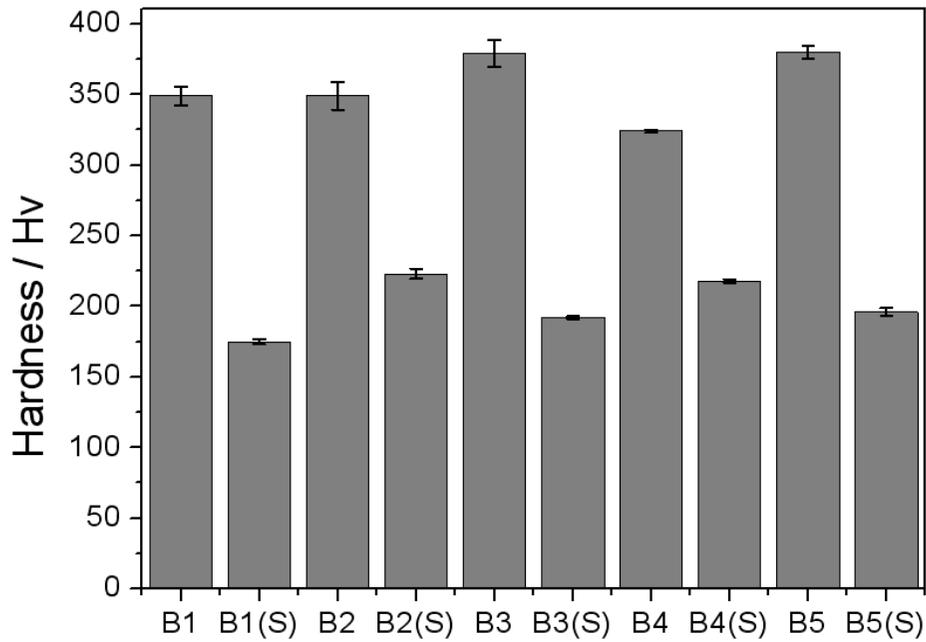
Figure 46: Hardness before and after spheroidization.

Table 2 : Details of hardness decrease and cementite fraction after spheroidization.

Alloys	Hardness (pearlite) [HV]	Hardness (spheroidization) [HV]	Hardness ratio (spheroidized/pearlite) [%]	Cementite fraction
B1	349±6.7	175±1.9	50	0.17±0.020
B2	349±9.8	223±3.6	64	0.15±0.002
B3	379±9.6	192±1.2	51	0.17±0.007
B4	324±1.0	218±1.2	67	0.16±0.005
B5	380±4.6	196±2.6	52	0.20±0.010

4.4 Bainite transformation kinetics of designed alloys

Bainite transformation kinetics were observed for each alloy using the method adopted for SAE52100, described in the previous chapter. Spheroidized specimen of each alloy was austenitized at 850℃ for 20 min, and then austempered at 250℃ for 2 h using dilatometry. Dilatometric data during austempering were measured to evaluate the kinetics. The microstructural changes as a function of time were observed using SEM.
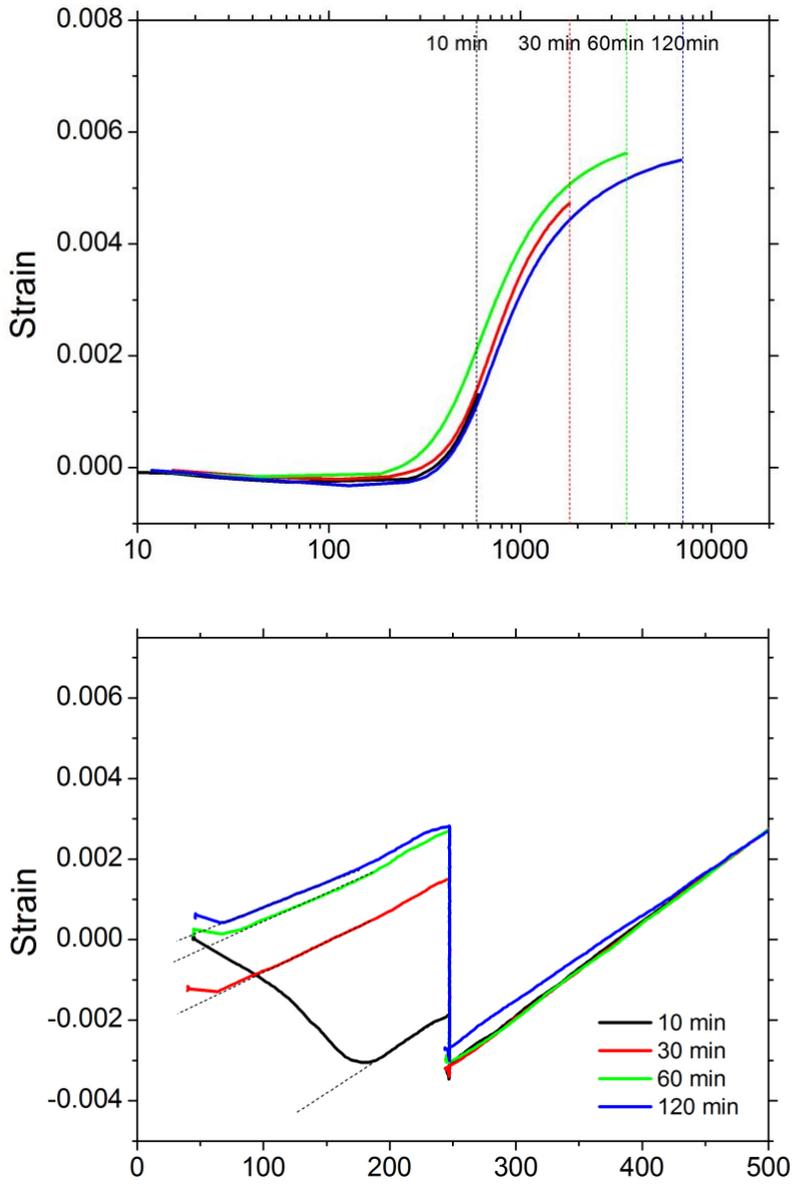
Figure 47: Bainite transformation kinetics of B2 specimen upon austempering at 250℃.
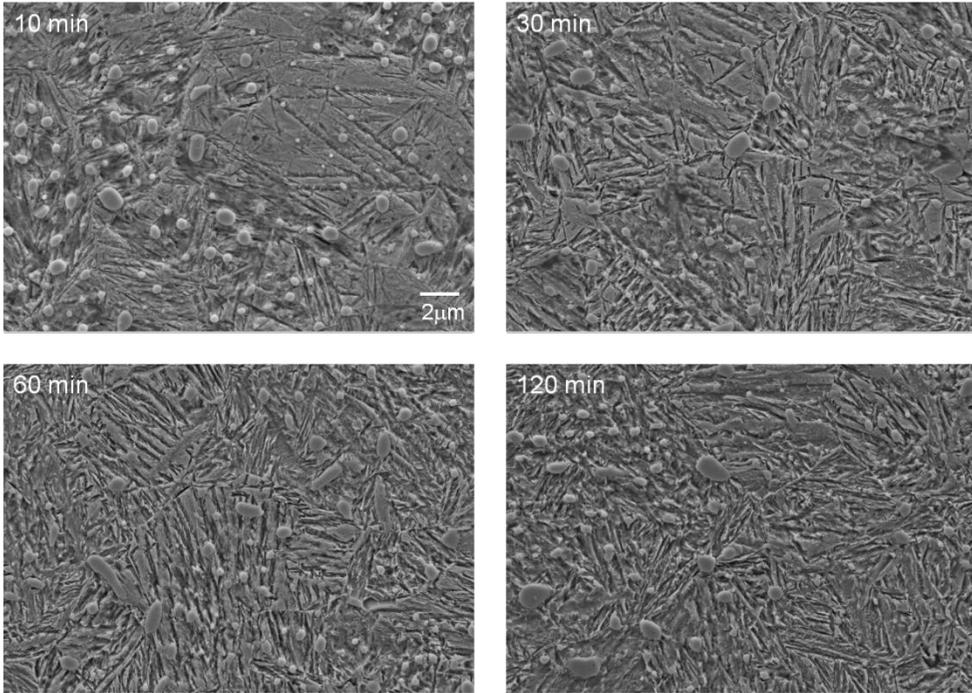
Figure 48: Microstructure of B2.
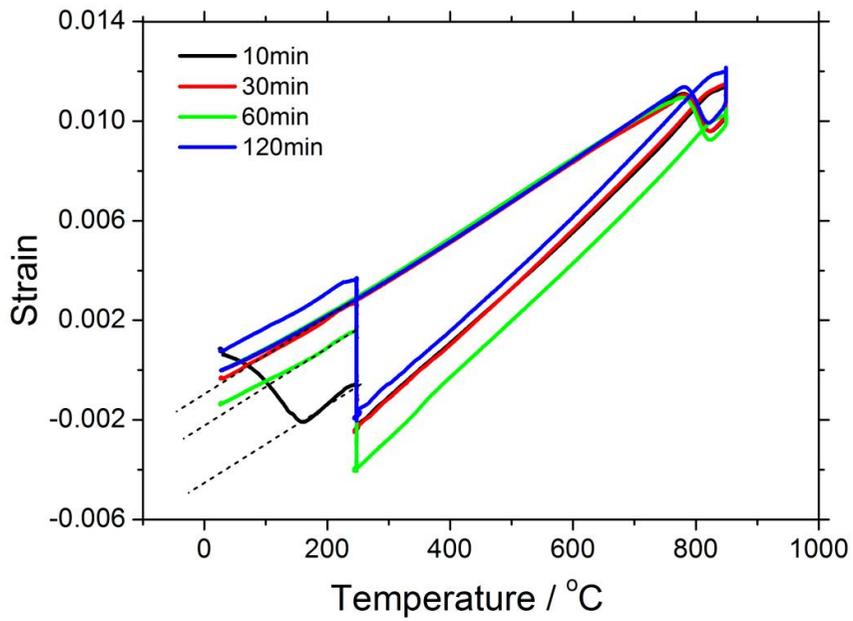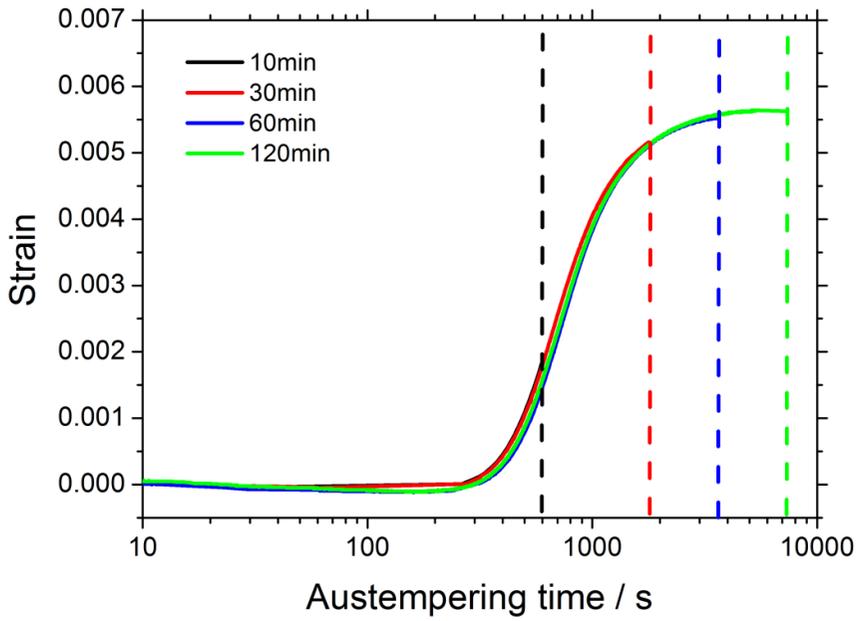
Figure 49: Bainite transformation kinetics of B3 specimen upon austempering at 250℃.
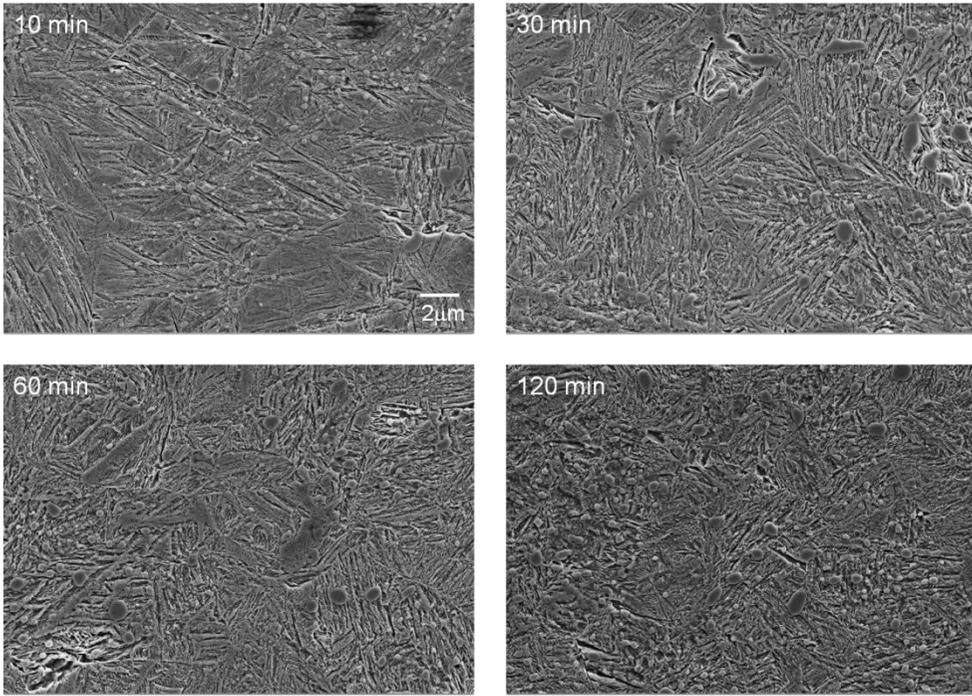
Figure 50: Microstructure of B3.
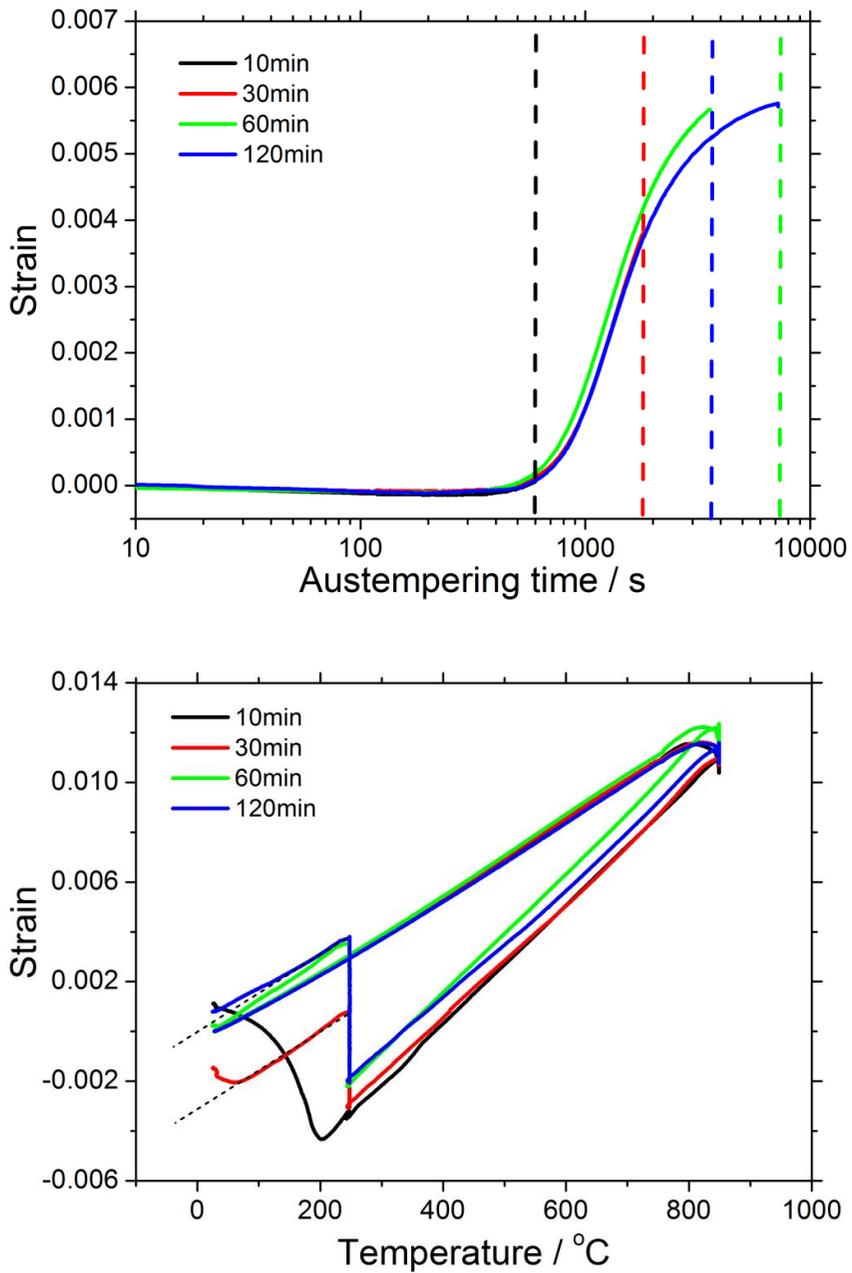
Figure 51: Bainite transformation kinetics of B4 specimen upon austempering at 250℃.
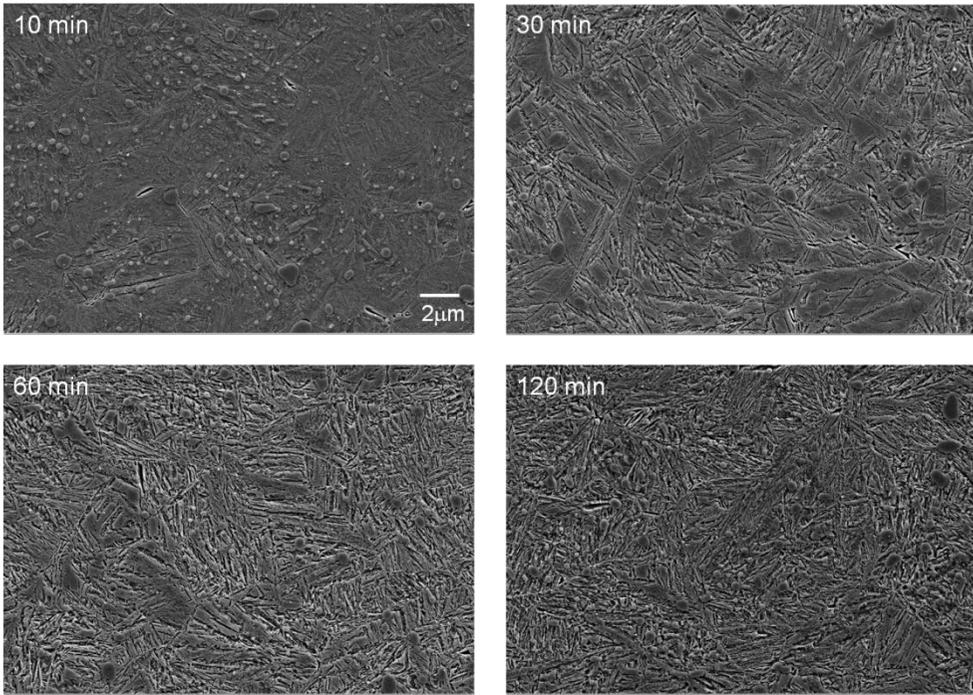
Figure 52: Microstructure of B4.
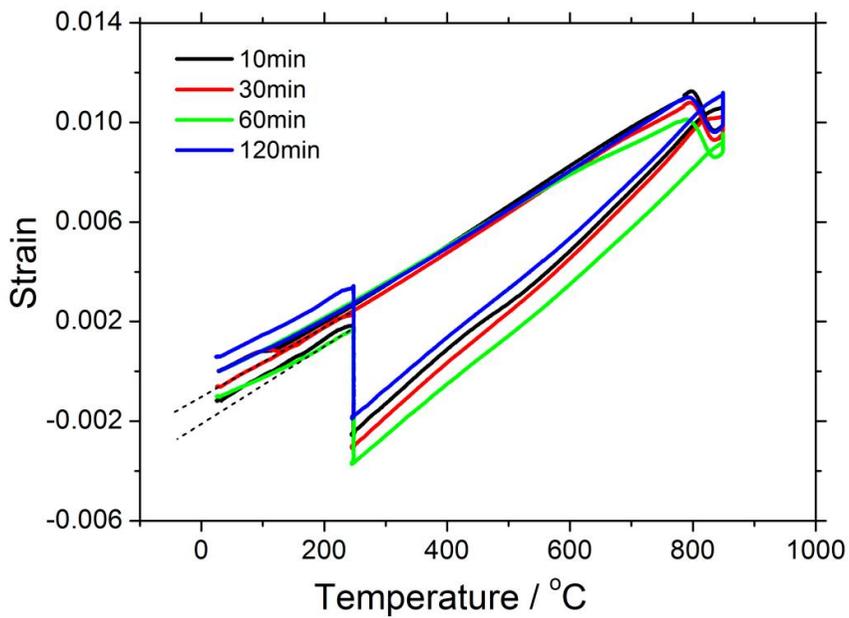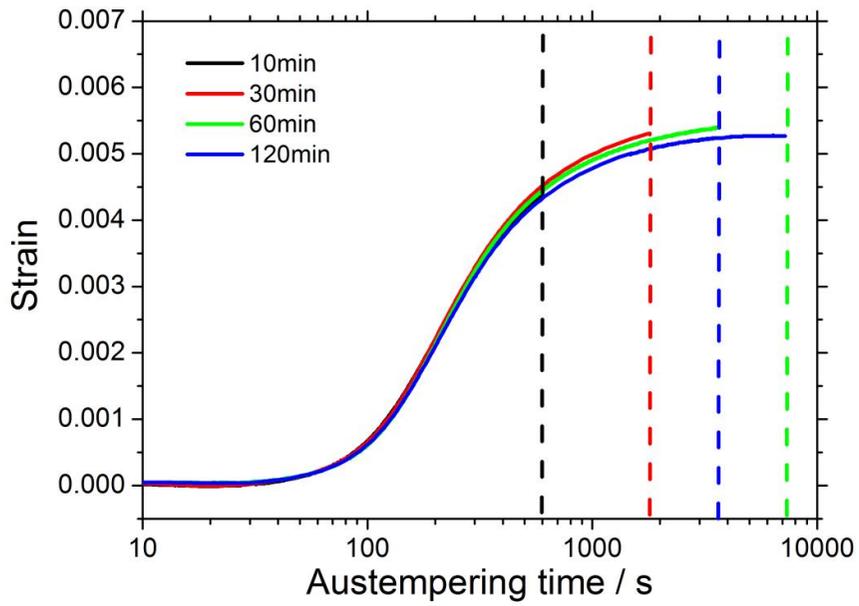
Figure 53: Bainite transformation kinetics of B5 specimen upon austempering at 250℃.
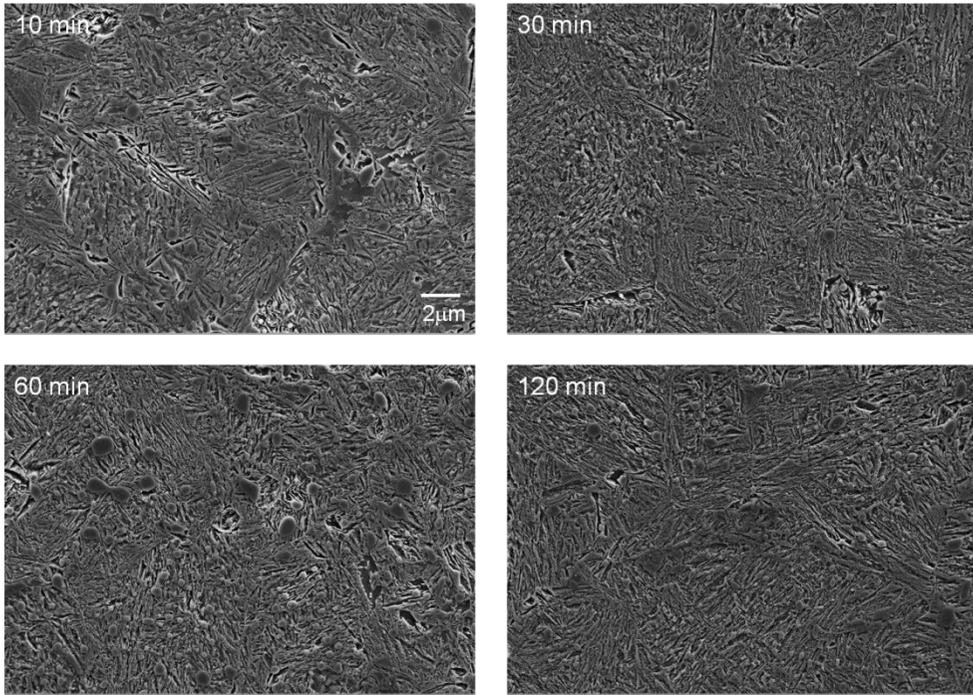
Figure 54: Microstructure of B5.

The dilatometric data and SEM images during bainite transformation are illustrated in Figs 5 to 12. The bainite completion times of each alloy can be inferred from the temperature-strain data. The expansions of specimens during cooling to room temperature were observed for the short austempering time conditions, and they indicated martensitic transformation of residual austenite after incomplete transformation of bainite. Thus, the time, when the expansion due to martensite is not observed, can be deduced as bainite completion time of each alloy. In the case of B2, the expansion of specimen during cooling to room temperature is observed even after 120 min of austempering, which means bainite transformation is not completed. In the case of B3 and B4, bainite transformation of each alloy seems to be completed in about 60 min of austempering. In the case of B5, the transformation progresses faster than other alloys. An appreciable amount of bainite

is already transformed even in 10 min of austempering in B5, and the reaction is completed in about 30 min. SEM images upon austempering time are also supporting the transformation process. The amount of bainite structure which is observed to consist of long sheaves in each image is naturally increased with the austempering time. And then, the microstructure seems not to change after some time, which agrees with the dilatometry data.
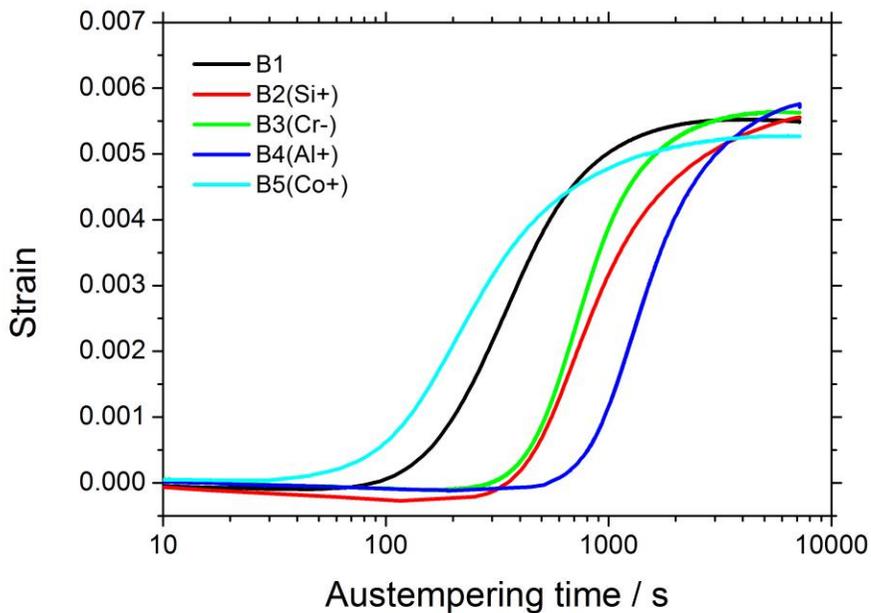
Figure 55: Overall bainite transformation kinetics upon austenitizing at 850℃ and austempering at 250℃.

The overall bainite transformation kinetics of the designed alloys are illustrated in Figure 13, with all the dilatometric data fitted to an origin corresponding to austempering process. From the result, only the Co added B5 alloy shows faster bainite transformation kinetics compared to SAE52100 (B1), while the other alloys exhibit delayed kinetics contrary to expectations.

4.5 Analytical approach to delayed transformation kinetics

The effect of cementite was considered in order to determine the reason for the unexpected delayed transformation kinetics. The bainite kinetics are strongly influenced by the chemical composition of austenite at the point that it reaches the isothermal transformation temperature. The influence of carbon is stronger than any of the other elements. In this study, certain amount of proeutectoid cementite is retained even after austenitizing process, instead of full austenitization. As shown in Figure 2, it is necessary to heat up above 900℃ to obtain a fully austenitic microstructure in the designed alloys, but austenitization was done at 850℃ in order to retain cementite. The purpose of the retained cementite in a bearing steel is generally to secure the wear resistance of the final bearing application (Hollox *et al.* 1981, Luzginova *et al.* 2007). However, the effect of alloying elements on the cementite dissolution behavior was not considered for the austenitization condition at 850℃. A change in solute concentration can affect not only the bainite kinetics but also cementite dissolution rates during austenitization. Thus, cementite fraction after austenitization may vary depending on alloy composition. Hence, the carbon concentration of the austenite that transforms into bainite may vary. That is, the overall bainite transformation kinetics illustrated in Figure 13 may be influenced strongly by the carbon concentration in solution within the austenite.
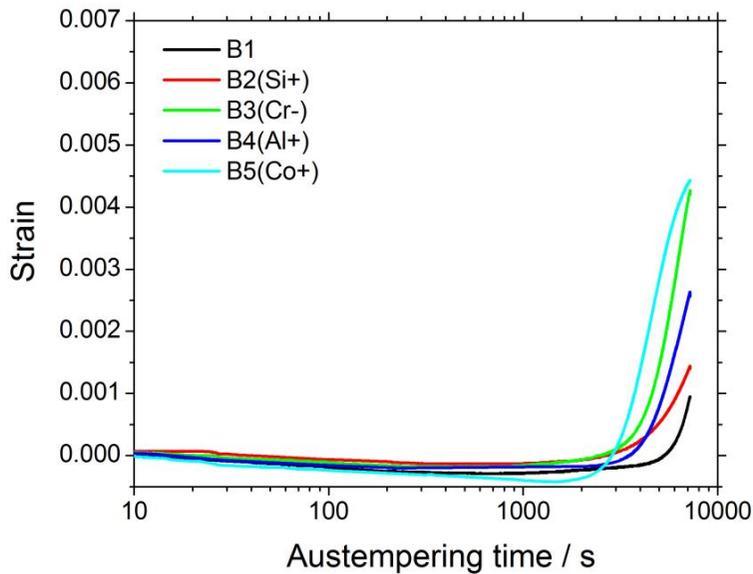
Figure 56: Overall bainite transformation kinetics upon austenitizing at 1100℃ and austempering at 250℃.

Several experimental approaches have been conducted to support that assumption. First of all, the designed alloys were all austenitized at 1100℃ which is in the fully austenitic phase field, and then austempered at 250℃. All the spheroidized cementite could be dissolved during austenitizing at that temperature. Then the effect of alloying elements (Si, Cr, Al and Co) on the bainite transformation could be checked without interference of cementite uninfluenced carbon concentration of austenite, since the concentration would then be same in all alloys. The overall bainite transformation kinetics are illustrated in Figure 14. Even though the bainite was delayed compared to austenitizing at 850℃, the effect of alloying elements on the acceleration of bainite transformation could be confirmed. Obviously, all the designed alloys showed faster initiation and progress of bainite transformation than B1. The result confirms that the unexpected transformation delay illustrated in Figure 13 is caused by carbon concentration variations in the austenite.

Table 3 : Measured martensite-start temperatures after austenitizing at 850℃ (M_S_850) and 1100℃ (M_S_850), and the gaps of them (M_S_850-M_S_1100).

	B1	B2	B3	B4	B5
M_S_850 (℃)	235	205	207	214	244
M_S_1100(℃)	146	140	161	165	168
M_S_850- M_S_1100(℃)	89	65	46	49	76

$$M_S(℃) = 539 - 423(\%C) - 30.4(\%Mn) - 17.7(\%Ni)$$
$$- 12.1(\%Cr) - 7.5(\%Mo)$$

(4-1)

Another experiment was designed to check the effect of differences in the carbon concentration in austenite on the transformation behavior. Using dilatometer the specimens of the designed-alloys were austenitized at 1100℃ and 850℃, and then rapidly quenched into room temperature to check their martensite-start temperatures. Then the gap between the martensite-start temperatures between 1100℃ and 850℃ were calculated for each alloy. The carbon concentration in austenite just after each austenitization would differ because of undissolved cementite at 850℃ austenitization condition. The martensite-start temperature is known to be strongly affected by the carbon concentration of austenite, more than other alloying elements (Equation 4-1) (Bhadeshia 1981). Hence the gap should be related with the amount of carbon which existed in undissolved cementite at 850℃. The calculation results are shown in Table 3. Comparing the gaps (M_S_850- M_S_1100), all designed alloys show lower values than B1. That is, the alloys have lower cementite fraction than B1 just after austenitization at 850℃. Hence, they have higher carbon concentration in austenite, by which the unintended delay of bainite transformation happened.

In conclusion, the effect of carbon on bainite transformation kinetics was more dominant than any other alloying elements such as Si, Cr, Al and Co. Therefore, an

unintended delay of bainite transformation kinetics happened as Figure 13, even though the alloying elements were expected to accelerate the transformation. It is necessary to control the carbon concentration of austenite in advance, to accelerate the bainite transformation by changing alloying elements. For that, the spheroidized cementite fraction should be controlled to be fixed, and that work can easily be implemented by changing the austenitization time and temperature.

4.6 Summary

The slow transformation kinetics of bainite in bearing steels are can in principle be improved by changing the chemical composition. Based on this, the acceleration of bainite in SAE52100 has been attempted by changing the concentration of Si, Cr, Al and Co. However, the transformation kinetics of most of the designed alloys were delayed, with the exception of Co added alloy for constant heat treatment conditions. It was determined that this is because of the difference in carbon concentration in austenite caused by corresponding variations in the quantity of proeutectoid cementite. Therefore, the carbon concentration of austenite should be controlled in advance to accelerate bainite transformation of SAE52100 by changing alloying elements. For the work, an understanding about cementite dissolution during austenitization is necessary.

Chapter 5: Dissolution of spheroidized cementite during austenitization

5.1 Introduction

It has been demonstrated in the previous chapter that the carbon concentration in austenite needs to be controlled in order to realize the influence of substitutional solutes on the rate of the bainite transformation in modified bearing steels. Since proeutectoid cementite is present in the microstructure, there is a close correspondence between carbon concentration in austenite and the amount of cementite. The spheroidized cementite comes from the divorced pearlite during the transformation of austenite during cooling, and is redissolved during the austenitizing process as discussed in Chapter 3 (Verhoeven *et al*. 1998, Verhoeven 2000, Luzginova *et al*. 2008). Thus, the amount of cementite is a function of both the spheroidization and austenitization processes. Work presented in this chapter focuses on the role of the austenitization process. The spheroidization process has not been changed.

Austenitization of the designed alloys has been done at a temperature just above Ae_1. The temperature is in the austenite and cementite two-phase region, and the equilibrium cementite fraction at the point is remarkably lower than observed at room temperature (Figure 1). Therefore, at equilibrium, much of spheroidized cementite must be dissolved during austenitization, and it takes some time to reach the equilibrium phase fraction. To obtain a lower bainitic microstructure with SAE52100 based alloys, 20 min of austenitization was implemented in the work presented in the previous chapter. However, the cementite dissolution reaction could not achieve equilibrium under these conditions, so a greater than equilibrium

fraction of cementite was retained in the final microstructure. Moreover, the cementite dissolution rate is influenced by the alloy compositions, as discussed in Chapter 4. This makes it necessary to investigate the dissolution of cementite in the different alloys, which is the subject of this Chapter.
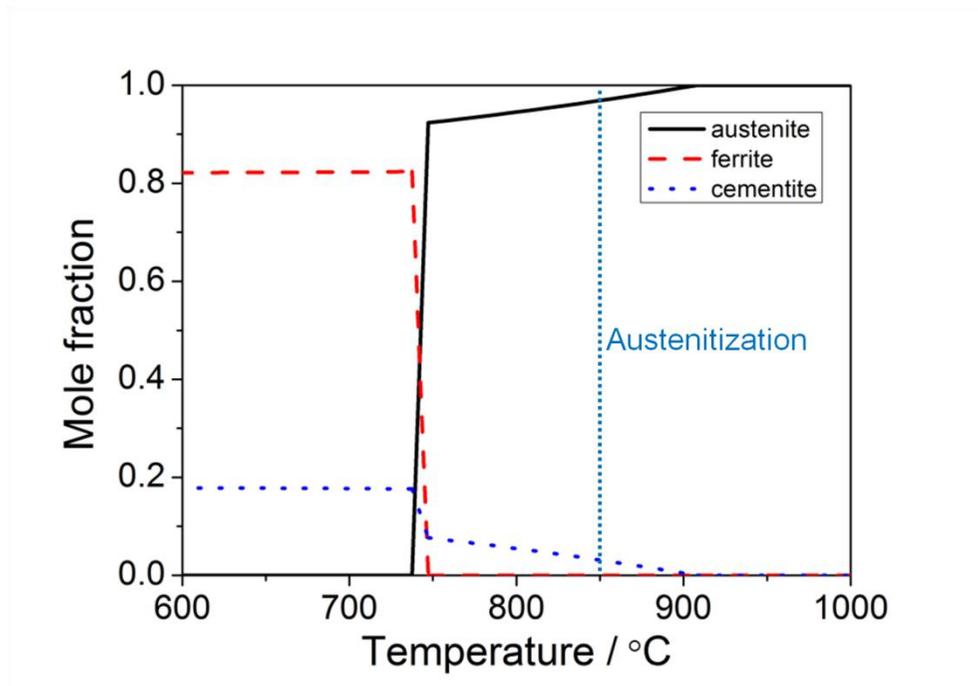
Figure 57: Calculated equilibrium phase fractions for SAE52100 using the ThermoCalc TCFE6 database. Dashed line indicates the austenitization temperature applied for SAE52100.
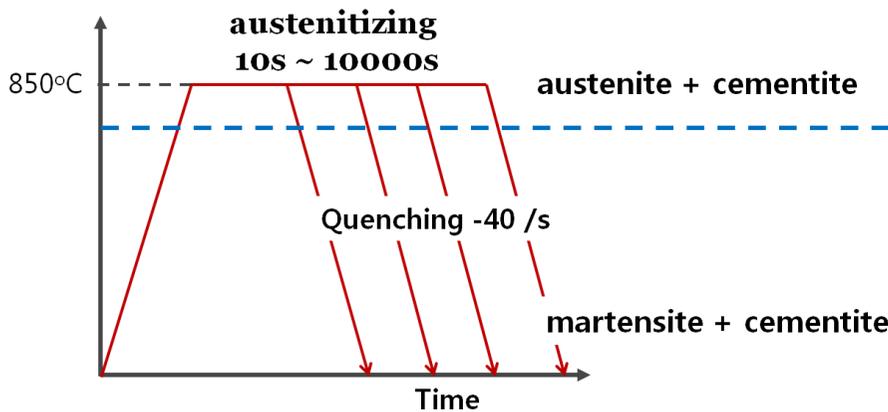
Figure 58 : Heat treatment process for measuring cementite fraction during austenitization as a function of austenitizing time.

5.2 Investigation methods

Three kinds of approaches have been attempted to investigate the dissolution behavior of spheroidized cementite during austenitization as a function of austenitization time, as follows.

In the first approach, a computational simulation was attempted using a combination of ThermoCalc and DICTRA. The size of a cementite particle could be calculated as a function of austenitization time using the mobility data for substitutional elements. Then, the phase fraction can be calculated using the size of cementite particle embedded in the defined volume of austenite.

From an experimental view, point counting was applied to analyze SEM images which represented the process of carbide dissolution. The spheroidized specimen was austenitized at 850℃ using a dilatometer. Then the sample was heated at the austenitization temperature for 10, 100, 1000 and 10000 s, before rapid quenching to room temperature to preserve the cementite (Figure 2). The resulting microstructure, which consists of martensite and spheroidized cementite, was

imaged using scanning electron microscopy on polished and etched (2% Nital) specimens. The point counting method was then applied to measure cementite fraction from those images.

Finally, the dilatometric data can be exploited to determine dissolution kinetics, by calculating the average atomic volumes of phases and carbon mass balance among them. The data for 10000 s of austenitization for the samples characterized by point counting method were studied for this purpose.

The overall results of three methods were evaluated to deduce optimum austenitization times for each alloy. Then, the controlled austenitization times were applied for each alloy, and bainite transformation kinetics were also evaluated at those cases.

5.3 Computational simulation using DICTRA and ThermoCalc

The calculation of cementite fraction using ThermoCalc and DICTRA was progressed based on the assumption that the whole system and its included phases have spherical shape as shown in Figure 3. The initial sizes of the phases were calculated from equilibrium phase fractions which were obtained using ThermoCalc with the TCFE6 database. The volume fractions of phases could be converted into the appropriate radius of the phase region using equation (5-1). During austenitization, the radius of cementite region would become smaller as cementite being dissolved. The movement of phase boundary in that situation can be predicted using the mobility data of the solutes involved, accessed via DICTRA. The radius of cementite phase region as a function of time is converted into volume fraction using equation (5-1). Although other substitutional solutes might affect the movement of phase boundary, only Cr was assumed to influence the movement for the sake of simplicity (Liu et al. 1991).

74
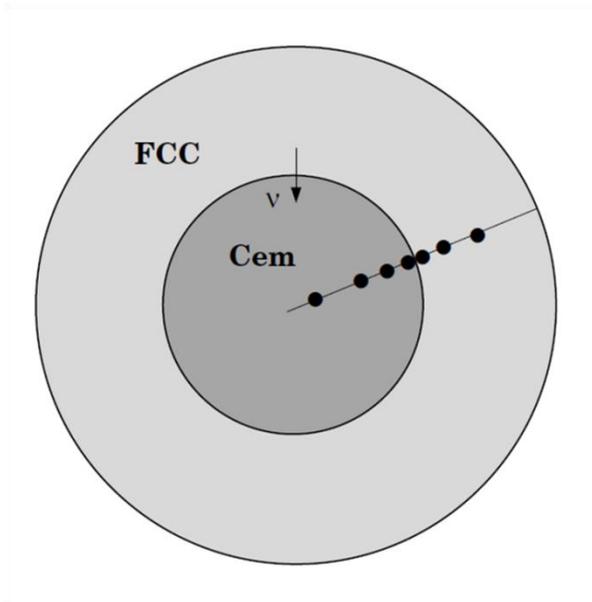
Figure 59 : A spherical phase region is assumed for DICTRA simulation (DICTRA examples version 26).

$$\frac{r_{cem}^3}{r_{total}^3} = \frac{V_{cem}}{V_{total}} = V_{cem}^f \qquad (5\text{-}1)$$
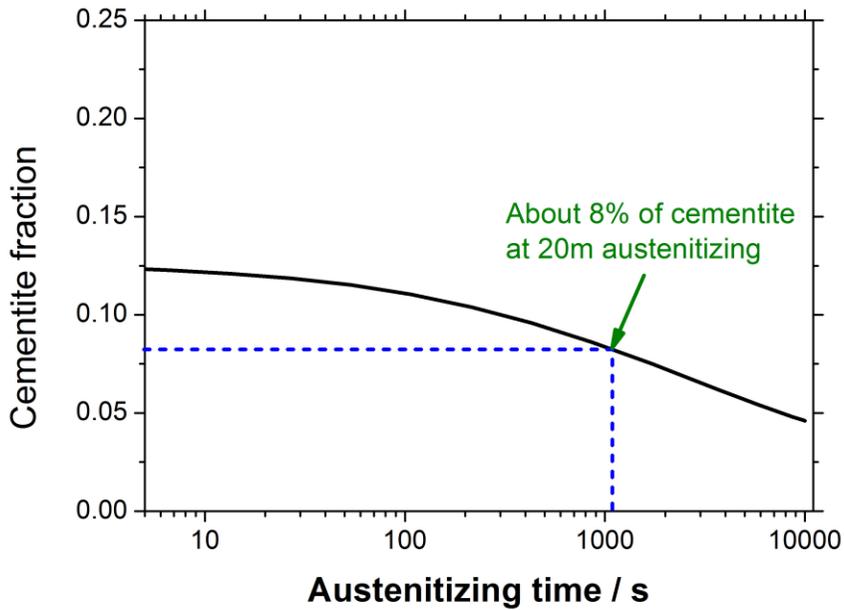
Figure 60 : Cementite fraction of SAE52100 as a function of austenitizing time at 850℃, calculated using ThermoCalc and DICTRA. The marked position indicates the cementite fraction after 20 min of austenitizing at 850℃.

The calculated result for SAE52100 is in Figure 4. The initial cementite fraction was about 0.13, which then decreased to 0.08 after about 20 min as marked in Figure 4. Cementite dissolution is therefore incomplete, even after 10000 s. The fraction after 10000 s was about 0.05, while the equilibrium fraction at 850℃ is about 0.03 (Table 1).

Table 4 : Equilibrium phase fractions at 850℃, calculated result using ThermoCalc.

	B1	B2	B3	B4	B5
Austenite	0.97	0.96	0.98	0.98	0.97
Cementite	0.03	0.04	0.02	0.02	0.03

The calculated results for the designed alloys (B2~B5) are shown in Figure 5. The marked point with a blue line indicates the austenitizing time when the cementite fraction reaches same level with that of SAE52100 after 20 min of austenitization (0.08). In the case of B2, B3 and B4, the initial cementite fractions are similar with SAE52100, and it takes a shorter time to reach a fraction 0.08 of cementite compared to SAE52100. While, B5 has a higher initial cementite fraction, it takes much longer to reach 0.08 of cementite.
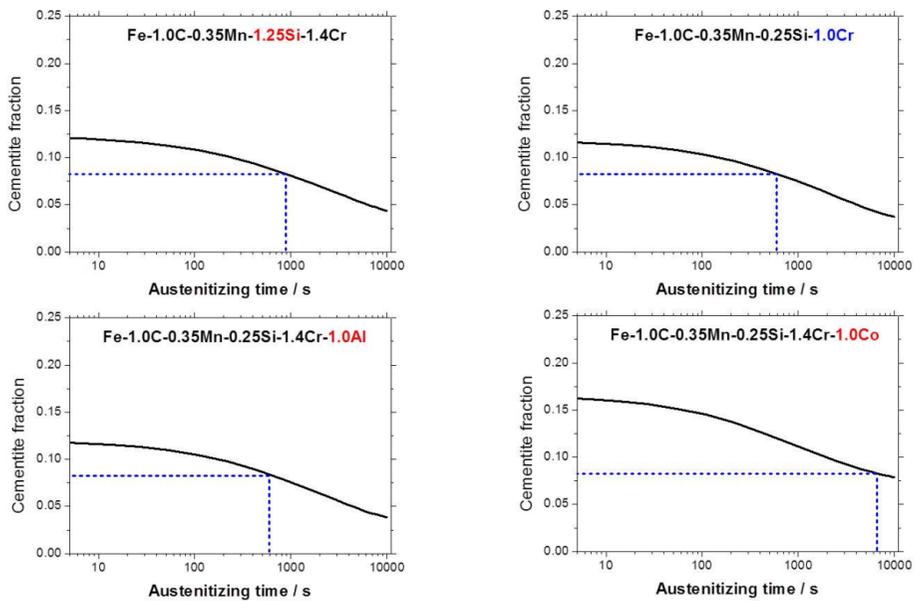
Figure 61 : Cementite fractions as a function of austenitizing time, as calculated using ThermoCalc and DICTRA. The dotted lines indicate the austenitizing time when the cementite fraction is identical to that of SAE52100 after 20 min of austenitization.

5.4 Point counting

Point counting is a simple and efficient method to estimate volume fractions in microstructures (ASM International, 2000). To implement the method, a grid was placed on the metallographic image. The number of grid points lying on the phase of interest was counted and divided by the total number of grid points. Then the point fraction was assumed to be equivalent to the area fraction and volume fraction of the phase of interest :

$$V_V = A_A = P_P = \frac{P_x}{P_T} \qquad (5\text{-}2)$$

P_P : point fraction

P_x : number of grid points lying inside x phase

P_T : total number of grid points

A_A : Area fraction

V_V : Volume fraction

The images for point counting were obtained by scanning electron microscopy of samples prepared using the heat treatment specified in Figure 2. Five SEM images were obtained for each austenitization condition, and the cementite fraction of each image was measured, and averaged to estimate the fraction.
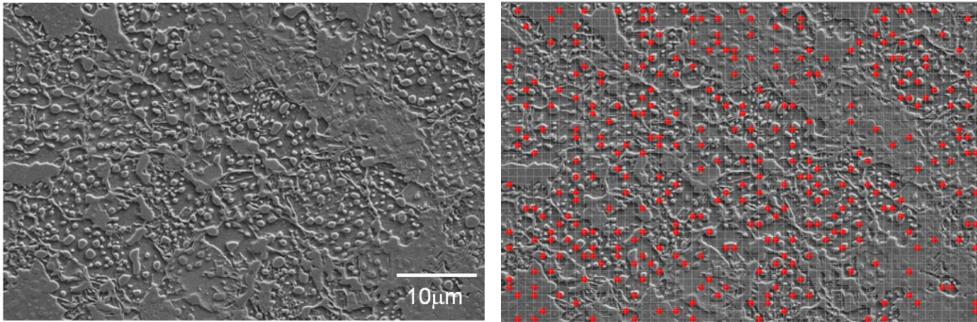
Figure 62 : SEM image of SAE52100 after heating at 850℃ for 10 s and then quenched to room temperature (left) and applying point counting as shown in the image at the right.

Figure 6 illustrates the SEM image of SAE52100 after heating at 850℃ for 10 s and then quenched to room temperature, subjected to quantitative analysis. The spacing between neighboring grid lines was an absolute length of $1\mu m$ representing 2320 points per image, with 371 points were judged as cementite in Figure 6; therefore, the cementite fraction of the image was assumed to be about 0.16±0.02.
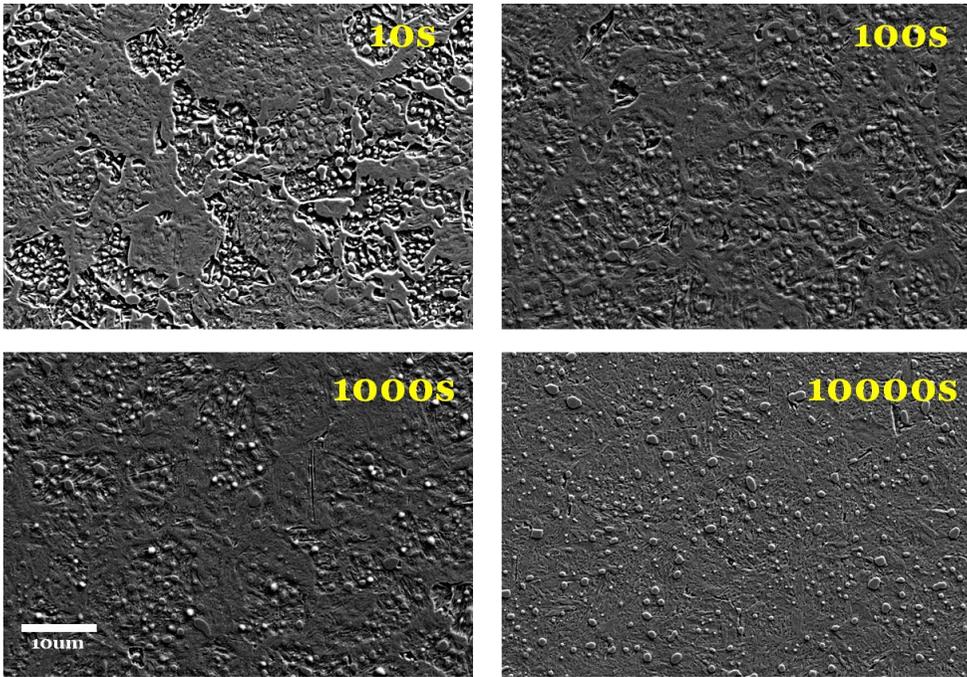
Figure 63 : SEM images of B1 as a function of austenitizing time. Each image was used for point counting.
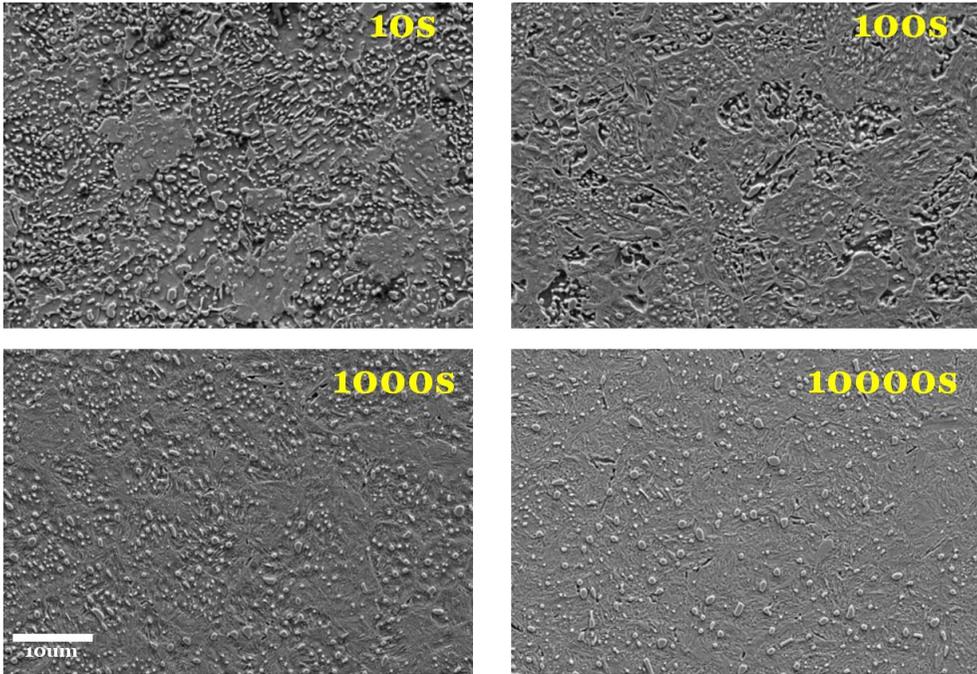
Figure 64 : SEM images of B2 as a function of austenitizing time. Each image was used for point counting.
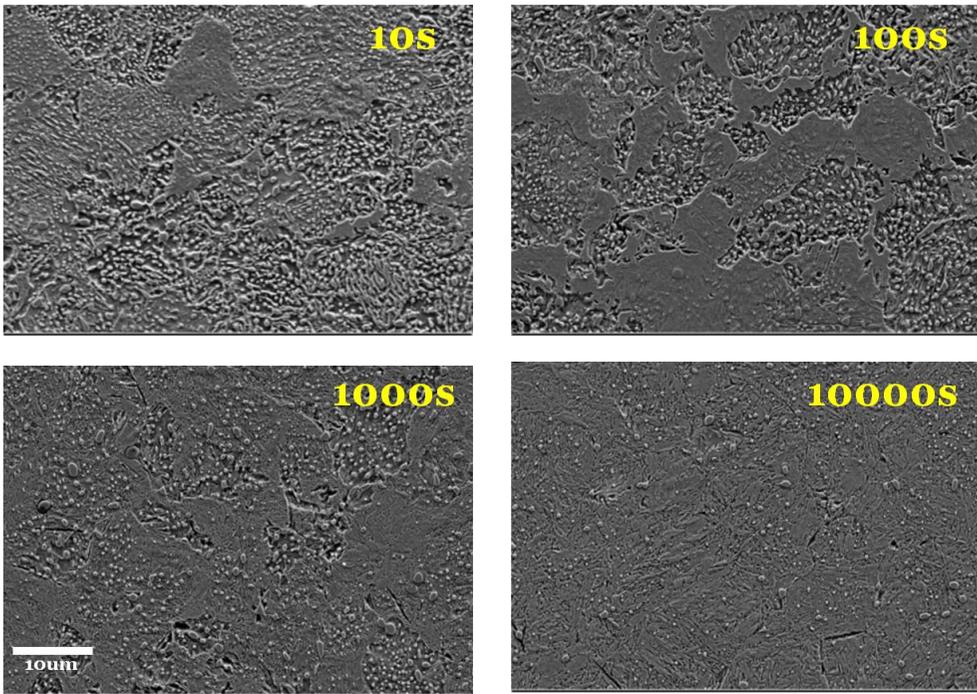
Figure 65 : SEM images of B3 as a function of austenitizing time. Each image was used for point counting.
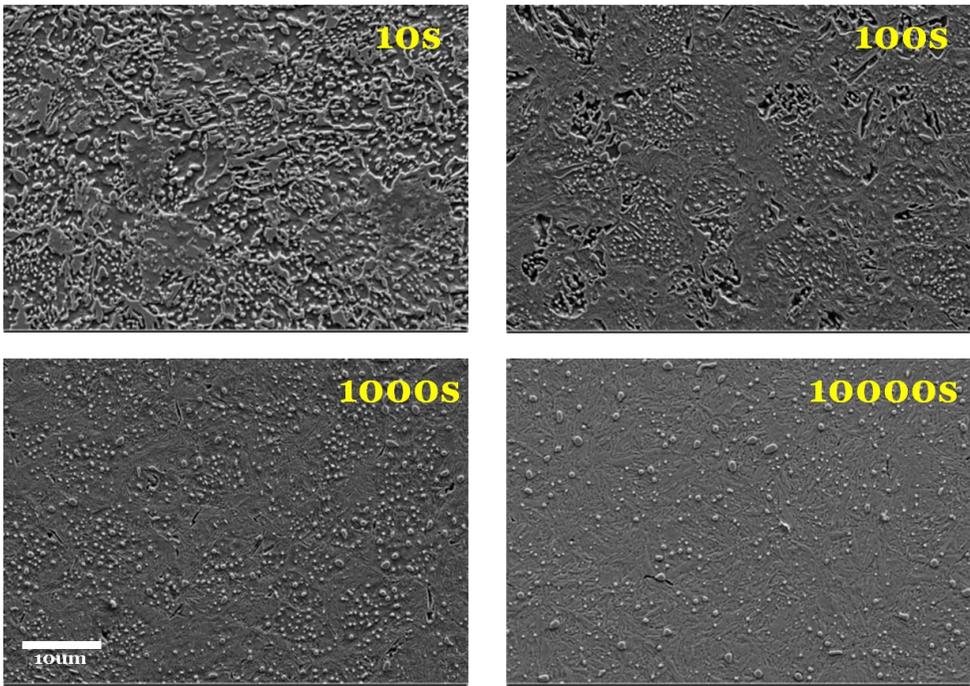
Figure 66 : SEM images of B4 as a function of austenitizing time. Each image was used for point counting.
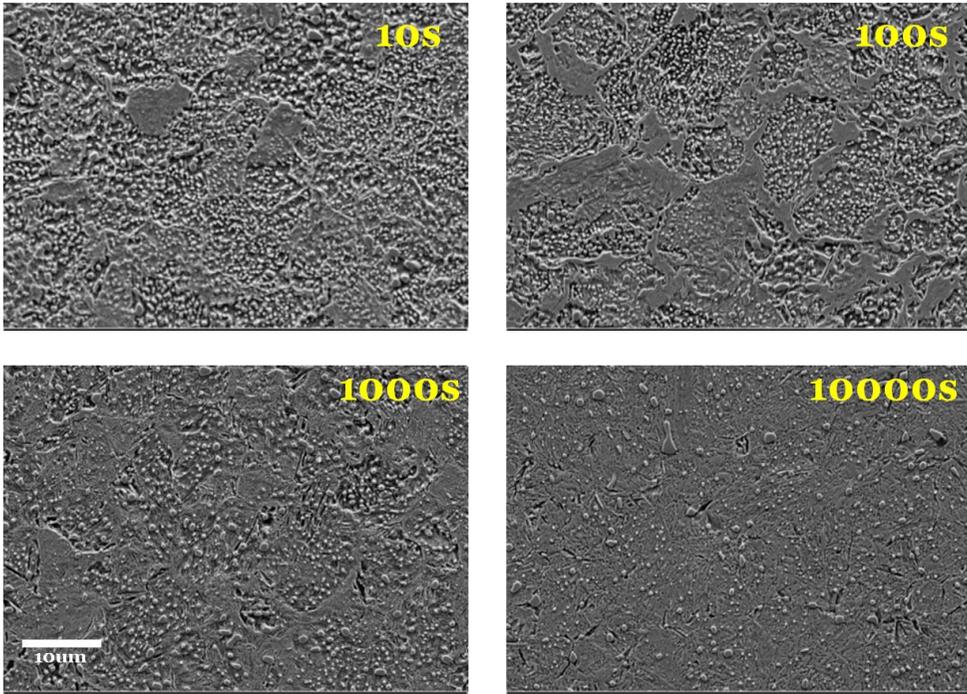
Figure 67 : SEM images of B5 as a function of austenitizing time. Each image was used for point counting.
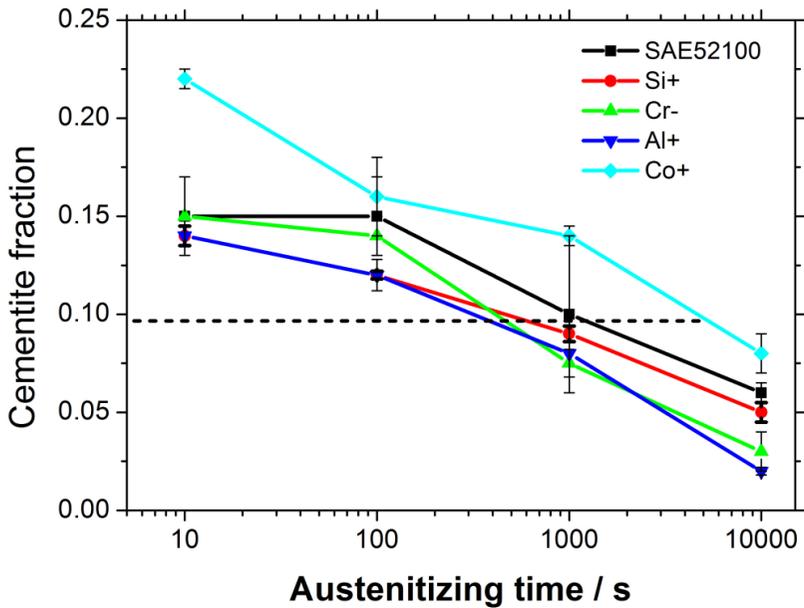
Figure 68 : Cementite fraction as a function of austenitizing time; data measured using point counting. The dashed line is explained later in the text.

Figures 7 to 11 illustrate the SEM images of B1 (SAE52100) to B5 alloys after austenitized for 10, 100, 1000, 10000 s at 850℃. Only B5, which has Co added, shows a higher cementite fraction than the other alloys, which exhibit similar cementite fractions for the same austenitization time (Figure 12). The trend of the results seems to be similar to the DICTRA simulations (Figures 4, 5). Because of its greater cementite fraction dissolution is incomplete even after 10000 s of austenitization. The dashed line in Figure 12 indicates the cementite fraction of SAE52100 after 20 min of austenitization. Thus, the austenitizing conditions, which the cementite fraction reaches same level with that of SAE52100 after 20 min of austenitization, could be identified using the intersection between dashed line and the result graphs of designed alloys. The optimum austenitization time of B2 was about 900 s, B3 and B4 were about 600 s, and B5 was about 7000 s. These match

well with the results by DICTRA simulation.

5.5 Dilatometric analysis

The phase fraction of a specimen can be determined by analyzing its dilatometer curve (ASTM 2000, Mittemeijer 1992, Li *et al*. 2001, Suh *et al*. 2007, Suh *et al*. 2008, Lee *et al*. 2010). The volume change due to transformation is related to the length change observed during dilatometry. Hence, the dissolution kinetics of cementite can be followed using this method.

If the expansion and contraction of dilatometer specimens is assumed to be isotropic, the volume and the length change are related as follows:

$$\left(\frac{\Delta V}{V_0}\right) = (1 + \frac{\Delta L}{L_0})^3 - 1 \approx \frac{3\Delta L}{L_0} \qquad (5\text{-}3)$$

$$V = k \cdot V_0 (\frac{3\Delta L}{L_0} + 1) \qquad (5\text{-}4)$$

where, V is atomic volume of the specimen, V_0 is average atomic volume at the reference temperature, L is specimen length, L_0 is specimen length at reference temperature, and k is a scale factor.

The atomic volume of the specimen at a specified temperature is the sum of the product of atomic volume and volume fraction of each phase. When ferrite, austenite and cementite are included in microstructure, the atomic volume of the

specimen can be expressed as follows:

$$V = f_\alpha \cdot V_\alpha + f_\theta \cdot V_\theta + f_\gamma \cdot V_\gamma$$

$$(f_\alpha + f_\theta + f_\gamma = 1)$$

(5-5)

where, f_i is volume fraction of i phase, and V_i is its atomic volume.

The atomic volume of each phase can be calculated from its lattice parameter and atomic structure of the phase as follows:

$$V_\alpha(T) = \left(\frac{1}{2}\right) \cdot a_\alpha^3$$

$$V_\theta(T) = \left(\frac{1}{12}\right) \cdot a_\theta \cdot b_\theta \cdot c_\theta$$

(5-6)

$$V_\gamma(T, C_\gamma) = \left(\frac{1}{4}\right) \cdot a_\gamma^3$$

where, a_i is the lattice parameter of i phase. The formulations used for the calculation of lattice parameters of austenite, ferrite, and cementite in this study are illustrated in Table 2 (Onink et al. 1993).

Table 5 : Lattice parameters of austenite, ferrite and cementite. C_γ is an atomic fraction of carbon in austenite, and T is temperature in Kelvin (Onink et al. 1993).

	Lattice parameter in Å
Austenite	$a_\gamma = (3.6306 + 0.78 \cdot C_\gamma) \cdot \{1 + (24.9 - 50 \cdot C_\gamma) \cdot 10^{-6} \cdot (T - 1000)\}$
Ferrite	$a_\alpha = 2.8863 \cdot \{1 + 17.5 \cdot 10^{-6} \cdot (T - 800)\}$
Cementite	$a_\theta = 4.5234 \cdot \{1 + (5.311 \cdot 10^{-6} - 1.942 \cdot 10^{-9} \cdot T + 9.655 \cdot 10^{-12} \cdot T^2) \cdot (T - 293)\}$
	$b_\theta = 5.0883 \cdot \{1 + (5.311 \cdot 10^{-6} - 1.942 \cdot 10^{-9} \cdot T + 9.655 \cdot 10^{-12} \cdot T^2) \cdot (T - 293)\}$
	$c_\theta = 6.7426 \cdot \{1 + (5.311 \cdot 10^{-6} - 1.942 \cdot 10^{-9} \cdot T + 9.655 \cdot 10^{-12} \cdot T^2) \cdot (T - 293)\}$

The mass fraction of carbon in each phase contributes to the overall concentration in proportion to the quantity of that phase as follows:

$$C_0 = \frac{C_\theta \cdot \rho_\theta \cdot f_\theta + C_\gamma \cdot \rho_\gamma \cdot f_\gamma}{\rho_\alpha \cdot f_\alpha + \rho_\theta \cdot f_\theta + \rho_\gamma \cdot f_\gamma}$$

(5-7)

where, C_i is mass fraction of carbon in i phase, and ρ_i is mass density of i phase. It is assumed that the concentration of carbon in ferrite is negligible. Mass density can be calculated by following formulations, when the effect of alloying elements except carbon is ignored:

$$\rho_\alpha = \frac{M_{Fe}}{V_\alpha}$$

$$\rho_\theta = \frac{12 \cdot M_{Fe} + 4 \cdot M_c}{12 \cdot V_\theta}$$

(5-8)

$$\rho_\gamma = \frac{M_{Fe} + \left(\frac{X_c}{1 - X_c}\right) \cdot M_c}{V_\gamma}$$

where, M_i is atomic mass of i phase, and X_c is carbon concentration in austenite.

The volume fraction of each phase as a function of temperature can be calculated by substituting the measured dilatometric data into the formulations above. Since the austenitization process in this study was progressed in two-phase region of austenite and cementite, the formulations can be simplified by neglecting the terms for ferrite. Therefore, equations (5-5) and (5-7) can be simplified as follows:

$$\begin{aligned} V &= f_\theta \cdot V_\theta + f_\gamma \cdot V_\gamma \\ &= V_\theta + (V_\gamma - V_\theta) \cdot f_\gamma \end{aligned}$$

(5-9)

$$(f_\theta + f_\gamma = 1)$$

$$C_0 = \frac{C_\theta \cdot \rho_\theta \cdot f_\theta + C_\gamma \cdot \rho_\gamma \cdot f_\gamma}{\rho_\theta \cdot f_\theta + \rho_\gamma \cdot f_\gamma} \tag{5-10}$$

By arranging equation (5-9) and (5-10), we obtain:

$$f_\gamma = \frac{(C_\theta - C_0) \cdot \rho_\theta}{[(C_0 - C_\gamma) \cdot \rho_\gamma - (C_0 - C_\theta) \cdot \rho_\theta]} \tag{5-11}$$

In equation (5-9), (5-10), and (5-11), V_θ is determined by temperature, and V can be obtained from dilatometer data after substituting to equation (5-4). Likewise, C_θ, C_0, and ρ_θ can also be calculated using the alloy composition. Then, the phase fractions f_γ and f_θ can be finally calculated at a certain temperature.
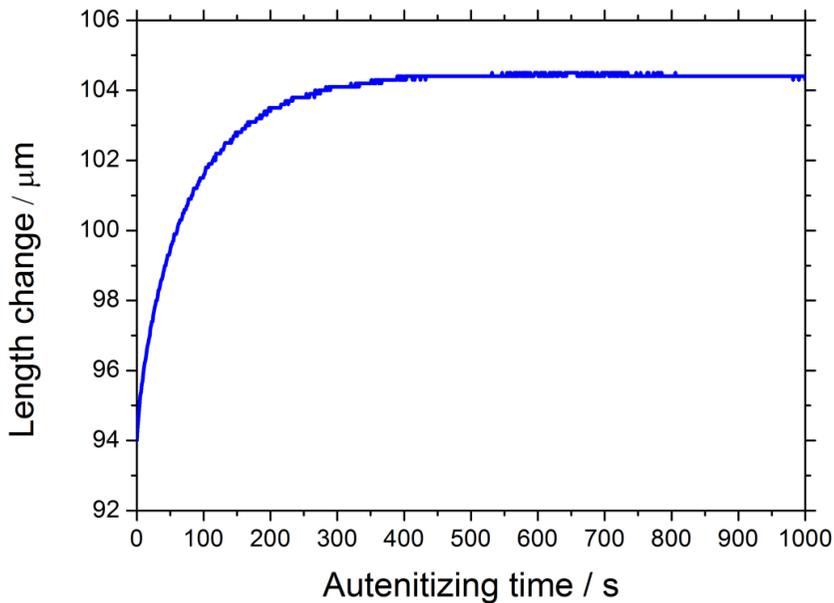
Figure 69 : Length change of a specimen during austenitizing process. Dilatometric data of SAE52100 austenitized at 850℃ for 1000 s.

The dilatometer curves used for the analysis were data from 1000 s for point counting method specimen as Figure 13, since 10000 s data were not suitable due to unknowable contraction of specimen. During austenitization process, a large amount of spheroidized cementite dissolves into austenite. Thus, the volume fraction of cementite is decreased, while the volume fraction and carbon concentration of austenite are increased. This also causes the increase of atomic volume of austenite. Therefore, the dilatometer specimen should expand, since the expansion due to austenite formation exceeds the contraction cementite dissolved.
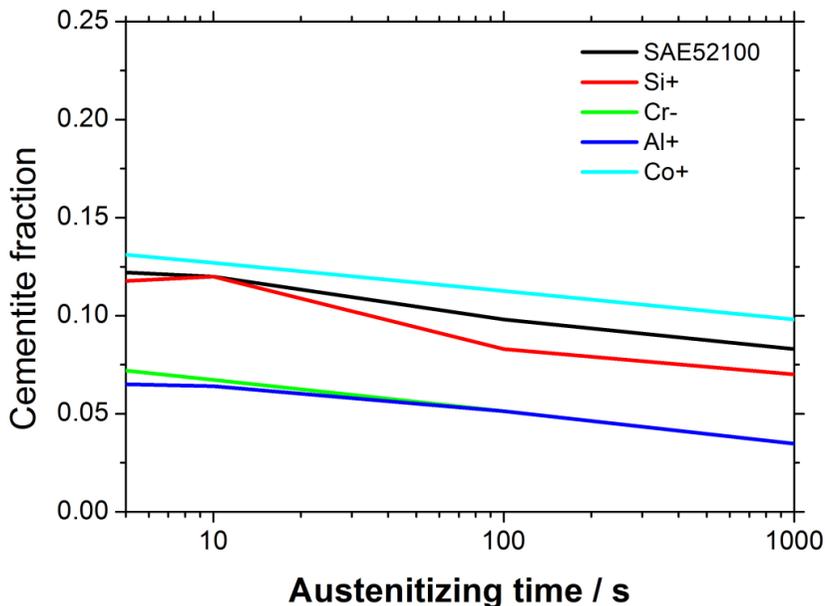
Figure 704 : Cementite fraction as a function of austenitizing time. Measured result by dilatometer analysis.

The cementite fraction as a function of austenitizing time, which was measured by dilatometer analysis, is illustrated in Figure 14. The trend of result seems to be similar with the outcome of DICTRA simulations and point counting methods. That is, the cementite fraction of B5 is higher than any other alloys after about 20 min,

and those of B2, B3 and B4 are lower than SAE52100. However, the overall cementite fraction of B3 and B4 are much lower level than that of SAE52100. Hence, the optimum austenitization time could not be determined using this method.

5.6 Bainite transformation kinetics after cementite fraction control

With the help of the cementite fractions determined in three ways, the optimum austenitization time for each of the alloys was determined. All the results indicate that B2, B3, and B4 contain less cementite, while B5 contains more at the same austenitization time compared with SAE52100. Thus, a shorter austenitization time was applied for B2, B3, and B4, while a longer time was applied for B5. Although the analysis suggested the trend in the adjustment of austenitization time, experimental try and error was required to determine the actual austenitization condition which could accelerate the bainite transformation. As a result, the austenitization time applied for B2 was 900 s, B3 and B4 were 600 s, and B5 was 1800 s.
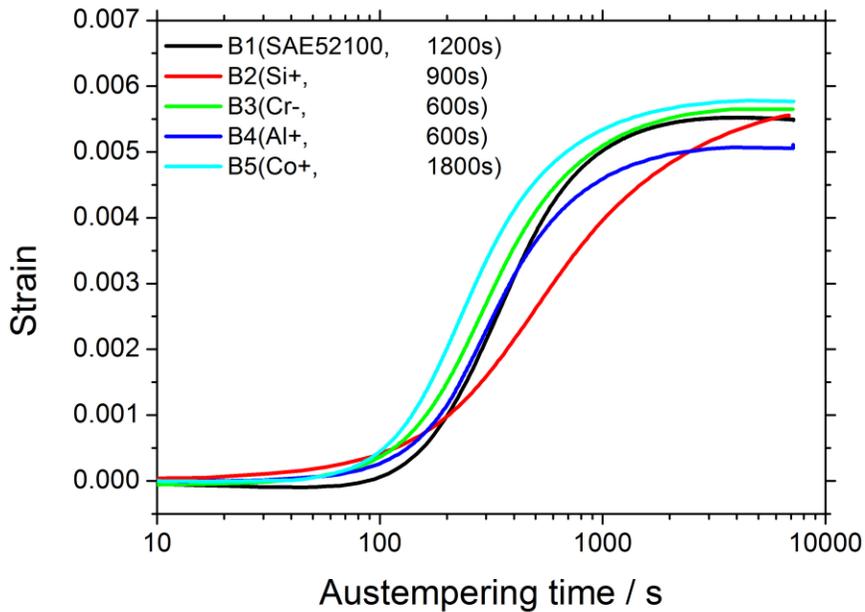
Figure 71 : Overall bainite transformation kinetics upon austenitizing at 850℃ and austempering at 250℃ after applying the adjusted austenitizing times.

The overall bainite transformation kinetics after applying the adjusted austenitization times is illustrated in Figure 15. The bainite transformation of every designed alloy initiates faster than SAE52100, and the kinetics of B2, B3, and B4 are accelerated compared to the results from the constant austenitization. Although the transformation is delayed in B5 due to the longer austenitization time to achieve the required cementite fraction, it is still faster than SAE52100. In the case of B2, the transformation obviously initiates faster than SAE52100, but slower at intermediate time relative to the other alloys, and is incomplete even after 2 h of austempering. Therefore, shorter austenitization times (180 s ~ 900 s) were tried for the acceleration of bainite transformation of B2. However, cementite dissolution did not progress sufficiently to avoid the formation of pearlite due to lower carbon concentration in austenite during cooling to 250℃. So the final austenitization time for B2 was determined to 900 s, after which the pearlite formation could be avoided.
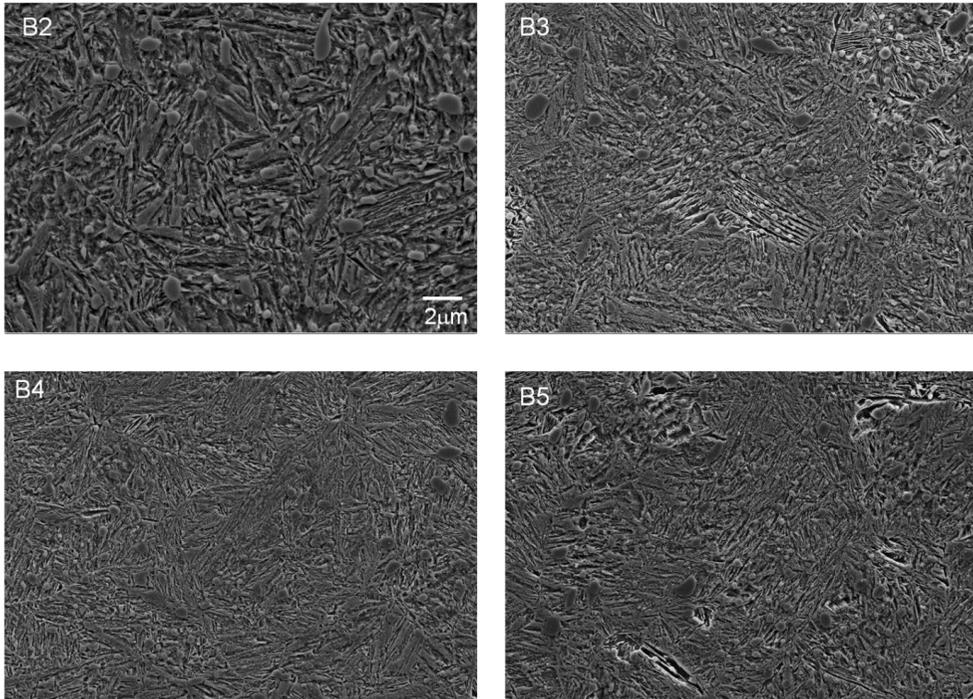
Figure 72 : SEM images of microstructures of B2~B5 upon austenitizing at 850℃ and austempering at 250℃ after applying controlled austenitizing time.

The SEM images for final microstructures of designed alloys are illustrated in Figure 16. However, the images look similar with the microstructure of uncontrolled austenitization (Figure 6, 8, 10, 12 of Chapter 4), since the change in cementite fraction between controlled and uncontrolled austenitization conditions is too small to generate microstructural change.

5.7 Summary

  It is necessary to control the carbon concentration in austenite for the acceleration of the bainite transformation of SAE52100 by changing alloy composition. For that, dissolution behavior of spheroidized cementite needs to be investigated in advance. Thus, the change in cementite fraction during austenitization was observed and estimated by DICTRA simulation, point counting method, and dilatometric analysis. Then optimum austenitization conditions, at which the cementite fraction becomes equivalent to that of SAE52100 after 20 min of austenitization, were determined for newly designed alloys. As a result, the bainite transformation kinetics of designed alloys could be accelerated compared to SAE52100, except B2.

Chapter 6: Mechanical properties of bainitic bearing steels

6.1 Introduction

The mechanical properties generally required for bearing steel are the hardness, tensile strength, fatigue property, toughness, wear resistance and shape stability. High-carbon steels such as SAE52100 alloy in a quenched and tempered condition have been widely used as a bearing material, as they can meet such requirements without special treatments. It is demonstrated in this study that hardness in the range of about 57-62 HRC can be obtained under tempering conditions of 180℃ to 250℃.

Lower bainite has been suggested in an initial stage as an alternative for martensite for the microstructure of bearing steel, as an equivalent or superior fatigue life to martensite could be derived in certain conditions without a major decrease in any of the other mechanical properties (Hollox *et al.* 1980). Based on this historical motivation, new bearing alloys for lower bainitic microstructures have been designed by changing the alloy compositions from SAE52100. The bainite transformation of the newly designed alloys showed improved kinetics compared to that of SAE52100, as intended. However, the mechanical properties of those alloys have yet to be evaluated. Therefore, in this chapter, the hardness and fatigue properties of designed alloys are evaluated.

6.2 Experimental

The hardness of designed alloys was measured using a Rockwell hardness tester (Mitutoyo HR-522). The specimens for the hardness test were spheroidized in a tube furnace in bulk and were then transformed into a bainitic structure using a dilatometer by a revised heat treatment process, as discussed in Chapter 5.

The fatigue properties of the alloys were evaluated by ultrasonic fatigue tests using a piezoelectric system at a high frequency of 20 kHz at room temperature. The specimens for the fatigue test were heat-treated in the same way as the hardness specimens, but the bainite transformation was performed in a salt bath instead of with a dilatometer. The heat-treated specimens were machined to the shape illustrated in Figure 1. The circular reduction of the cross-sectional area in the centers of the specimens serves to magnify the strain amplitude. The specimens were ground with a grinding disc to produce surface conditions as close to actual conditions as possible. About 20 specimens were tested for each alloy.
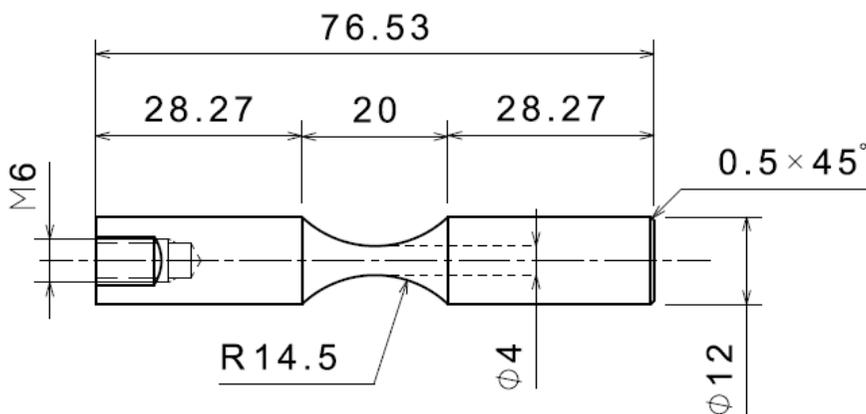
Figure 73: The specimen used in ultrasonic fatigue test. All dimensions are in ㎜.

6.3 Hardness

The hardness of the lower bainite microstructure of SAE52100 was compared with that of the martensitic microstructure in Chapter 3. This comparison showed about 60HRC of hardness when the transformation was complete, which was a level equivalent to the martensitic microstructure of SAE52100 tempered at 250℃ for 120 min. The hardness of other designed alloys is also illustrated in Figure 2.
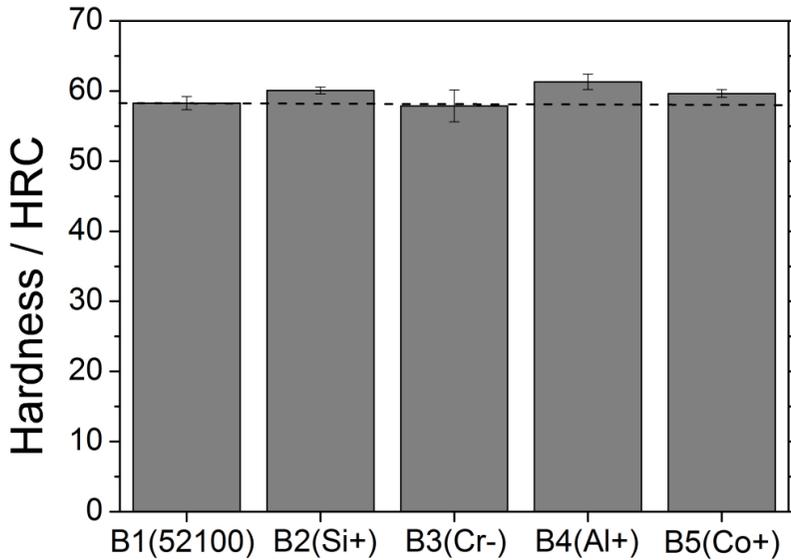
Figure 74 : Hardness of lower bainite microstructure of the designed alloy. The dashed line marks the hardness of SAE52100. The hardness presented is the average of at least five measured values.

All of the five alloys demonstrate a similar level of hardness close to 60HRC. B2, B4, and B5 showed slightly higher hardness values than the SAE52100 alloy, while B3 showed a lower value. Because the hardness was measured after the bainite transformation was complete, the microstructure of each alloy may consist of an equivalent phase fraction of the spheroidized cementite and lower bainite. The hardness of the steel can be typically expressed as a linear combination of the contributions from individual phases:

$$H = \sum V_i H_i \qquad (6\text{-}1)$$

Here, V_i is the volume fraction of the i phase, and H_i is the specific hardness of the i phase. The change in the hardness in the designed alloys may come from the

change in the specific hardness of each phase, as the volume fractions of the phases are controlled and are thus equivalent. Figure 3 illustrates the amounts of substitutional alloys in the austenite (martensite at the room temperature) of each alloy just after the austenitization process, as measured by energy dispersive x-ray spectroscopy (EDS). The result confirms that there are some differences in the alloy compositions of austenite, which transformed to lower bainite later. The added alloys may contribute to the substitutional solid solution strengthening of bainite. Consequentially, the hardness illustrated in Figure 2 appears to be the outgrowth of the composition change effect rather than stemming from a phase fraction change.
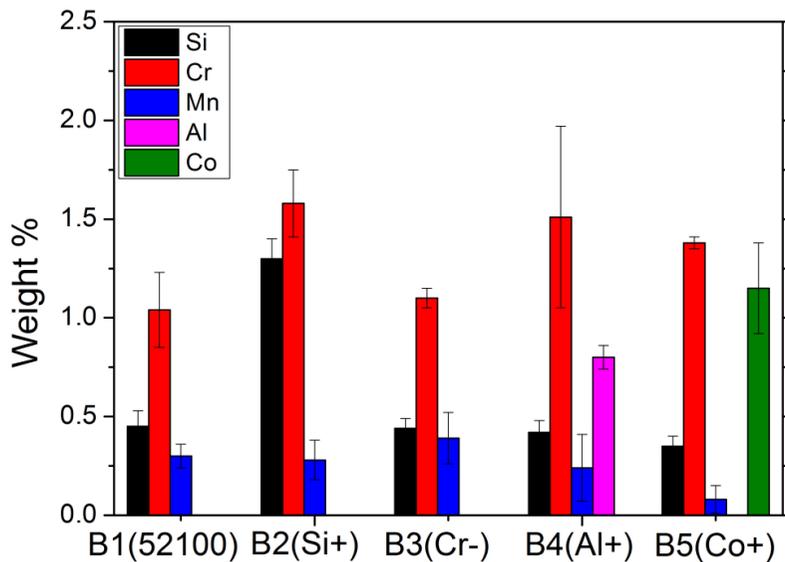
Figure 75: Mass percent of substitutional elements in austenite after austenitization for 20 min at 850℃. The results were measured by energy dispersive X-ray spectroscopy (EDS).

6.4 Fatigue property

Fatigue tests were carried out for the alloys of B1, B3, B4, and B5, which showed accelerated bainite transformation kinetics compared to that of B1. The results are expressed as "S-N" curves by plotting the alternating stress amplitude versus the logarithm of the number of cycles leading to failure. The S-N curves obtained from the tests are shown in Figure 4.

Figure 76: *S-N* curves for the alloys of B1, B3, B4 and B5. The arrows represent the specimens which did not fail during the experiments.

The results indicate that B3, B4, and B5 yield longer fatigue life than B1 at all stress amplitudes; B5 shows the longest fatigue life, followed by B4, B3, and B1, respectively. Therefore, changes in the alloy elements seem to contribute to the enhancement of the fatigue property of lower bainitic 52100 alloys.

However, the overall result demonstrates a shorter fatigue life than other reported results. Figure 5 illustrates the reported fatigue life of 52100-type steels, which were also evaluated by ultrasonic testing at a frequency of 20 kHz (Bathias 2010, Marines *et al.* 2003, Mayer *et al.* 2009). All of these samples yield longer fatigue lifetimes at all stress amplitudes compared to B5, which recorded the best fatigue property among the designed alloys in this research. Particularly, the bainitic structure in Mayer's research, in which SAE52100 was austenitized at 850℃ and austempered at 220℃ for 5 hours, showed enhanced fatigue properties compared to other results. The hardness levels in these studies showed levels similar to those of the designed alloys in this study, which were also about 60 HRC.
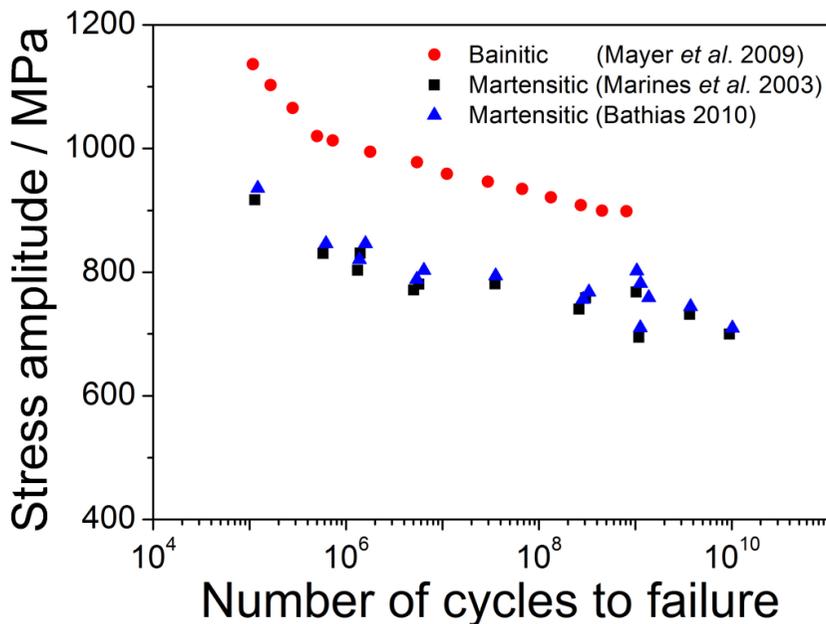
Figure 77: Reported S-N data for SAE52100-type steels (Bathias 2010, Marines *et al.* 2003, Mayer *et al.* 2009). The data were obtained by ultrasonic testing at a frequency of 20 kHz.

In order to verify the cause of the shorter fatigue life of the designed alloys, the fracture surfaces of several broken specimens were observed using SEM. Figure 6 illustrates the fracture surfaces of the samples, showing the maximum ((a), (c), (e), (g)) and minimum ((b), (d), (f), (h)) fatigue lifetimes in the B1, B3, B4, and B5 alloys, respectively. In every specimen, a crack initiates on the surface of the specimen without any inclusion and propagates to the interior. The dotted circles in Figure 6 mark the crack initiating sites in each specimen. B1 and B3 have one crack initiation site, while B4 and B5 have multiple crack initiation sites. This tendency is reasonable, as a single crack initiation site usually indicates a failure with a low level of stress, while multiple initiation sites may be a result of high stress (Sachs 2005). Every fracture surface reveals the same macroscopic features of typical fatigue failure. These results can be commonly divided into the three regions of the crack initiation site, the fatigue zone, and an instantaneous zone. Figure 7 illustrates the fracture surface of B1 (showing the same image shown in Figure 6(a)) at 406 MPa, with enlarged images in the dotted region. Figure 7(a) is the crack initiation site at the surface of the specimen. Figure 7(b) is the fatigue zone, where the crack growth is slow. Then, it is followed by an instantaneous zone in Figure 7(c), where the final failure occurs.
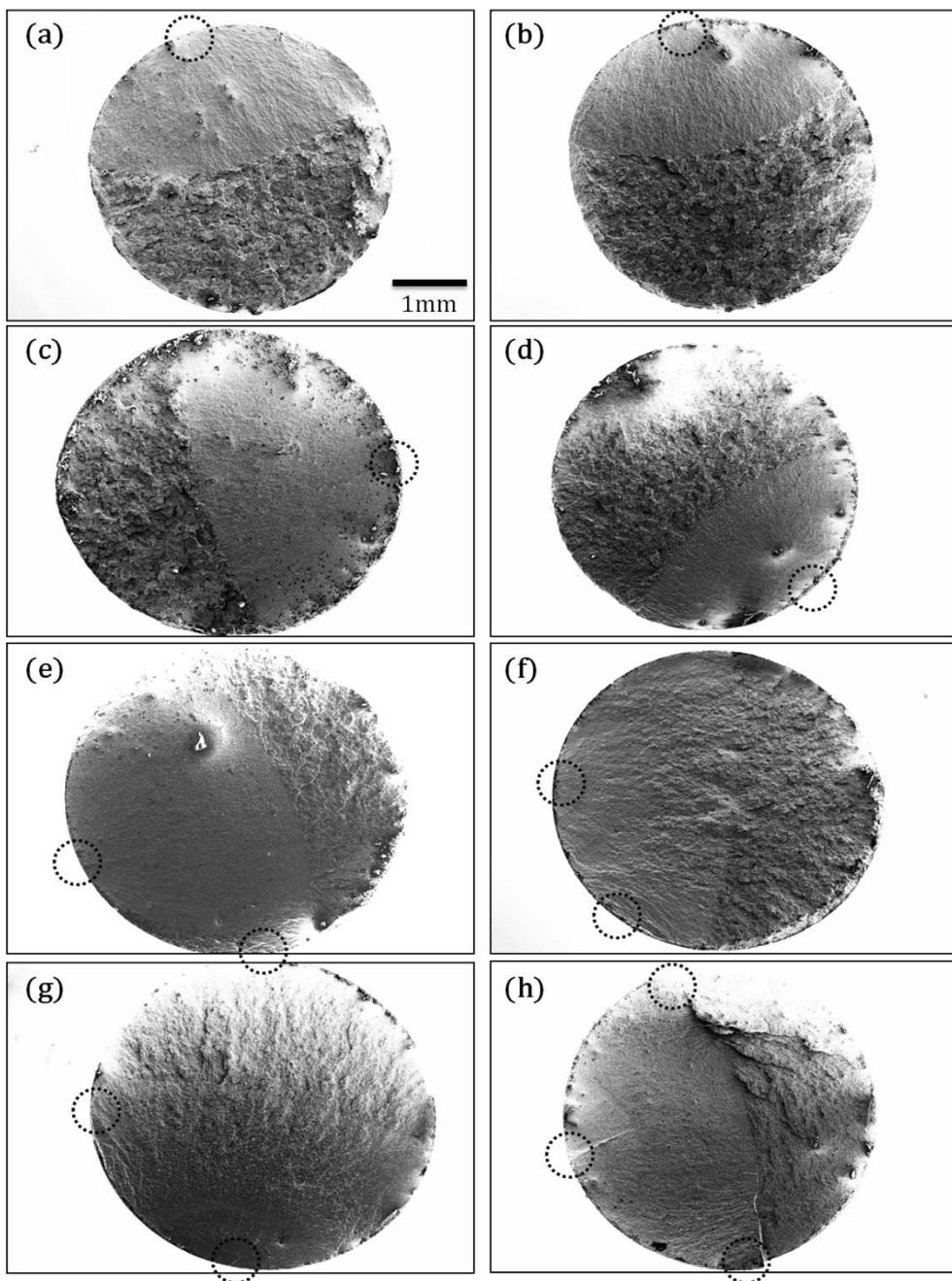
Figure 78: SEM observations of the fracture surfaces of the designed alloys:
B1 specimens of (a) $4.24*10^8$ cycles at 406MPa and (b) $3.90*10^5$ cycles at 420MPa
B3 specimens of (c) $1.44*10^8$ cycles at 434MPa and (d) $8.40*10^4$ cycles at 479MPa
B4 specimens of (e) $4.36*10^8$ cycles at 522MPa and (f) $5.19*10^4$ cycles at 540MPa
B5 specimens of (g) $8.65*10^5$ cycles at 571MPa and (h) $6.70*10^4$ cycles at 602MPa
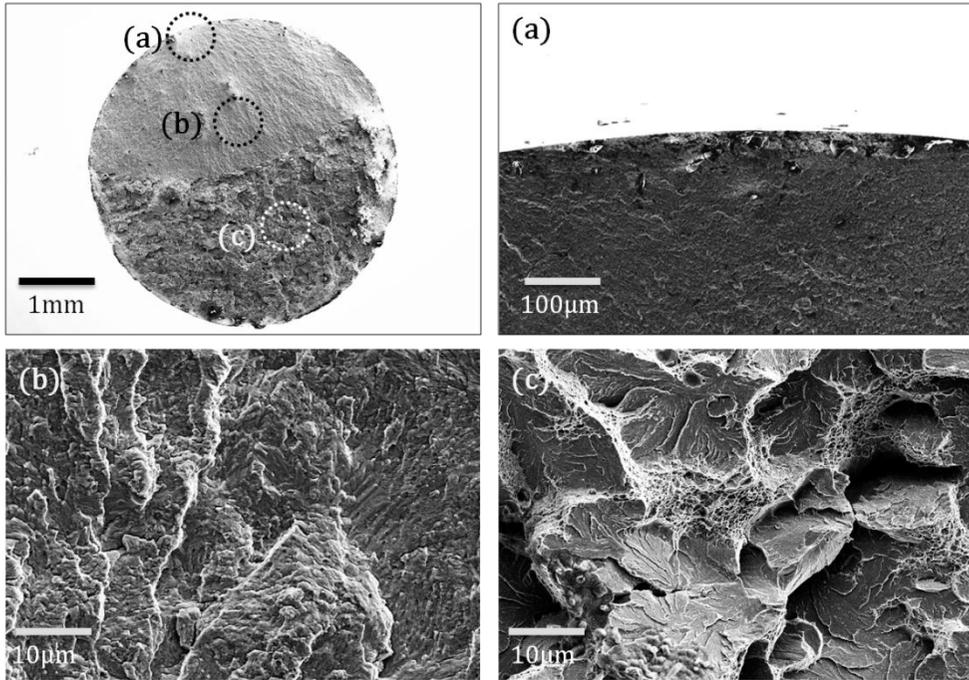
Figure 79: Fracture surface of B1 (the same image shown in Figure 6(a)) at 406 MPa, with enlarged images of dotted circle regions. (a) The crack initiation site on the surface of the specimen. (b) Fatigue zone, where crack growth is slow. (c) Instantaneous zone, where the final failure occurs.

On the other hand, the fracture surfaces in earlier studies, as noted in Figure 5, reveal typical 'fish-eye' failure modes in which the crack initiates from an internal nonmetallic inclusion (Oguma *et al.* 2001, Saki *et al.* 2006; 2010). Figure 8 illustrates the fish-eye type fracture surface in Marines' research (Marines *et al.* 2003). It is clearly distinct from the fracture surfaces of the samples in this research, as shown in Figure 6.
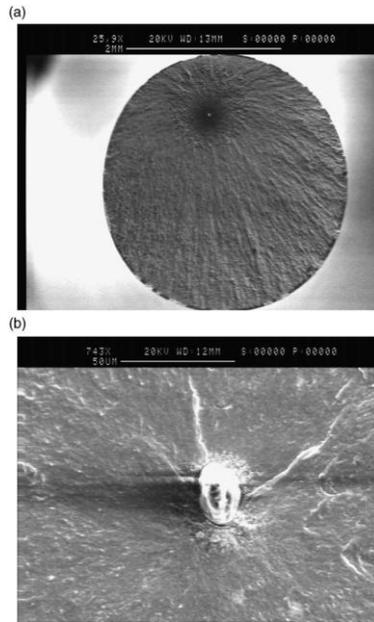
Figure 80: Internal crack initiation of martensitic 52100-type steel tested at a cyclic stress level of $2.52*10^8$ at 860 MPa. (a) Internal fish-eye structure. (b) Al_2O_3 inclusion (Marines *et al.* 2003).

It is not clear why the lower bainitic structure in this study shows a lower fatigue life compared to earlier martensitic or same bainitic structures despite the similar hardness level. Considering the factors which can affect the fatigue property of lower bainitic 52100 steel, the effect of spheroidized cementite in the microstructure was initially suspected. The final microstructure is controlled so that it consists of about 8% of spheroidized cementite, with the rest being lower bainite in this study, whereas the bainite structure in Mayer's research had no spheroidized cementite. Thus, some portion of the alloying elements is constructing spheroidized cementite instead of constructing lower bainite. This can cause a decline in the strength and hardness of bainite on the microscale, even when the overall properties in the bulk scale are maintained. It has been reported in several studies that a longer fatigue life

can be obtained by an enhancement of the surface hardness of the steel (Glaeser 1977, Boardman 1990, Sasahara 2005). Therefore, the lower micro-hardness of the lower bainite caused by the existence of spheroidized cementite may lead to a shorter fatigue life of the steel. This assumption is reasonable only when the spheroidized cementite does not contribute to the crack propagation or stress concentration during the fatigue test. Unfortunately, a recent study reported a contrary effect of spheroidized cementite on tempered martensitic bearing steel. Kim showed that spheroidized cementite contributes to the enhancement of the fatigue life of tempered martensitic 52100 bearing steel. The spheroidized cementite is regarded to strengthen the tempered martensite matrix and to make the stress concentration not on the surface but around the internal inclusion. Figure 9 illustrates the fatigue mechanisms of tempered martensitic bearing steels with spheroidized cementite and without them (Kim *et al.* 2012). However, the role of spheroidized cementite on the hardness or stress concentration of lower bainite has not been established yet.
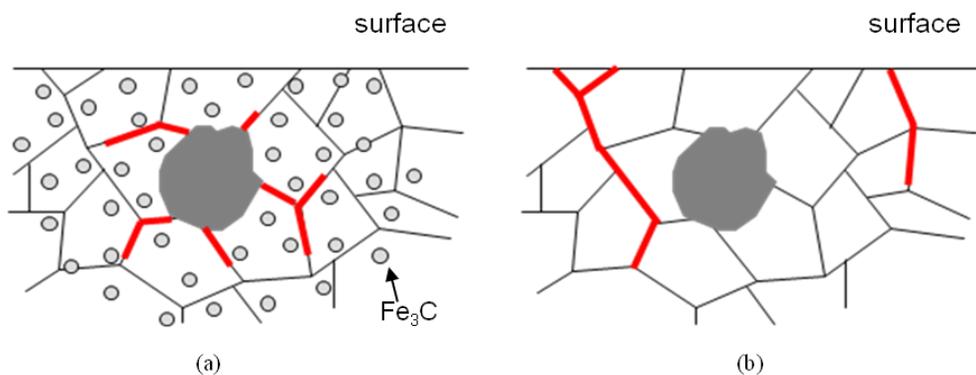
Figure 81: Schematic illustration of the fatigue mechanisms of bearing steels (a) with spheroidized carbides and (b) without them. The crack initiation and propagation paths assumed to occur are expressed as thick lines (Kim *et al.* 2012).

6.5 Summary

The hardness and fatigue property of lower bainitic bearing steels as designed in this study were evaluated. All alloys demonstrate similar levels of hardness close to 60HRC. Si-, Al-, and Co-added alloys showed slightly higher hardness values than the SAE52100 alloy, while the Cr-decreased alloy showed a lower value.

The fatigue property was evaluated by an ultrasonic fatigue testing method. The results demonstrated that changing in Cr, Al, and Co concentrations seemed to contribute to the enhancement of the fatigue property as well as to the acceleration of bainite transformation for lower bainitic 52100 alloys. However, the overall fatigue property was inferior to the reported results of tempered martensite and the lower bainite structure of 52100 steel. To clarify why this occurred, it is necessary to establish how spheroidized cementite affects the micro-hardness or fatigue stress concentration of lower bainite.

Chapter 7: Conclusion

The bainite transformation of SAE52100 bearing steel, with a microstructure containing spheroidized cementite in a ferrite matrix, could be completed in 30 min at 250℃, which is much faster than previous studies based on a non-spheroidized starting structures. The resultant lower bainitic microstructure showed a similar hardness level compared with martensite at the same transformation temperature. Moreover, an enhancement of hardness could be achieved by lowering the isothermal transformation temperature, without retardation of transformation kinetics.

The bainite transformation could be accelerated by changing alloying elements of SAE52100 steel. The bainite transformation of Al-, Co-added, and Cr-decreased alloys has been completed in shorter isothermal transformation time compared with SAE52100, while the transformation kinetics of Si-added alloy was delayed.

Changing alloying elements influenced cementite dissolution kinetics during austenitization as well as bainite transformation. The quantity of spheroidized cementite is relevant to the carbon concentration of austenite, which is the biggest affecting factor on bainite transformation kinetics. Therefore it was necessary to investigate the cementite dissolution behavior, in order to understand the effect of various solutes on the acceleration of bainite. Several techniques were applied to measure the cementite fraction during austenitization. Based on the results, the spheroidized cementite fraction was controlled to be fixed by changing the austenitization time.

The fatigue property of lower bainitic SAE52100 could be enhanced by changing the concentration of Cr, Al, and Co, without a particular change in hardness. However, the presence of spheroidized cementite particle was adversely affected on the fatigue property of bainitic SAE52100 steel, since the measured results were inferior to the reported results with non-spheroidized microstructures. It is

inconsistent with martensitic SAE52100 steel, in which the microstructure with spheroidized cementite showed enhanced fatigue property compared with non-spheroidized microstructure.

The Al-added alloy can be the most viable candidate for the new generation bainitic SAE52100 steel. Since fully bainitic microstructure could be obtained in shorter transformation time, and the mechanical properties of the resultant microstructure was also improved. Cr-decreased alloy revealed similar performance with Al-added alloy, except the insignificant hardness reduction. Co-added alloy showed the longest fatigue life, but the longer austenitization was required for the alloy due to slow cementite dissolution kinetics.

References

A. R. Kiani-Rashid and D. V. Edmonds. "The bainitic phase transformation in aluminum containing ductile irons after short time of austempering." *International Journals of ISSI* 1: 8-14, 2004.

B. Boardman. "Fatigue resistance of steels." *Properties and Selection: Irons*, ASM International, 1: 673-688, 1990.

C. A. Stickels. "Carbide refining heat treatment for 52100 bearing steels." *Metallurgical Transactions A*, 5:865–874, 1974.

C. Bathias and J. Ni. "Determination of fatigue limit between 10^5 and 10^9 cycles using an ultrasonic fatigue device." *Advances in fatigue lifetime predictive techniques*, ASTM International 1211:141–52, 1993.

C. Bathias. "Gigacycle fatigue properties of bearing steels." Journal of ASTM International,7:JAI102712, 2010.

C. Berger, B. Pyttel, and D. Schwerdt. "Beyond HCF – is there a fatigue limit?" *Materialwissenschaft und Werkstofftechnik*, 39:769–776, 2008.

C. Garcia-Mateo, F. G. Caballero, and H. K. D. H. Bhadeshia. "Acceleration of Low-temperature Bainite." *ISIJ Intermational*, 43:1821-1825, 2003.

C. Garcia-Mateo, F. G. Caballero, and H. K. D. H. Bhadeshia. "Development of hard bainite." *ISIJ Intermational*, 43:1238-1243, 2003.

C. M. Li, F. Sommer, E. J. Mittemeijer (2001). "Quantitative dilatometric Analysis of the Isothermal Decomposition of Hypereutectoid Fe-C austenite." *Zeitschrift für*

Metallkunde, 92:32-36, 2001.

D. Umbrello, A. D. Jayal, S. Caruso, O. W. Dillon, and I. S. Jawahir. "Modeling of white and dark layer formation in hard machining of AISI 52100 bearing steel." *Machining Science and Technology*, 14:128–147, 2010.

D. Umbrello, A. D. Jayal, S. Caruso, O. W. Dillon, and I. S. Jawahir. "Modeling of white and dark layer formation in hard machining of AISI 52100 bearing steel." Machining Science and Technology, 14:128–147, 2010.

D. W. Suh, C. S. Oh, and S. J. Kim. "Dilatometric analysis of austenite formation during intercritical annealing." *Metals and Materials International*, 14:275-282, 2008.

D. W. Suh, C. S. Oh, H. N. Han, and S. J. Kim. "Dilatometric analysis of austenite decomposition considering the effect of non-isotropic volume change." *Acta Materialia*, 55: 2659-2669, 2007.

E. Girault, A. Metens, P. Jacques, Y. Houbaert, B. Verlinden, and J. V. Humbeeck. "Comparison of the effects of silicon and aluminium on the tensile behavior of multiphase trip-assisted steels." *Scripta Materialia*, 44:885-892, 2001.

E. J. Mittemeijer. "Review Analysis of the kinetics of phase transformations." *Journal of Materials Science*, 27:3977-3987, 1992.

F. C. Akbasoglu and D. V. Edmonds. "Rolling contact fatigue and fatigue crack propagation in 1C-1.5Cr bearing steel in bainitic condition." *Metallurgical Transactions A*, 21:889–893, 1990.

F. C. Akbasoglu. "The effect of microstructure on the performance of bearing steels

with particular reference to their operation with water containing lubricants." *PhD thesis*, University of Oxford, 1988.

F. G. Caballero and H. K. D. H. Bhadeshia. "Very strong bainite." *Current Opinion in Solid State and Materials Science* 8(3-4): 251-257, 2004.

F. G. Caballero, H. K. D. H. Bhadeshia, K. J. A. Mawella, D. G. Jones, and P. Brown. "Very Strong Low Temperature Bainite." *Materials Science and Technology* 18: 279-284, 2002.

F. Hengerer. "The history of SKF3." *Ball Bearing Journal*, 231:2–11, 1987.

G. E. Hollox, R. A. Hobbs, and J. M. Hampshire. "Lower bainite bearings for adverse environments." Wear 68(2): 229-240, 1981.

G. E. Hollox, R. A. Hobbs, and J. M. Hampshire. "Lower bainite bearings for adverse environments." *Wear*, 68:229–240, 1981.

Glaeser, Ludema and Rhee. "Wear of Materials." ASME, 1977.

H. K. D. H. Bhadeshia. "Thermodynamic analysis of isothermal transformation diagrams." *Metal Science* 16(3):159-166, 1982.

H. K. D. H. Bhadeshia. *Bainite in Steels, 2nd edition.* Institute of Materials, 2001.

H. K. D. H. Bhadeshia. *Steels for Bearings.* Progress in Materials Science, 2012.

H. Kuhn. "Ultrasonic fatigue testing." *Mechanical testing and evaluation*, Vol 8, ASM International, 8:717-729, 2000.

H. Mayer, W. Haydn, R. Schuller, S. Issler, B. Furtner, and M. Bacher-Hochst. "Very high cycle fatigue properties of bainitic high carbon–chromium steel." International Journal of Fatigue 31: 242–249, 2009.

Hiroyuki Sasahara. "The effect on fatigue life of residual stress and surface hardness resulting from different cutting conditions of 0.45%C steel." *International Journal of Machine Tools and Manufacture*, 45(2):131-136, 2005.

I. Marines, G. Dominguez, G. Baudry, J.-F. Vittori, S. Rathery, J.-P. Doucet, and C. Bathias. "Ultrasonic fatigue tests on bearing steel AISI-SAE 52100 at frequency of 20 and 30 kHz." International Journal of Fatigue 25: 1037–1046, 2003.

J. Cappel, M. Weinberg, and R. Flender. "The metallurgy of roller–bearing steels." *Steel Grips*, 2:261–268, 2004.

J. Chakraborty, D. Bhattacharjee, and I. Manna. "Development of ultrafine bainite + martensite duplex microstructure in SAE 52100 bearing steel by prior cold deformation." *Scripta Materialia*, 61: 604–607, 2009.

J. D. Verhoeven. "The role of the divorced eutectoid transformation in the spheroidization of 52100 steel." *Metallurgical & Materials Transactions A*, 31A:2431–38, 2000.

J. D. Verhoeven and E. D. Gibson. "The divorced eutectoid transformation in steel." *Metallurgical & Materials Transactions A*, 29A:1181–89, 1998.

J. M. Beswick. "Fracture and fatigue crack propagation properties of hardened 52100 steel." *Metallurgical & Materials Transactions A*, 20:1961–1973, 1989.

J. M. Hare. "Fatigue failure of a circulating water pump shaft." *Handbook of case*

histories in failure analysis, ASM International, 2:348-353, 1993

K. H. Kim, J. S. Lee, and D. L. Lee. "Effect of silicon on the spheroidization of cementite in hypereutectoid high carbon chromium bearing steels." *Metals and Materials International*, 16:871–876, 2010.

K. H. Kim, S. D. Park, J. H. Kim and C. M. Bae. "The role of spheroidized carbides on the fatigue life of bearing steel." *Metals and Materials International*, to be submitted, 2012.

K. Hokkirigawa, K. Kato, and Z.Z. Li. "The effect of hardness on the transition of the abrasive wear mechanism of steels." *Wear*, 123:241–251, 1988.

K. Monma, R. Maruta, T. Yamamoto, and Y. Wakikado. "Effect of particle sizes of carbides and amounts of undissolved carbide on the fatigue life of bearing steel." *Journal of the Japan Institute of Metals*, 32:1198–1204, 1968.

K. Tsubota, T. Sato, Y. Kato, K. Hiraoka, and R. Hayashi. "Bearing steels in the 21st century." *Bearing Steels: into the 21st Century*, 202–215, American Society for Testing of Materials, 1998.

Krauss, G. "Principles of heat treatment of steel." *American Society for Metals*, 291, 1980.

M. Guillot and G. Dudragne. "Optimisation of the thermal treatment of a roller bearing steel 100Cr6." *Memoires Etudes Scientifiques Rev. Metallurg.*, 79:493, 1982.

M. J. Caton, J. W. Jones, H. Mayer H, S. Stanzl-Tschegg, and J. E. Allison. "Demonstration of an endurance limit in cast 319 aluminum." *Metallurgical Transactions A*, 34A:33-41, 2003.

M. Onink, D. Tichelaar, M. Brakman, J. Tittemeijer, S. Van Der Zwaag, and J. H. Root. "The lattice parameters of austenite and ferrite in Fe-C alloys as Functions of Carbon Concentration and Temperature." *Scripta Metallurgica*, 29, 1993.

M. Y. Huh, K .K. Bae, and S. J. Kim. "A study on the mechanical properties and sub-structures of 1.0%C-1.4%Cr bearing steel." *Journal of the Korean Institute of Metals*, 20:987–994, 1982.

N. Sakanaka. "Axial loading fatigue properties of bainite SUJ2 bearing steels." *ISIJ International*, 22:1292, 2009.

N. V. Luzginova, L. Zhao, and J. Sietsma. "Evolution and thermal stability of retained austenite in SAE52100 bainitic steel." *Materials Science and Engineering: A*, 448:104-110, 2006.

N. V. Luzginova, L. Zhao, and J. Sietsma. "Bainite formation kinetics in high carbon alloyed steel." *Materials Science and Engineering A*, 481–482:766–769, 2008.

N.V. Luzginova, L. Zhao, and J. Sietsma. "The cementite spheroidization process in high-carbon steels with different chromium contents" *Metallurgical and Mateials Transactions A*, 39(A):513-521, 2008.

N. W. Sachs. "Understanding the surface features of fatigue fractures: How they describe the failure cause and the failure history." *Journal of Failure Analysis and Prevention*, 5(2):11-15, 2005.

NPL. MTDATA. Software, National Physical Laboratory, Teddington, U.K., 2006.

P. R. T. Silva. "Analysis of the fatigue behavior of SAE52100 steel under different microstructural conditions." *PhD thesis*, Porto Alegre, 2001.

Q. Y. Wang, C. Bathias, S. Rathery, and J. Y. Berard. "Fatigue of a spheroidal graphite cast iron in the very high cycle range." *Revue de Metallurgie*, 96(2):221–226, 1999.

R. F. Mehl and W. C. Hagel. "The austenite: pearlite reaction." *Progress in Metal Physics*, 6:74–134, 1956.

R. W. K. Honeycombe and H. K. D. H. Bhadeshia. *Steels: Microstructure and Properties, 2nd edition.* Butterworths−Hienemann, 1995.

S. J. Lee, K. D. Clarke, and C. J. Van Tyne. "An on-heating dilation conversional model for austenite formation in hypoeutectoid steels." *Metallurgical Transactions A*, 41A: 2224-2235, 2010.

T. Oyama, O. D. Sherby, J. Wadsworth, and B. Walser. "Application of the divorced eutectoid transformation to the development of fine-grained, spheroidized structures in ultrahigh carbon steels." *Scripta Metallurgica*, 18:799–804, 1984.

T. R. McNelley, M. R. Edwards, A. Doig, D. H. Boone, and C. W. Schultz. "The effect of prior heat treatments on the structure and properties of warm-rolled AlSl 52100 steel." *Metallurgical & Materials Transactions A*, 14:1427–1433, 1983.

T. Sakai, B. Lian, M. Takeda, K. Shiozawa, N. Oguma, Y. Ochi, M. Nakajima, and T. Nakamura. "Statistical duplex S–N characteristics of high carbon chromium bearing steel in rotating bending in very high cycle regime." *International Journal of Fatigue*, 32: 497, 2010.

T. Sakai, Y. Sato, Y. Nagano, M. Takeda, and N. Oguma. "Effect of stress ratio on long life fatigue behavior of high carbon chromium bearing steel under axial loading." *International Journal of Fatigue*, 28:1547–1554, 2006.

T. Sakai, Y. Sato, Y. Nagano, M. Takeda, and N. Oguma. "Effect of stress ratio on long life fatigue behavior of high carbon chromium bearing steel under axial loading." *International Journal of Fatigue*, 28: 1547, 2006.

W. Li, Y. Wang, and X. Z. Yang. "Frictional hardening and softening of steel 52100 during dry sliding." *Tribology Letters*, 18:353–357, 2005.

Y. Hirotsu and S. Nagakura. "Crystal structure and morphology of the carbide precipitated from martensitic high–C steel during the 1st stage of tempering." *Acta Materialia*, 20:645–655, 1972.

Y. Nadot, J. Mendez, N. Ranganathan, and A. S. Beranger. "Fatigue life assessment of nodular cast iron containing casting defect." *Fatigue & Fracture Engineering Materials & Structures*, 22(4):289–300, 1999.

Y. Wang, T. C. Lei, and C. Q. Gao. "Influence of isothermal hardening on the sliding wear behaviour of 52100 bearing steel." *Tribology International*, 23:47–53, 1990.

Z. K. Liu, L. Hoglund, B. Jonsson, and J. Agren. "An experimental and theoretical study of cementite dissolution in an Fe-Cr-C Alloy." *Metallurgical Transactions A*. 22A: 1745-1752, 1991.

Acknowledgements

CURRICULUM VITAE

Name: Chae, Jae-Yong (채 재 용)
E-mail: exfeel@potsech.ac.kr; exfeel@posco.co.kr
Date of birth: 12th July, 1981
Place of birth: Pohang, South Korea

Education
Ph. D. 2012, POSTECH (Pohang, Korea), Graduate Institute of Ferrous Technology, Computational Metallurgy Group.

M. S. 2008, POSTECH (Pohang, Korea), Graduate Institute of Ferrous Technology, Computational Metallurgy Group.

B. S. 2006 POSTECH (Pohang, Korea), Department of Computer Science and Engineering.

Publications

J. Y. Chae, J. H. Jang, G. Zhang, K. H. Kim, J. S. Lee, H. K. D. H. Bhadeshia, and D. W. Suh, "Dilatometric analysis of cementite dissolution in hypereutectoid steels containing Cr." *Scripta Materialia*, 65:245-248, 2011.